Planning for Sun-Synchronous Lunar Polar Roving

Nathan D. Otten

CMU-RI-TR-18-21

Submitted in partial fulfillment of the requirements for the degree of Doctor of Philosophy in Robotics.

The Robotics Institute
Carnegie Mellon University
Pittsburgh, Pennsylvania 15213

May 2018

Thesis Committee:
David Wettergreen, Co-chair
William "Red" Whittaker, Co-chair
Alonzo Kelly
Anthony Colaprete, *NASA Ames*
Paul Tompkins, *SpaceX*

Copyright © 2018 by Nathan Otten. All rights reserved.

Abstract

Lunar polar resources can accelerate deep space exploration by resupplying missions with oxygen, water, and propellent. Before lunar resupply can be established, the distribution and concentration of water ice and other volatiles abundant at the poles of the Moon must be verified and mapped. The need for affordable, scalable exploration of the lunar poles motivates the deployment of solar-powered rovers and planning strategies that sustain robotic missions beyond a single two-week period of lunar daylight.

Reliance on solar power at the lunar poles gives rise to significant challenges—and opportunities—for individual rovers to achieve multi-lunar-day longevity. Solar-powered rovers require persistent sunlight for power and heat, lest they succumb to the cryogenic temperatures of lunar night. Although constrained by thermal conditions and available power, opportunistic polar rovers can maintain warmth and ample solar power for several months by following sun-synchronous routes. Strategic, informed route planning that exploits polar lighting enables sustained lunar polar roving and resource prospecting not possible by other means.

This research develops polar roving strategies and applies global path planning methods to generate spatiotemporal routes that provide multiple lunar days of uninterrupted sunlight while satisfying constraints on rover speed, terrain slope, and direct-to-Earth communication. The existence of feasible sun-synchronous routes on the South Pole of the Moon is demonstrated by proof-of-concept examples that last multiple lunar days. These are generated using spatiotemporal predictive models of dynamic surface illumination and Earth view based on ephemeris data and global topographic maps derived from Lunar Orbiter Laser Altimeter data.

In addition, this research addresses issues of route robustness. Predictive model uncertainty stemming from topographic measurement error presents substantial risk to rovers dwelling at predicted local peaks of persistent sunlight. This thesis presents a strategy to selectively deploy limited rover autonomy to reduce risk during unavoidable communication blackouts. Finally, this thesis presents a method of identifying viable landing sites amenable to sustained lunar polar roving. Together, these contributions advance capabilities to plan safe, reliable routes that extend lunar missions by an order of magnitude and enable a future of sustainable exploration.

Acknowledgments

No Ph.D. thesis is a solo act, but even soloists rely on directors, rhythm sections, and active supporters to pull off a successful performance. This dissertation is no exception, and I owe a lot to those who guided, backed, and helped me along the way.

First, I thank my advisors, Dave Wettergreen and Red Whittaker, for instructing and mentoring me as I navigated my graduate education and research and for enabling me to pursue topics I care about. They read my roughest drafts, listened to my greenest ideas, and pushed me to be a better student and scholar. Without them, I wouldn't be where I am today, nor would I be on my current trajectory.

I also thank the rest of my thesis committee, Al Kelly, Paul Tompkins, and Tony Colaprete, for sharing their perspective and constructive commentary. Their interest in my topic is genuine, and their contributions have kept me and my work grounded.

Many of the results presented in this dissertation depend on predictive models made possible by members of the Planetary Robotics Lab at CMU and our partners at Astrobotic. I especially want to thank Heather Jones and Eric Amoroso for pouring countless hours into developing the systems used to process lunar data and generate models of the lunar polar environment that are foundational to this work.

In addition to my research colleagues, I'm thankful to all of my friends in the Robotics Institute, particularly the Nebraska cohort, Nate Wood, Joe Bartels, and Eric Markvicka, for their camaraderie and commiseration during our shared time in Pittsburgh. I believe those college football Saturdays spent together were important for my own well-being, and I'd like to think my company was good for them too.

My family deserves a lot of credit as well. I thank my parents, Kim and Yvonne, and my sisters, Heather and Heidi, for their love, encouragement, belief, and not questioning whether six more years of school was really a good idea. Thanks to my French Bulldog, Merry, for always lifting my spirits with unconditional companionship and endless kisses. Finally, I can't acknowledge enough my girlfriend, Cait, for always being there for me and listening to my unfiltered thoughts, both good and bad. Our relationship is without a doubt the single most valuable thing I'll take away from CMU and Pittsburgh. Thank you.

This work was sponsored in part by the NSF Graduate Research Fellowship Program and NASA Innovative Advanced Concepts.

Contents

1 Introduction **1**
- 1.1 Motivation . . . 1
  - 1.1.1 Lunar Prospecting . . . 2
  - 1.1.2 Sustainable Exploration . . . 4
  - 1.1.3 Sun-Synchronous Route Planning . . . 6
- 1.2 Approach . . . 8
- 1.3 Thesis Statement . . . 10
- 1.4 Contributions . . . 11
- 1.5 Overview . . . 11

2 Background **13**
- 2.1 The Lunar Polar Environment . . . 14
  - 2.1.1 Water . . . 14
  - 2.1.2 Sunlight . . . 15
  - 2.1.3 Earth View . . . 17
  - 2.1.4 Terrain . . . 17
  - 2.1.5 Thermal . . . 17
- 2.2 Prior Lunar Roving . . . 18
  - 2.2.1 Lunokhod . . . 18
  - 2.2.2 Apollo Lunar Roving Vehicle . . . 19
  - 2.2.3 Chang'e Yutu . . . 19
- 2.3 Relevance to other Planetary Bodies . . . 19
  - 2.3.1 Mercury . . . 20
  - 2.3.2 Venus . . . 20
  - 2.3.3 Earth . . . 20
  - 2.3.4 Mars . . . 21
  - 2.3.5 Others . . . 21

3 Related Work **23**
- 3.1 Polar Mission Planning . . . 23
  - 3.1.1 Modeling Lunar Polar Illumination . . . 23
  - 3.1.2 Circumnavigation and Sun-Synchronous Planning . . . 24
- 3.2 Path Planning . . . 25
  - 3.2.1 Deterministic Path Planning . . . 26
  - 3.2.2 Randomized Path Planning . . . 26

3.2.3 Temporal and Resource Path Planning . . . 27
3.2.4 Replanning . . . 28
3.3 Summary . . . 29

4 Spatiotemporal Constraint Models **31**
4.1 Gridded Models . . . 31
4.2 Lunar Data . . . 32
4.3 Modeling Spatiotemporal Constraints . . . 33
4.3.1 Surface Insolation . . . 34
4.3.2 Earth Visibility . . . 37
4.3.3 Terrain Slope . . . 37

5 Planning for Sunlight **39**
5.1 Routes of Continuous Illumination . . . 39
5.1.1 Sunlight as a Hard Constraint . . . 39
5.1.2 Deterministic Path Planning . . . 40
5.2 Connected Component Analysis . . . 43
5.2.1 Connected Component Pruning . . . 44
5.2.2 Planning within Connected Components . . . 48
5.3 Other Improvements . . . 48
5.3.1 Temporal Pruning . . . 48
5.3.2 Time-Independent Waypoints . . . 50
5.4 Summary . . . 52

6 Planning for Communication **53**
6.1 Supervised Teleoperation . . . 54
6.1.1 Constraints . . . 54
6.1.2 Planning Method . . . 55
6.1.3 Example Route . . . 56
6.2 Route Analysis . . . 56
6.2.1 Visualizing 3D Route Constraints in 2D . . . 58
6.2.2 Computational Method . . . 58
6.2.3 Interpretation . . . 59
6.3 Summary . . . 60

7 Planning for Uncertainty **63**
7.1 Sources of Error and Uncertainty . . . 64
7.2 Strategic Autonomy . . . 65
7.2.1 Singularities . . . 65
7.2.2 Constraints . . . 67
7.2.3 Planning Method . . . 67
7.2.4 Example Route . . . 68
7.2.5 Discussion . . . 68
7.3 Quantifying Risk and Route Sensitivity . . . 70
7.4 Summary . . . 72

8 Planning for Longevity **73**
8.1 Introduction . . . 73
8.2 Method . . . 74
8.2.1 Model . . . 74
8.2.2 Preprocessing . . . 76
8.2.3 Route Planning . . . 78
8.3 Results . . . 79
8.4 Summary . . . 80

9 Planning for Landing **85**
9.1 Data . . . 85
9.2 Method . . . 87
9.3 Results . . . 91
9.3.1 Route Validation . . . 91
9.3.2 Route Seeding . . . 91
9.4 Summary . . . 91

10 Planning for the Future **97**
10.1 Planning for Shadow . . . 97
10.1.1 Rover Stored Energy State . . . 97
10.1.2 Maximizing Solar Array Configurations . . . 99
10.2 Planning for Efficiency . . . 99
10.3 Planning for Thermal . . . 101
10.4 Planning for Science . . . 102
10.4.1 Mission Enhancement . . . 102
10.4.2 Mixed-Initiative Planning . . . 104
10.5 Planning for Perpetual Exploration . . . 105
10.6 Planning a Sustainable Power Grid . . . 107

11 Conclusion **109**
11.1 Summary . . . 109
11.2 Conclusions . . . 110
11.3 Contributions . . . 111

A Acronyms **113**

List of Figures

1.1 Solar-powered lunar polar rovers 3

2.1 Estimated depth of permafrost at Nobile Crater rim 15
2.2 Average illumination and communication at Nobile Crater rim 16
2.3 10-meter LOLA DEM to 85°S 18

4.1 Digital terrain models of the lunar South Pole 32
4.2 3D mesh model of the Moon's South Pole 33
4.3 Illumination maps of Malapert Peak and Shackleton Crater 34
4.4 Binary illumination maps of Malapert Peak and Shackleton Crater . . 35
4.5 Simulated illumination map accuracy 36
4.6 Slope maps of Malapert Peak 38

5.1 Routes via deterministic path planning 41
5.2 Lighting, slope, and connected components 45
5.3 Pruned connected component and route 47
5.4 Two examples of prolonged solar-powered polar traverses 49

6.1 Nobile route demonstrating *Supervised Teleoperation* constraints . . . 57
6.2 Route Proximity to *Supervised Teleoperation* Constraint Conditions . 59
6.3 Nobile route 61
6.4 Nobile route close-up 62

7.1 Average sunlight and DTE communication at Nobile Crater rim . . . 64
7.2 10-meter LOLA DEM to 85°S 65
7.3 Nobile route demonstrating *Strategic Autonomy* constraints 68
7.4 Route Proximity to *Strategic Autonomy* Constraint Conditions 69
7.5 Supervised Teleoperation vs. Strategic Autonomy 70

8.1 Nobile Crater Rim slope 75
8.2 Solar disk visibility model 75
8.3 Solar flux and terrain slope at Nobile Crater Rim 77
8.4 Longest connected component vs. solar disk visibility 77
8.5 Relative frequency of connected component durations 78
8.6 RRT staring points, graph structure, and solution 79
8.7 RRT solution 80
8.8 RRT solution close-up 81

8.9 RRT top view 82
8.10 RRT side view 83

9.1 Malapert Massif percent illumination 86
9.2 Malapert Massif local principal terrain slope 87
9.3 Malapert Massif DTE communication conditions 87
9.4 Malapert Massif longest periods of uninterrupted sunlight 89
9.5 Malapert Massif safe landing targets 90
9.6 Malapert Massif viable landing areas and target sites 92
9.7 Seeded sun-synchronous route average illumination 93
9.8 Seeded sun-synchronous route uninterrupted sunlight 93
9.9 Seeded sun-synchronous route terrain slope 94
9.10 Seeded sun-synchronous route DTE communication 94

Chapter 1

Introduction

> "All civilizations become either spacefaring or extinct."
>
> - Carl Sagan

Sustained lunar polar roving is key for enabling human exploration and habitation of the Moon and elsewhere in the Solar System. Robotic lunar rovers will precede human outposts and settlements to scout locations, survey the environment, transport cargo, and prospect for resources. Abundant resources, particularly frozen water, and abundant sunlight make the lunar poles an attractive destination for both human and robotic activity. Many lunar polar rovers will rely on solar power due to its availability and affordability relative to radioisotope power systems.

Although abundant, polar sunlight is not constant, and lunar darkness brings with it temperatures cold enough to threaten even robust electromechanical systems. Solar-powered rovers are therefore constrained to strongly favor paths of persistent if not continuous sunlight for both warmth and power. Sustaining productive operation of individual rovers for multiple lunar days is important for achieving ambitious missions and programs, yet the harsh and dynamic nature of low-angle polar sunlight makes planning sustained paths nontrivial. This thesis addresses many of the challenges and complications that arise when planning for sun-synchronous lunar polar roving and presents routes that achieve up to 6 months of uninterrupted sunlight.

1.1 Motivation

The development of planning methods that enable sun-synchronous lunar polar roving is motivated by a variety of possible applications, including some not yet imagined. One of the most compelling applications in the near future is resource prospecting.

Prospecting for natural resources at the lunar poles is an important precursor to human habitation of the Moon and Mars. Observations made by orbiting satellites indicate that the lunar poles are rich with frozen volatiles. The most prominent of these is water ice, which can be extracted and processed to produce drinkable water, breathable oxygen, and liquid rocket propellent. These supplies are vital for expanding

and sustaining human presence in space yet prohibitively expensive to continually transport in substantial quantities from Earth due to their weight. Because of the Moon's weak gravity relative to Earth's and its lack of atmosphere, supplies derived from the Moon's in-situ resources can be placed in lunar orbit far more efficiently than equivalent supplies from Earth. Once the necessary infrastructure is in place, the Moon's resources could be utilized not only to support lunar bases and settlements but also to reduce the cost of deep space exploration by resupplying spacecraft that are in lunar orbit and bound for more distant destinations such as Mars. Before a lunar resupply depot can be established, the concentration and distribution of lunar polar ice must be thoroughly verified, quantified, and mapped. Robotic rovers are well-suited to precede human expeditions to the Moon's poles, where they can physically probe subsurface ice deposits and take local ground measurements not possible via orbiters.

Robotic lunar prospecting will succeed on a global[1] scale only if done in a manner that is sustainable both programmatically and at the level of individual rovers. The same is true more generally of lunar exploration. A sustainable lunar program requires *affordability*, *scalability*, and *longevity*. In the case of lunar prospecting, affordability and scalability can be addressed primarily by selecting a suitable fleet size and power architecture, the combination of which has crucial implications on the longevity required of each rover. Longevity is addressed in turn by rover designs, mission concepts, and planning methods that enable lunar polar roving to be sustained for long distances and durations. In large part, *sustainable* lunar exploration and resource prospecting is enabled by *sustained* lunar polar roving.[2]

Thorough exploration of the lunar poles will require tens of thousands of kilometers driven over decades of cumulative operating time. The sheer scope of such a campaign discourages nuclear-powered rovers as a viable near-term solution, since few can be produced with existing stockpiles. Solar-powered rovers are an affordable, scalable alternative; however, reliance on solar power at the lunar poles gives rise to significant challenges—and opportunities—for individual rovers to achieve the necessary longevity. On the Moon, solar-powered rovers are severely limited by thermal constraints and available power, but near the poles, rovers following routes that provide persistent sunlight and avoid long exposure to shadows can maintain favorable thermal and power states for extended distances and durations. Strategic, informed route planning that exploits lunar polar sunlight to achieve sustained lunar polar roving is therefore a key enabling technology for sustainable exploration.

1.1.1 Lunar Prospecting

The discovery of water on other planets is a vital clue in the search for extraterrestrial life, but it may also hold the key to human colonization of the Solar System. Practical, economical sources of air, water, and fuel are critically important for humans to live

[1] Usage of the word 'global' throughout this dissertation generally refers not to the entire globe of the Moon but rather the two polar regions. It is also used in the context of global path planning.

[2] A subtle distinction is made between 'sustainable' and 'sustained,' where the former refers to entire programs, and the latter refers to individual missions that comprise a given program.

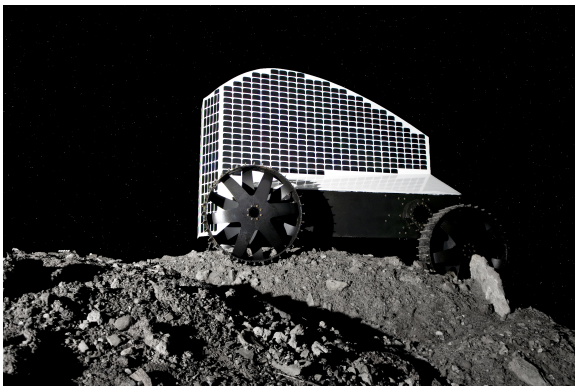

Figure 1.1: Prototype solar-powered lunar polar rovers. **Left**: "Polaris" (Image credit: Astrobotic Technology, Inc.) **Right**: "Resource Prospector" (Image credit: NASA)

and work in space. Planetary colonists will depend on in-situ water and oxygen, and deep space scenarios are enabled by oxygen–hydrogen propellents. All three are available from ice deposits that await at the lunar poles. Water is essential for human survival, and if decomposed into its constituent elements, it can be utilized as gaseous oxygen for human respiration and as liquid oxygen and liquid hydrogen for rocket propellent. Early explorers and subsequent settlers alike will benefit from abundant and accessible lunar resources, since the alternative of maintaining supply lines from Earth is energetically expensive and financially unsustainable.

In-situ resource utilization (ISRU) and in-situ propellent production (ISPP) have long been seen as an enabling technology for future space exploration [1]. This is because of the potential to substantially reduce long-term costs by minimizing the mass of supplies and materials that must be launched from Earth. In 2013, the market price of available launch vehicles was estimated to range between $3,200 and $18,700 per kilogram transported to low Earth orbit (LEO)[2]. Lifting payloads completely out of Earth's gravity well costs even more [3]. Since then, SpaceX has successfully launched dozens of Falcon 9 rockets at an advertised base price of approximately $2,700 per kilogram to LEO [4] and has repeatedly demonstrated booster recovery and reuse that promise to further reduce price. Falcon Heavy, launched for the first time in 2018, projects as low as $2,350 per kilogram to LEO, $5,600 per kilogram to geosynchronous transfer orbit (GTO), and $8,900 per kilogram to Mars [4, 5], figures that would lead the industry. While the continued development of reusable rocket technology and added competition from new launch providers such as Blue Origin will continue to drive down launch costs, it is unlikely that operating perpetual resupply missions solely from Earth to support exploration and habitation of deep space will ever be financially viable or sustainable.

ISRU concepts envision production of life support consumables, rocket propellent, construction materials, and solar cells all made from indigenous resources in environments that would otherwise be uninhabitable [1]. Near-Earth resources (primarily those on the Moon) could also be used to reach more distant destinations. Journeys to Mars or one of Jupiter's moons might begin by bringing just enough fuel, water, and oxygen to reach the Moon, where spacecraft would then dock with an orbiting

resupply station that provides the additional supplies needed to reach the ultimate destination. Leveraging in-situ resources will enable humans and robots to explore farther than otherwise possible and accomplish more science and discovery for less total expense.

Interest in ISRU has grown in recent decades as the abundance of water in the Solar System has become increasingly apparent. Orbiting satellites have collected overwhelming evidence for the existence of vast quantities of frozen water ice concentrated near the poles of the Moon [6, 7], Mercury [8], and Mars [9, 10, 11]. Lunar water is especially valuable due to its proximity to Earth and the Moon's advantageous gravity and atmosphere. NASA planned a solar-powered robotic surface mission to measure and characterize the constituents and distribution of water and other volatiles at the poles of the Moon as soon as the early 2020s [12, 13, 14]. While it is unclear if the Resource Prospector mission will proceed as originally envisioned, similar robotic missions will soon lead the way for widespread lunar prospecting campaigns and the subsequent in-situ utilization of resources present on the Moon and throughout the Solar System. Many of these missions will benefit from sun-synchronous operation.

1.1.2 Sustainable Exploration

Long-term sustainable exploration of the Moon and Solar System will depend on ISRU and maximizing the return on investment of future missions, prospecting or otherwise. For ISRU to truly become a game-changing capability, lunar prospecting must go beyond a single rover operating at a single site for a single daylight period (which last about two weeks). Completing a thorough survey of the poles will require many miles over many moons[3] (pardon the expression). Doing so in a reasonable time frame will require parallel exploration by a fleet of rovers. Doing so for a reasonable price will require a balance between the size of the fleet, individual rover cost, and the capability demanded of each rover in terms of lifespan and range. The interrelated considerations of affordability, scalability, and longevity drive the need for sustained solar-powered roving—and therefore, sun-synchronous roving—especially on the poles of the Moon.

Affordability The many technological challenges associated with spaceflight are often superseded by economic challenges. For a space exploration program to be funded, publicly or privately, it must be affordable and deemed more valuable than the total cost. In the case of lunar prospecting, total cost is the product of two key factors: number of rovers and cost per rover. The cost per rover is in part a function of the number of rovers produced, due to economies of scale. This encourages an inexpensive, scalable design. Solar power systems are substantially cheaper to implement on rovers than radioisotope power systems (RPSs). The estimated total cost of development, production, and deployment of the multi-mission radioisotope thermoelectric generator (MMRTG) used to power Mars Science Laboratory (MSL)

[3] A 'moon' in this sense literally means one month, one lunar day, one diurnal cycle, or one synodic period, all of which are equivalent to approximately 29.5 Earth days.

"Curiosity" exceeds $192 million in 2015 dollars, not including costs from NASA staff or facilities nor other indirect costs [15]. While a fleet approach requires additional flight hardware production and added launch and landing operations, the sum of development and production costs per unit decreases with increased fleet size. The total program cost can be further mitigated by increasing the share of the program objectives accomplished by each individual rover, thereby moderating the size of the fleet.

Scalability Prospecting both lunar poles requires a minimum of two rovers, but timely, broad, dense coverage requires a fleet. Sampling the total surface area above 85°N and below 85°S at a resolution of 4 km × 4 km would require approximately 36,000 km of driving. Alternatively, an equivalent distance could instead be spent focusing a subset of that area (for example, regions with the highest expected water content) to achieve denser coverage. If divided evenly between two rovers with an average operating speed of 5 cm/s, that would take approximately 12 years of continuous operation (23 rover-years). Ignoring the likelihood of a mechanical failure, such a pace is likely unsustainable for that long regardless of power source; but even if it were achievable, broad coverage would take over a decade. A fleet of a dozen rovers of the same speed could complete the same campaign in two years. Deploying additional rovers not only reduces the time to completion but also spreads out early data coverage and provides redundancy in the event of unexpected failures.

RPSs are not feasible for fleets larger than a few rovers in the near term due to a lack of available Plutonium-238, the fuel used to power radioisotope thermoelectric generators (RTGs) and radioisotope heater units (RHUs). Pu-238 is a scarce, tightly-controlled national resource. Existing U.S. stockpiles available to NASA are enough for just three MMRTGs like the one used to power MSL [16]. This is just sufficient for planned missions through the mid-2020s [17]. The United States recently began production of new Pu-238 for the first time since 1988; however, full-scale production is not expected before 2023 at the earliest [16]. Even at the targeted production level of 1.5 kg per year, producing enough new Pu-238 for a single MMRTG will take approximately three years. Additionally, any new and existing supplies of Plutonium are generally prioritized for missions to remote deep space destinations where solar power is not viable, leaving less for lunar missions.

Due to current scarcity and long-term production challenges of Plutonium, deploying a fleet of nuclear-powered rovers to the Moon will likely remain infeasible for decades. Unlike RPSs, efficient space-grade solar arrays are relatively inexpensive and readily producible. Besides being more economically feasible, solar power is the only scalable means of lunar prospecting for the foreseeable future.

Longevity Despite the advantages of solar power, the need for program affordability applies downward pressure on fleet size. A moderate number of rovers demands that each unit must cover long distances and operate for long durations, thereby reducing the total number of rovers needed to survey the polar regions. To be successful and cost-effective, individual rovers must cover hundreds or thousands of kilometers.

Covering long distances at a reasonable pace demands that each rover must operate for many months. On the Moon, this equates to many day–night cycles. This requirement gives rise to non-trivial challenges to lunar polar route planning due to the unique constraints of solar-powered rovers with respect to dynamic sunlight and thermal conditions. Addressing these route planning challenges and thereby enabling sustained sun-synchronous lunar polar roving is the primary contribution of this thesis.

Immediate and Broad Relevance

The relevance of this thesis research is not limited to exhaustive lunar prospecting campaigns executed by large, distributed rover fleets. Although the desire for timely, broad coverage motivates a scalable approach, affordability and longevity are equally relevant to solo robotic exploration. This thesis seeks to sustain lunar polar roving by any surface vehicle that happens to be solar-powered. A prime example is NASA's planned Resource Prospector mission, which was intended to send a single solar-powered rover to a lunar pole to characterize the makeup and distribution of polar resources and demonstrate ISRU technologies [12]. Applying sun-synchronous planning concepts to missions like Resource Prospector has the potential extend operations by an order of magnitude—from a single daylight period lasting a couple weeks to many daylight periods spanning several months—by taking advantage of unique polar lighting conditions.

The importance of this capability was recently reinforced when NASA deemed that a one-day Resource Prospector mission was "too limited in scope for the agency's expanded lunar exploration focus" and called instead for "many missions to locate, extract and process elements across bigger areas of the lunar surface" [18]. Sun-synchronous mission concepts that cover larger areas over the course of multiple lunar days are an attractive alternative to single-site, single-day missions. The benefits of sun-synchronous lunar polar roving not only aligns with NASA's vision for lunar exploration but also extends to a wide variety of other mission concepts including sustainable solar power grids, permanent manned lunar outposts, and commercial mining operations.

1.1.3 Sun-Synchronous Route Planning

Sun-synchronous lunar roving and resource prospecting, be it by one or many robots, is enabled by high-fidelity lunar models and thoughtful route planning. Robotic missions to prospect lunar resources will face many challenges. As rovers explore the poles of the Moon in search of ice, they will encounter transient illumination, volatile thermal conditions, rugged terrain, and intermittent communication, all of which pose substantial risk. Rovers must successfully navigate these hazards while accomplishing their scientific objectives. Doing so requires extensive planning to account for the time-varying lighting, temperature, and communication conditions. This is especially true for solar-powered rovers, which must take advantage of natural sunlight both to generate power and to remain within acceptable temperature ranges.

Venturing into darkness, particularly permanently shadowed regions (PSRs), will be necessary to complete key science and survey objectives, but these short forays need to be planned strategically as part of a complete rover traverse plan to reduce risk to the rover.

Generating detailed traverse plans prior to launch is critical due to the complex nature of polar surface lighting and the limited capability of planetary rovers to sense, plan, and react effectively in real time. Limitations include not only hardware and software capabilities (e.g., sensor range, computational resources, and drive speed), which are generally less than that of terrestrial rovers, but also a myopic perspective inherent to surface exploration. Even rovers equipped to perceive their local surroundings are generally unable to effectively perceive the global environment due to their low point of view. In the case of solar-powered polar exploration, the relevant environment is not only too large and rough to be perceived at once but also dynamic, since surface lighting changes with time. This makes reliance on in-situ perception infeasible, since future surface lighting cannot be observed. Without detailed knowledge of how sunlight and shadows evolve in both space and time on a global scale, rover traverse planners are ill-equipped to generate safe and robust plans that prevent mission-ending missteps. Generating reliable plans requires complete, detailed, accurate data describing the surface geometry of the Moon so that surface lighting can be confidently predicted prior to pre-mission planning.

Until recently, no such data existed [19]. The Lunar Reconnaissance Orbiter (LRO) satellite, launched in 2009, has provided global altimeter data used to produce high-resolution digital elevation models (DEMs) covering the entire surface of the Moon [20, 21]. The highest-resolution DEM available for a given location varies with latitude. DEMs covering the poles range between about 100 meters per pixel extending out to 45°N/45°S and 5 meters per pixel poleward of 87.5°N/87.5°S [22]. The resolution of these models is orders of magnitude higher than the best available data prior to LRO [19].

Elevation models can be used in conjunction with solar and lunar ephemerides to predict future surface lighting conditions at any location. Generating predictive lighting maps covering an area of interest over a time sequence produces a discretized, three-dimensional, spatiotemporal predictive model of surface lighting. These 3D models of future sunlight conditions can then be used to inform route planning algorithms designed to maintain adequate solar power or constant sunlight. A similar process can be used to predict all states for which rovers will be in direct view of the Earth—or more specifically, the Deep Space Network ground stations—for direct-to-Earth (DTE) communication. This method produces a predictive model of when and where communication systems are able to send and receive commands, telemetry, and scientific data.

Not only does LRO data enable mission designers to plan safer, more reliable rover traverses, it also provides the opportunity to plan prolonged routes that extend solar-powered lunar polar exploration by an order of magnitude relative to traditional mission plans. For example, baseline Resource Prospector mission designs assumed rover operations not exceeding 14 Earth days [23] and did not intend to survive the lunar night [13]. This duration is approximately half of a full lunar day. In general,

lunar sites receive 15 Earth days of continuous sunlight followed by 15 Earth days of total darkness. Although many polar sites receive additional seasonal sunlight, conservative missions may not take full advantage of it due to landing time and limited range. A mission that lands 2 or 3 Earth days after local sunrise at a non-polar latitude is left with about 10 days of guaranteed solar-power before local sunset, at which time thermal conditions begin to drop below rover-survivable limits. Without sun-synchronous planning, short-range polar rovers might recoup those 2–3 days but not much more.

Because rovers are not constrained to a fixed location, they can follow routes that move in sync with the sunlight, prolonging their access to solar power and moderate temperatures for several months. Furthermore, the radius and angular velocity of the Moon are such that many routes of multi-month solar power can be executed at modest speeds, even by planetary roving standards. The challenge is solving for routes that enable extended operation, satisfy science objectives, and have a low risk of catastrophic failure.

Despite the availability of LRO data, identifying and planning multi-month routes is challenging. Challenges arise from the size and complexity of the relevant path planning problem. To maximize reliability, rover traverses must be planned on maps with the finest spatial resolution possible, ideally at a resolution similar to the scale of the rover's wheels (sub-meter). The current best available lunar polar models are limited to about 5–10 meters per pixel, but this resolution is still high for global maps. In addition to being high resolution, maps must cover large areas, up to thousands of square kilometers, to include all potential regions of interest that an extended route might explore.

This combination of resolution and scale yields a spatially expansive state space much too large for effective manual search. The goal of sun-synchronous planning is to extend lunar polar roving to achieve many months of operation, but achieving this goal requires an increase to the size of the spatiotemporal models used for planning of up to an order of magnitude in the time dimension. Long time durations and temporal granularity multiplies the depth of the search space and magnifies the complexity of the problem exponentially. In the case of sun-synchronous planning, this often makes the search space too large for optimally efficient deterministic algorithms to find solutions in a tractable runtime. The greater the extent and resolution of predictive models, both spatially and temporally, the more likely it is that the path planning problem becomes intractable for deterministic, grid-based planning methods.

1.2 Approach

This thesis presumes that affordability and scalability of robotic lunar polar exploration programs—resource prospecting or otherwise—can be addressed by opting for solar-powered rovers in favor of nuclear power and does not deal explicitly with these considerations beyond this introduction. Further, it asserts that the resulting challenges to individual rover longevity can be sufficiently addressed through novel application of informed route planning techniques and predictive models. The work

detailed herein focuses on sun-synchronous planning methods that enable sustained, long-distance, long-duration exploration by solar-powered rovers at the poles of the Moon.

This research implements planning algorithms and utilizes high-fidelity predictive models to generate route solutions that demonstrate sun-synchronous lunar polar roving. Initial results make simplifications to reduce the size and complexity of the planning problem. Subsequent results demonstrate methodology capable of efficiently solving increasingly relevant versions of the planning problem. This research builds on concepts of prior related work in the areas of sun-synchronous circumnavigation and mission-directed path planning. These notions combine the ideas of resource-constrained temporal planning with predictive models of how sunlight and shadows evolve over time on planetary surfaces. This thesis research generates large-scale, long-duration, shortest-distance routes that satisfy resource constraints on uninterrupted sunlight, direct-to-Earth communication, rover speed, and terrain slope. This work improves the resolution at which these routes are generated, taking advantage of the latest high-resolution topographic maps of the Moon.

The methods presented treat both sunlight and communication as binary conditions and enforce a hard constraint on lighting. For a majority of the examples provided, sunlight is modeled as a directional source, in which all rays are parallel to a vector passing through the center of the Sun. This results in hard shadow boundaries corresponding roughly to where half of the solar disk is visible (or where 50% of the maximum solar flux is available). This differs from actual insolation conditions, but only slightly, since most lunar shadows have hard boundaries. The largest discrepancies occur where shadows are cast by distant geometry, which creates a penumbra or gradient from light to dark over tens or sometimes hundreds of meters. Results presented in later chapters utilize models that approximate the Sun as a uniform area source and maps representing the percentage of the solar disk that is visible from the surface. This improves model accuracy and enables better control of planned solar flux levels.

In this thesis research, as long as the rover stays in direct sunlight, it is assumed to stay warm and generate sufficient electrical power to operate all of its necessary subsystems, including mobility. Although these assumptions oversimplify the complexity of actual rovers, they produce reasonable solutions that are conservative with regard to battery power, since all planetary rovers incorporate batteries, but stored energy is not relied upon in this research. An articulated solar array delivers approximately 400 W/m^2 of electric power continuously regardless of driving direction given the hard constraint on sunlight. Thermal systems can be designed to tolerate lunar daylight conditions as demonstrated by prior lunar exploration. Although battery-stored energy is not explicitly modeled, the inclusion of batteries will only expand rover capabilities beyond the routes presented. In this way, the routes presented are conservative.

Sun-synchronous lunar polar routes in this research are generated using both a deterministic grid-based graph search approach and a randomized sampling-based path planning approach—specifically A* and RRT, respectively. The former produces optimal shortest-distance paths (given the suboptimality of the grid and intermediate

waypoints), and the latter produces non-optimal random walk paths. Constraints are enforced at plan time, using binary arrays representing spatiotemporal lighting, communication, and slope conditions. The solutions presented serve to demonstrate a valuable proof of concept—that moderately paced rovers can achieve multiple lunar days of solar-powered exploration by traversing sun-synchronous lunar polar routes.

This thesis also applies elements of connected component analysis to aid waypoint selection and computation time and presents a method of identifying landing sites useful for verifying and seeding sun-synchronous routes.

1.3 Thesis Statement

This thesis asserts that 1) sun-synchronous spatiotemporal routes exist near the geographic poles of the Moon that enable solar-powered rovers to operate for multiple lunar days; 2) these routes satisfy constraints on uninterrupted sunlight, direct-to-Earth communication, terrain slope, and rover speed; and 3) these routes can be planned using high-fidelity predictive models based on lunar topography data.

Definitions

- **sun-synchronous**: maintaining uninterrupted sunlight for all states
- **spatiotemporal route**: ordered sequence of states defined in both physical space and time
- **lunar day**: one full rotation of the Moon with respect to the Sun; equivalent to one month, one diurnal cycle, one synodic period, or approximately 29.5 Earth days
- **uninterrupted sunlight**: continuous direct illumination by at least half of the solar disk
- **direct-to-Earth communication**: direct line-of-sight view of Earth and/or the specific locations of Earth-based communication assets
- **terrain slope**: shall not exceed 15–20 degrees principal slope at the resolution of lunar topography data
- **rover speed**: shall not exceed 2–10 cm/s depending on communication availability
- **high-fidelity**: at the full resolution of the best available lunar topography data
- **lunar topography data**: digital elevation models derived from Lunar Orbiter Laser Altimeter data

1.4 Contributions

This thesis research contributes to future lunar polar missions in two major capacities: 1) the ability to plan detailed sun-synchronous rover traverses, defined by spatiotemporal routes and science activities, prior to launch that sustain solar-powered lunar polar roving for multiple diurnal cycles and 2) the ability to inform on-ground decisions during mission operations through better understanding of the global mission-level repercussions. This thesis focuses on the former but contributes to the latter as well. The primary contribution is a pair of ground-based route planning methods that handles dynamic resources and constraints characteristic of polar exploration and generates large-scale, long-duration, global routes that enhance and extend robotic missions. During mission design, this technology aids the selection of landing sites, rover routes, and science activities. During mission operations, it can provide anytime contingencies in response to new discoveries. The following contributions will improve the mission longevity, range, efficiency, safety, and scientific return of robotic rovers exploring the poles of the Moon.

1. A grid-based method to plan sun-synchronous routes that sustain solar-powered polar roving on the Moon to durations lasting multiple diurnal cycles while satisfying constraints on
   (a) direct exposure to sunlight
   (b) direct-to-Earth communication
   (c) maximum terrain slope
   (d) maximum rover speed
2. Identification and analysis of feasible sun-synchronous routes lasting multiple diurnal cycles on the Moon with direct relevance to resource prospecting missions.
3. A strategy to selectively employ limited rover autonomy to reduce risk of sun-synchronous lunar polar exploration.
4. A sampling-based method to efficiently plan sun-synchronous lunar polar routes lasting up to 6 months while satisfying constraints on sunlight, terrain slope, and rover speed.
5. A method of selecting landing sites amenable to lunar prospecting missions and used both to validate and seed sun-synchronous routes.

1.5 Overview

The remainder of this dissertation is organized roughly in order of the listed contributions. Chapter 2 provides background information pertaining to the lunar polar environment, past lunar roving, and possible relevance to planetary bodies other than

the Moon. Chapter 3 describes prior work by others in published literature related to polar mission planning and path planning. Chapter 4 describes the process used to generate high-fidelity predictive models of lunar sunlight and communication availability using existing data products from lunar orbiting satellites.

Chapter 5 describes a deterministic, grid-based method to plan paths that maintain continuous uninterrupted sunlight, which is essential to sun-synchronous lunar polar roving. Chapter 6 adds methodology to satisfy constraints on drive-time direct-to-Earth communication. Chapter 7 introduces the concept of strategic autonomy, in which limited rover autonomy is selectively deployed to safely overcome some of the limitations of strict DTE communication requirements. This and other methods are proposed as possible solutions to dealing with uncertainty in predictive models and reduce risk associated with lunar polar roving. Chapter 8 presents a sampling-based method to plan sun-synchronous routes that achieve up to 6 months of uninterrupted sunlight. Chapter 9 describes a method to identify landing sites amenable to lunar prospecting and polar roving useful for both validating and seeding sun-synchronous routes.

Chapter 10 suggests future topics and approaches related to sun-synchronous lunar polar planning, including considerations for solar-powered batteries, thermal conditions, science objectives, year-long routes, perpetual exploration, and sustainable power grids. Chapter 11 summarizes the thesis, its conclusions, and its contributions.

Note on Publications

Portions of this thesis research have been published previously in [24] and [25].

Chapter 2

Background

Solar-powered planetary rovers will encounter transient sunlight yet must generate adequate power to drive, sense, reason, and perform science activities, often while navigating hazardous terrain. Planetary surface lighting, temperature, and available communication with Earth all vary temporally due to the combination of orbits, rotations, and axial tilts, which leads to the ever-changing insolation conditions on the surface of planetary bodies. On the Moon, sunlight varies periodically on a month-long diurnal cycle and evolves more subtly on an annual cycle. Seasonal effects are much less pronounced than those of Earth due to the Moon's axial tilt of just 1.5 degrees relative to the ecliptic, but these slight variations are amplified at the pole, where lower Sun angles generate longer shadows. Diurnal fluctuations in solar illumination induce equally dramatic swings in surface temperature, particularly on airless bodies such as the Moon and Mercury, which have no appreciable atmosphere. At night, lunar surface temperatures plunge below 100 K (-173 °C) [26, 27], and daytime temperatures reach 390 K (117 °C) at the equator [26, 28].

These extreme temperatures pose a significant challenge to rovers exploring the surface. Solar-powered rovers that linger in a single locale will experience intermittent lighting, power, and long nighttime periods of extreme cold—more than 14 Earth days on the Moon and 88 Earth days on Mercury. Passive thermal management is incapable of tolerating both hot and cold extremes observed in these environments, and battery capacities are insufficient to actively heat rover electronics for the entire night. This makes solar-powered rovers particularly vulnerable to the cold night temperatures, typically limiting them to a single daylight period of exploration. Prior lunar rovers have mitigated the extreme cold by using the heat generated by radioisotopes, but this comes at great cost in terms of money, time, and mass.

Planetary rovers have a unique opportunity to take advantage of close proximity to the pole, provided that the planetary body is sufficiently small in diameter and slow in angular velocity with respect to the Sun. Under these conditions, solar-powered rovers can move in sync with the Sun and stay continuously insolated for multiple diurnal cycles. The Moon and Mercury are prime candidates for this kind of sustained solar-powered polar exploration. Using this strategy, solar-powered rovers can operate for 3–6 months on the Moon and perhaps indefinitely on Mercury. Although this thesis deals specifically with the Moon, this strategy is a viable anywhere that the Sun's

ground speed is less than than the rover's average drive speed and where atmospheric conditions (e.g., lack of atmosphere) permit reliable prediction of sunlight. With detailed topographic maps of the terrain, the global surface lighting conditions can be reliably predicted, and path planning algorithms can leverage these models to generate detailed routes that satisfy the constraints on critical resources, avoid hazards, and meet mission objectives. This capability can have an immediate and lasting impact on robotic and human exploration. The following sections provide additional background on the lunar polar environment, prior lunar rovers, and other destinations where sustained roving might be possible.

2.1 The Lunar Polar Environment

As rovers explore the poles of the Moon in search of ice, they will encounter transient illumination, intermittent communication, and steep terrain, all of which pose risk. At polar latitudes, sunlight grazes the surface as the Sun circles low in the sky, skimming just above the horizon. The motion of the Moon with respect to the Sun causes the surface lighting to evolve dramatically over the 29.5-day diurnal cycle in addition to the more subtle seasonal effects of the annual cycle [29]. In this low-angle light, polar terrain casts long shadows that stretch tens of kilometers and sweep widely across the surface. Without direct sunlight, a solar-powered rover will quickly deplete the energy stored in its batteries and cease to function. Rovers exposed to the cryogenic temperatures of lunar night [30] are unlikely to be operational by the time sunlight returns.

Despite the tidal locking that keeps the same hemisphere of the Moon always facing Earth, direct line-of-sight to Earth, or "Earth view," at the lunar poles is not static. Due to the inclination of the Moon's orbit from the ecliptic, rovers near the pole will observe the Earth rising and setting across the near-side horizon each lunar day. As the Earth sets, all direct communication is cut off. A rover without communication for teleoperation must be either be autonomous or stationary and is at risk of becoming stranded in shadow. In addition to the dynamic insolation and communication conditions introduced here, the lunar poles feature transient thermal environments and terrain that is hazardous but static. All of these factors must be considered and planned for to reach polar deposits of frozen water.

2.1.1 Water

The abundance of water on the Moon is well-documented, and the next steps of exploration are surface missions to visit and characterize local concentrations. Lunar water is a key resource because it can be converted into breathable air, drinkable water, and combustible propellent, all three of which are vital to sustaining exploration beyond Earth. Orbiting satellites have collected overwhelming evidence of vast quantities of frozen water ice concentrated at the lunar poles [6, 7], and NASA is planning a solar-powered robotic surface mission to verify and quantify this water and other frozen volatiles [12]. The estimated subsurface depth of frozen water permafrost [30]

at a candidate landing site near the lunar south pole is shown in Fig. 2.1. In addition to accessible water, Nobile exhibits a combination of topography and latitude ideal for demonstrating the advantages of sustained lunar polar roving.

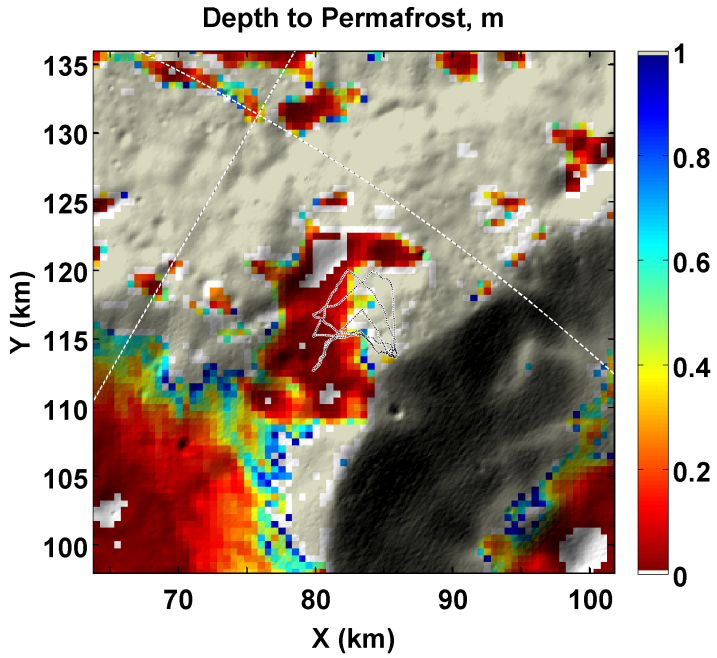

Figure 2.1: Estimated depth of permafrost below the lunar surface for a roughly 40-by-40-km area of the Nobile Crater rim near 86°S [30]. Gray terrain indicates an estimated permafrost depth of greater than 1 meter. A 74-day sun-synchronous route, which crosses the steep gradient between deep and shallow permafrost several times, is located near the center of the area shown. Image credit: Richard Elphic

2.1.2 Sunlight

Because the synodic period of the Moon averages approximately 708 hours and the Moon is tidally locked with Earth, a single lunar day is equivalent to about 29.5 Earth days [29]. At non-polar latitudes, this yields alternating day and night periods of sunlight and darkness averaging 14.75 Earth days each. Limited to 2 weeks of solar power, rovers traveling at modest drive speeds [1] without a sustainable internal heat source (e.g., nuclear isotopes) are doomed by the unavoidable cryogenic temperatures characteristic of lunar night [31, 30, 32].

Near the poles, however, seasonal effects and local topography dominate, resulting in more dynamic and complex lighting conditions. The Moon's 1.5-degree axial tilt relative to the ecliptic induces seasons that are subtle relative to Earth's yet pronounced enough to leave the poles almost completely dark during winter and predominately lit during the summer. The Sun circles the summer pole once per lunar day and

[1] Drive speeds on the order of 10 cm/s will are considered modest relative to the minimum speed required to circumnavigate the equator, which is $\sim$ 4.3 m/s.

never deviates far above (or below) the horizon; thus, sunlight grazes the lunar polar surface. The low-angle light renders shadows that stretch many kilometers and sweep across the rough terrain, locally blocking out sunlight for days at a time. Although there exists no "peak of eternal light" lit 100% continuously [33], modest-paced rovers can maintain uninterrupted solar power for 3–6 months by navigating strategically planned sun-synchronous routes. This enables mission durations an order of magnitude greater than what is possible at lower latitudes or without sun-synchronous planning.

A 4-month composite of polar illumination based on spatiotemporal predictive models is shown in Fig. 2.2a. This is the same area as that shown in Fig. 2.1. The permanently shadowed regions (PSRs) generally correspond to high concentrations of ice, while the small points of maximum illumination indicate important sites of persistent sunlight.

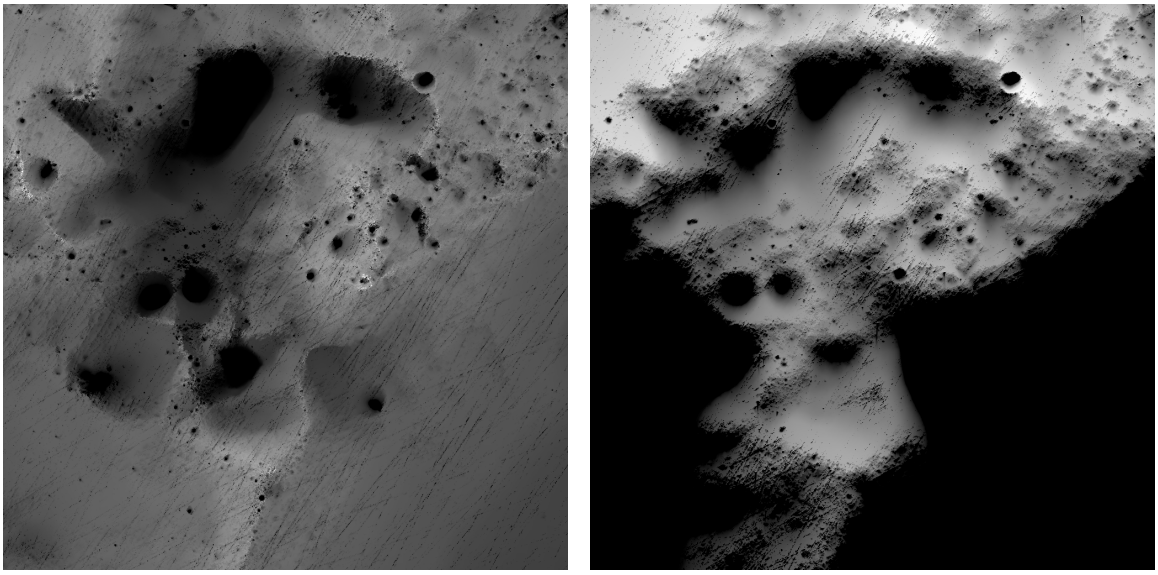

(a) Average Illumination **(b)** Average Communication

Figure 2.2: These images represent the average illumination (**a**) and communication (**b**) coverage over a 4-month period of a 20-by-20-km area on the rim of Nobile Crater near the lunar south pole. Brighter values indicate greater cumulative exposure (to the Sun or Earth, respectively) as a percentage of total time: *white* indicates 100%, while PSRs appear as *black*. Earth is upward.

In addition to solar power, sunlight provides passive illumination for rover perception. The harsh contrast characteristic of lunar light, especially at the poles, challenges navigation with visual cameras, but in shadow, visual perception without active illumination is virtually impossible. This further motivates rovers to favor routes of persistent sunlight, regardless of the rover's power system. Navigating in PSRs will require some form of active illumination.

2.1.3 Earth View

After power, the most critical resource for lunar rovers is communication with Earth. Without frequent communication, rovers cannot adequately receive commands nor transmit telemetry and scientific data. A satellite relay system can provide (near) constant communication with polar rovers, but such infrastructure is costly to deploy. Many polar rovers will rely on direct-to-Earth (DTE) communication. Due to tidal locking, only one hemisphere of the Moon ever faces Earth; however, at the poles, the Moon's axial tilt causes the Earth to rise and set periodically as viewed from the surface. This induces intermittent communication coverage with periodic blackouts, most commonly at local depressions and on slopes facing away from Earth. These conditions are not conducive to highly supervised autonomy or teleoperation; however, planning for communication blackouts can mitigate the associated risks. A 4-month composite of Earth-view representing DTE communication availability is shown in Fig. 2.2b.

2.1.4 Terrain

Another important aspect of the lunar polar environment is local topography, which not only influences the sunlight and communication available to rovers but also defines the terrain that must be negotiated. While rover-scale (sub-meter) terrain features cannot yet be resolved from orbit, topographic maps can be used to model gross ground slope. Because much of the polar terrain is too steep for typical wheeled rovers to traverse reliably, path planners often treat ground slope as a static constraint defining obstacles or hazardous areas that must be avoided. The rugged nature of lunar terrain is most pronounced at the poles and presents substantial limitations in many regions of interest.

2.1.5 Thermal

The Moon's thermal environment is ultimately what drives the need for sun-synchronous operation of rovers without a radioisotope heat source. Day–night temperature swings are accentuated due to the lack of an atmosphere to regulate heat transfer. Radiation dominates minimal conduction and nonexistent convection. The peak surface temperature experienced on the Moon is primarily a function of latitude, with temperatures reaching as high as 390 K (117 °C) at the equator [26, 28]. Minimum surface temperature, however, is a much weaker function of latitude, since all locations experience long periods of total darkness. Overnight, surface heat is radiated to the near-perfect black body of space (3 K), and temperatures drop below 100 K (-173 °C) regardless of latitude [26, 27]. This means in general that no matter where a robot is on the Moon, it will have to survive cryogenic thermal conditions to continue operating beyond a single lunar day. Historically, this has only been achieved with heat sourced from a combination of RTGs and RHUs. The only viable survival strategy for rovers powered solely by solar radiation is to avoid these extreme cold temperatures. Fortunately, polar rovers have that opportunity. Solar-powered rovers achieve two major objecti-

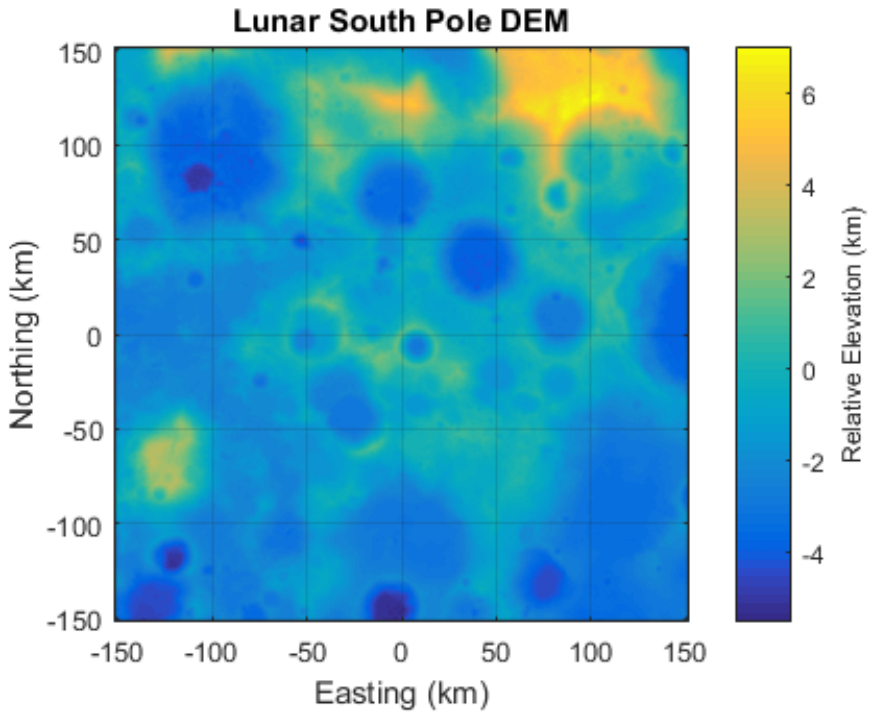

Figure 2.3: This 10-meter LOLA DEM covers the lunar south pole out to 85°S [34]. The Nobile Crater rim is among the peak elevations.

ves by staying in the sunlight: they stay warm, and they maintain electric power. Both enable sustained lunar polar roving.

[figure of surface temperature]

2.2 Prior Lunar Roving

To date, total of six wheeled rovers have operated on the Moon as part of three separate exploration programs: Lunokhod, Apollo, and Chang'e. All prior lunar rovers operated at mid-latitudes. The Lunokhod and Chang'e programs deployed robotic designs that were intended to to survive the lunar night using heat from radioisotopes. While the two Lunokhod rovers successfully demonstrated multi-day operation, both ultimately failed for thermal reasons, as did the Chang'e "Yutu" rover. The Apollo rovers were human-driven and designed to operate for a single daylight period using battery power. These prior missions illustrate some of the challenges and demonstrated capabilities of lunar roving.

2.2.1 Lunokhod

Two Soviet lunar rovers, Lunokhod-1 and Lunokhod-2, demonstrated multiple lunar days of operation in 1970 and 1973, respectively. They were powered by solar batteries and heated by an active thermal management system using an isotopic source [35]. A

clam-shell design enabled the rovers to generate solar power and radiate excess heat with the lid open during the day and insulate against the cold with the lid closed during the night. Lunokhod-1 traversed a total of 9.9 km over the span of 11 lunar days [36], and Lunokhod-2 traversed 39.2 km over 5 lunar days [37]. Ultimately, both rovers failed due thermal issues—Lunokhod-1 due to cold when its isotope stopped generating sufficient heat, Lunokhod-2 due to overheating when its radiator became insulated by lunar regolith [38].

2.2.2 Apollo Lunar Roving Vehicle

The Lunar Roving Vehicle (LRV) was used to transport astronauts and cargo during each of the Apollo 15, 16, and 17 missions flown by the U.S. in 1971 and 1972. Each LRV was driven manually by an astronaut and powered by two primary (non-rechargeable) batteries designed to last up to 78 hours [39]. The LRV was designed for a maximum range of 65 kilometers but was operationally limited to a 9.5-kilometer radius from the Lunar Module. The designed top speed was 13–14 km/hr, but Eugene Cernan reported attaining an actual top speed of 18 km/hr during Apollo 17 [40]. For context, this speed is sufficiently fast that, if sustained continuously, the LRV could have circumnavigated the Moon's equator in a single lunar day.[2]

2.2.3 Chang'e Yutu

The Chinese Chang'e-3 mission [41], launched in late 2013, featured a 140-kg rover called "Yutu" (meaning "Jade Rabbit") that was designed to operate for three months using plutonium heaters [42]. To survive the lunar night, Yutu was commanded to fold its mast and one of its two solar panels to insulate its interior during hibernation, which was kept warm by the RHU [43]. However, a "mechanical control abnormality" caused a drive unit malfunction that prevented proper dormancy preparations as sunset approached on the second lunar day [44]. Yutu awoke on its third lunar day but was immobile and continued to lose functionality with each lunar night [45]. Although Yutu operated in a limited capacity for a total of 31 months [46], it traveled a total of just 114 meters [47].

2.3 Relevance to other Planetary Bodies

Solar-powered roving for multiple diurnal cycles is possible on planetary bodies other than the Moon; however, in most cases the motivation is far less compelling. The exception is Mercury, where sun-synchronous roving is perhaps just as relevant as it is on the Moon. Key considerations include atmosphere, weather, solar intensity, thermal environment, planet diameter and angular velocity, terrain, and topographic data.

[2] lunar circumference / lunar day $\approx$ 10,921 km / 708 hr = 15.4 km/hr = 4.3 m/s

2.3.1 Mercury

Mercury shares many characteristics with the Moon that make both prime candidates for sustained polar roving and resource prospecting. Like the Moon, Mercury has no appreciable atmosphere or weather that might diffuse or obscure sunlight. Being much closer the the Sun, Mercury receives more intense solar radiation, which is ideal for electric power generation. Thermally, Mercury is hot during the day and cold at night with a longitudinal temperate band that moves with the day-night terminator. Because Mercury is smaller than the Moon and has a much longer rotational period, very little speed is required to circumnavigate the planet once per diurnal cycle. Mercurian terrain is navigable, and global topographic maps of Mercury have been compiled using orbital data from the 2004-launched MESSENGER spacecraft [48].

Even slow-moving rovers could conceivably keep pace with Mercury's temperate thermal band and achieve continuous solar-powered operation for years. While Mercury presents a scenario for sustained sun-synchronous roving that is perhaps even more favorable than do the lunar poles, quasi-static local lighting conditions and the minimal speed required make equatorial route solutions almost trivial. The planning methods applied to the Moon in this dissertation are highly relevant to robotic exploration of Mercury, but no Mercurian routes were studies as part of this thesis research.

2.3.2 Venus

Venus is blanketed by a dense atmosphere comprised primarily carbon dioxide, which contributes to a runaway greenhouse effect. This results in extreme surface conditions with temperatures exceeding 460 °C and a pressure of 92 Earth atmospheres []. Thick clouds obscure sunlight, only a small fraction of which reaches the surface. The atmosphere also contains sulfur dioxide, which combines with water to form sulfuric acid. The extreme temperature, pressure, and corrosiveness of the environment make Venus make an inhospitable destination for robots, which are challenged to operate for mere hours, much less months or years.

2.3.3 Earth

Sustained solar-powered polar roving is possible on Earth but unnecessary for rover survival due to its mild temperatures. A sun-synchronous rover can, however, increase its productivity by optimizing its global path to maximize solar battery levels. This was demonstrated on Devon Island above the Arctic Circle in 2001 by the "Hyperion" rover [49]. Because of the Earth's large axial tilt of 23.5°, this can be done relatively easily on a local scale a substantial distance from the geographic pole. Unpredictable cloud cover limits the accuracy of predictive models of sunlight and shadow on Earth. In addition, the radius and angular velocity of the Earth is such that circumnavigating the pole in continuous sunlight is infeasible for rovers of modest speed anywhere but the very highest latitudes. These factors limit the usefulness of applying this thesis' planning methods to terrestrial rovers.

2.3.4 Mars

While Mars might seem like a reasonable candidate for deploying sustained polar roving, it shares many characteristics with Earth that limit its efficacy and necessity. Mars has a similar combination of atmosphere, size, and rotational period as Earth. Sun-synchronous roving is unnecessary for rover survival on Mars as demonstrated by NASA's Mars Exploration Rovers (MERs) "Spirit" and "Opportunity." One Martian sol is nearly identical in length to an Earth day, so even with a diameter between that of Earth and the Moon, polar circumnavigation requires either great speed or very high latitudes. While feasible in some scenarios, sun-synchronous polar roving is not generally compelling.

2.3.5 Others

Beyond the four rocky planets are the gas giants, Jupiter and Saturn, and the ice giants, Uranus and Neptune, which are unsuitable for surface exploration. Many moons of these large planets are compelling targets for robotic investigation; however, their great distance from the Sun makes solar power far less practical—or even nonviable—compared to radioisotope power systems. Nearer to the Sun are many asteroids, but even the largest of these have short rotational periods and only microgravity, conditions which are not conducive to surface roving.

The key distinctions that motivate sun-synchronous polar roving are highly-predictable lighting conditions, dramatic day–night thermal swings, and particular combinations of planet size, rotational speed, and axial tilt. In the Solar System, only the Moon and Mars meet all of these criteria. The planning methods described in this dissertation are not generally relevant beyond those two bodies.

Chapter 3

Related Work

3.1 Polar Mission Planning

3.1.1 Modeling Lunar Polar Illumination

The recent availability of lunar orbital data and global topographic maps has lead to several notable studies on lunar polar illumination. Studies simulate lunar surface lighting conditions based on solar ephemeris and digital elevation models (DEMs) derived from altimeter data. This is done using one of two general methods: the ray-tracing method or the horizon method. The ray-tracing method renders illumination by projecting simulated rays of light from the position of the modeled light source (the Sun) onto a DEM-based surface model (the Moon) and computing the response from the perspective of a simulated camera pose [50]. To study temporal aspects of illumination, this process must be repeated for each time step in a sequence. The horizon method instead computes the profile of the horizon from the perspective of each surface element comprising the surface model and then determines if (or how much of) the light source is visible above (or occluded by) the horizon [33]. This is repeated for each surface element and for each time step in a sequence to generate a spatiotemporal model of illumination. The two methods have particular trade-offs related to efficiency in various scenarios, but both are computationally expensive and produce similar results.

Studies then analyze the simulated illumination model to draw conclusions about sites that may be amenable to robot and/or human exploration. Sites are often ranked by metrics such as the percentage of the total time duration for which they receive direct or indirect lighting, longest uninterrupted period of illumination, and shortest night periods. These studies offer insight to the problem of sustained lunar polar roving but don't take full advantage of the rich spatiotemporal illumination models. For example, several studies have demonstrated that there exists no site on either lunar pole that receives sunlight for 100% of a year and that uninterrupted sunlight lasting multiple lunar days is very localized and rare [50, 33], but this should not imply that rovers are limited to these sites or durations. The primary objective of this thesis is to demonstrate planning methods that take advantage of spatiotemporal information to generate routes that enable sustained lunar polar roving.

3.1.2 Circumnavigation and Sun-Synchronous Planning

Sun-synchronous circumnavigation routes for maximizing solar power and extending missions were first envisioned without the benefit of high-fidelity lunar terrain models [51]. The concept was later partially demonstrated in field experiments each spanning a single day on Earth [49]. The concept of mission-directed path planning was developed to enable global planning and navigation capabilities for planetary rovers over large scales and long durations amenable to sun-synchronous exploration [52]. The TEMPEST planner embodied a sun-synchronous navigation strategy tailored to solar-powered polar exploration and was demonstrated onboard the "Hyperion" rover on Devon Island north of the Arctic Circle. It was not extended to multiple diurnal periods, interplanetary communication, nor the use of lunar data.

Prior work by the author presents examples of sun-synchronous lunar polar routes generated using data from Lunar Reconnaissance Orbiter (LRO) [24, 53]. This work is detailed in Chapter 5. South polar routes at Malapert Massif and Shackleton Crater maintain uninterrupted sunlight and traversable slopes for 2 months with maximum driving speeds of 1 centimeter per second and 1 millimeter per second, respectively, but do not account for communication [24]. A route near Nobile Crater (similar to the routes presented in this paper) achieves 74 days with a strict requirement for direct line-of-sight to Earth when driving [53] (see Chapter 6). Chapter 7 introduces the concept of a *singularity* caused by the interaction of dynamic sunlight and communication and suggests a strategy to mitigate the associated risk [25].

This thesis advances the concept of *nomadic exploration*, in which rovers execute planned routes that follow the ever-shifting regions of solar power, moderate temperatures, and reliable communication [24]. Sun-synchronous circumnavigation routes that circle geographic features to maximize solar power were previously envisioned [51] and demonstrated on a small scale using terrestrial analogs [54] but without Moon-relevant lighting. This behavior could be applied around small, local geographic features (e.g., mountain peaks near the Lunar poles), mid-sized regions (e.g., large polar craters), or global routes (e.g., the equatorial circumference of the Moon or Mercury). The primary distinction between these scenarios is the speed required to complete the circuit and the amount of time available for performing experiments and collecting scientific data. Circling a 200-meter-diameter peak or crater near the Moon's pole while remaining in sunlight requires an average speed of only about 1 meter per hour. This is approximately 10% of the Mars Exploration Rover's overall drive speed [55]. This type of repetitive local route provides opportunities for densely distributed science sampling over a long period of time. Traveling faster enables exploration of larger regions and forays to more diverse science targets. At the other extreme, circumnavigating the Moon's equator in a single lunar period requires an average speed of about 16 kilometers per hour, which is about the maximum velocity of the Apollo Lunar Roving Vehicle [56].

Chapter 5 includes examples of local and regional routes, specifically at Malapert Peak, Shackleton Crater, and the Nobile Crater rim, all of which are near the Lunar South Pole [24, 53]. This work demonstrates a route planning method that utilizes connected component analysis to plan nomadic routes that never pass through

shadows or over steep terrain but provide continuous illumination, traversable slope, and communication while driving.

Prior work by others has addressed similar path planning problems, some with solutions specific to planning traverses for solar-powered planetary rovers under dynamic lighting conditions. Tompkins presents a concept of mission-directed path planning designed to enable global planning and navigation capabilities for planetary rovers over large scales and long durations. The heart of this work is the development of TEMPEST (TEmporal Mission Planner for the Exploration of Shadowed Terrain), a planning architecture that facilitates a variety of constraints and optimizations on time, distance, battery energy, terrain slope, communication availability, mission returns, and others under dynamic world models, such as time-varying lighting and communication [57]. Route segments are generated using an incremental heuristic search algorithm called Incremental Search Engine (ISE), which is akin to D* [58]. Route segments connecting waypoints and goal actions are planned individually, and the timing of the partially defined segments are then optimized to maximize the rover's energy state. Although TEMPEST was suited to handle many different types of constraints (e.g., communication, thermal state, data storage), Tompkins demonstrates only instances considering distance, time, slope, and energy. Generated plans are also purposely limited to coarse resolutions for practical computation reasons. Typical terrain models used are 10–30 meters/pixel, and typical routes presented are on the order of single-digit kilometers over single-digit days.

TEMPEST was incorporated into a sun-synchronous navigation strategy specific to solar-powered polar exploration. In this strategy the rover circles either the pole or a polar mountain or hill in sync with the Sun such that its fixed solar array is always directed generally toward the Sun. Sun-synchronous navigation was demonstrated with the solar-powered Hyperion rover on Devon Island above the Arctic Circle. The TEMPEST planner was used to generate 24-hour cyclic routes, aided by handpicked waypoints, timed to maximize battery energy. The planning state space included position, time, and energy. Routes of approximately 6 and 9 km were executed over separate 24-hour periods. The routes were generated offline and required approximately 6 hours to compute on a laptop computer.[1] Though suggested as a means to improve planetary roving, this work did not study lunar-specific routes nor did it incorporate orbital lunar elevation models, the most recent and high-resolution of which were not yet available at the time.

3.2 Path Planning

This section provides a brief overview of prior work in robotic path planning that is relevant to sustained lunar polar roving in a more general context. Additional related work is cited throughout the following chapters.

[1] with a 400 MHz Pentium II and 128 MB of RAM

3.2.1 Deterministic Path Planning

Deterministic path planning algorithms generate the same output every time they are executed for a given set of inputs. Common examples include breadth-first search, depth-first search, Djikstra's algorithm [59], and A* search [60]. Breadth-first and depth-first search are both brute-force graph search methods that are complete under certain conditions, meaning they will find a solution if one exists, but they are both inefficient with respect to the time needed to find a solution (exponential in depth). Breadth-fist search is optimal only if step costs are all identical, and depth-first search is not guaranteed to find the optimal solution. Djikstra's algorithm is a uniform-cost search that keeps track of the lowest total path cost from the start to each expanded node in the search space and expands nodes in order of minimum path cost. This algorithm is complete and optimal (under certain conditions) but may expand many more states than necessary to generate a solution. A* search extends this idea by expanding search tree nodes in the order of the estimated cost of the cheapest solution through each node. It uses a heuristic function to estimate a lower bound on the remaining cost to the goal from each state. This estimate plus the computed total cost from the start is the cheapest possible total solution cost. Given and admissible and consistent heuristic, A* is not only complete and optimal, but also optimally efficient, meaning it explores no unnecessary nodes to find the optimal solution. This is extremely advantageous, but unfortunately, A* is still impractical for large-scale problems because of its space and time complexity. Still, A* is valuable as a method to generate proof-of-concept routes and as a reference against which to compare the performance and solution quality of randomized path planning approaches.

3.2.2 Randomized Path Planning

Rapidly-exploring random tree (RRT) algorithms use a stochastic sampling-based approach, which avoids discretizing the state space and generates a search tree that explores the state space much more rapidly than do algorithms like A* [61]. The tradeoff is that because RRTs are not deterministic, they do not produce optimal plans (e.g., of minimal path length), and the generated paths tend to "wander" through the environment before arriving at the goal. RRTs are also only probabilistically complete, meaning that the probability of finding a solution approaches unity as time approaches infinity. This completeness guarantee is weaker than that of A*.

More recently, the RRT* algorithm addressed the suboptimality of RRTs by introducing an iterative anytime approach that is asymptotically optimal, meaning that over time, the solution converges to the optimal solution (e.g., one that minimizes path length) [62]. RRT* works by constantly updating the search tree's parent-child relationships as uniform samples are generated, effectively finding the optimal path to every sampled point in the state space. Because only a single path to a single query is needed, much of the computation is wasted effort. The amount of time it takes for the algorithm to converge grows arbitrarily large with increasing dimensionality of the state space. Another drawback, is that like standard RRTs, RRT* tends to have trouble exploring narrow passageways due to the reduced probability

of randomly sampling these areas. A recently published algorithm, Informed RRT* addresses both of these issues by directly sampling from the n-dimensional ellipsoid defining all search nodes that can theoretically improve the current best solution [63]. This modification improves performance compared to RRT* by an order of magnitude in complex environments. BIT* [64] and RABIT* [65] further improve planning performance.

Informed RRT* begins the search the same way as RRT*, but once an initial solution is found, the sampling is restricted to the exact area in which new samples can improve the solution. Informed RRT* retains the anytime nature of RRT*, meaning that at any point after the initial solution is found, the search can be halted and a viable solution is output. The quality of this solution is a non-decreasing function of the run time, so the longer the algorithm is allowed to run, the better the solution it will produce [63]. This characteristic is beneficial during polar mission operations, since new discoveries may require alternative solutions to be generated quickly due to the dynamic lighting conditions. The planner can be allowed to run and improve its solution until a final decision is needed.

3.2.3 Temporal and Resource Path Planning

SEXTANT (Surface Exploration Traverse Analysis and Navigation Tool) is a mission tool designed to plan extravehicular activities (EVAs) for human mission to the Moon and Mars [66]. Waypoints are selected on a 3D map by an astronaut, and SEXTANT plans EVA traverses between waypoints. The planner can optimize the traverse for either distance, time, or energy consumption measured in kilocalories. Predicted energy consumption is computed as a function of mass, slope, gravity, velocity, and time. Alternatively, energy consumption can be treated as rover energy consumption [67]. Rover energy consumption is a function of terrain slope, and the total rover energy consumed can be minimized using A* search. Surface lighting and shadows are computed using LOLA DEMs, and the energy generation is computed along the route. Combining energy generation and energy consumption, the rover battery energy level is computed along the entire route, but only after the route has been generated. This can lead to suboptimal or even negative battery energy states, so this method is not reliable for solar-powered polar exploration.

While TEMPEST demonstrated both temporal and resource path planning through consideration of position, time, and energy [57], other time-dependent planners have incorporated thermal state as well [68]. This hierarchical planner constructs a low-resolution graph by applying a quadtree decomposition to a series of illumination maps to generate a sparse set of nodes that is densest near shadow boundaries. Then edges are formed between neighboring nodes in position and time. A high-resolution planner precomputes the cost of each of these long edges. Simple models of power and thermal state are used along with dynamic state generation to conduct an A* search through the low-resolution graph from a start state to a goal position while minimizing time duration. The hierarchical nature of this planner is necessary to generate routes within practical time limits but leads to suboptimal, indirect paths. Also, altering the density or placement of the low-resolution graph to better suit a

particular traverse plan requires that edge cost be recomputed. More recent work enforces constraints on solar power, communication, and slope while implementing temporal compression for improved efficiency [69]; however, the routes presented are limited to 80 meters per pixel resolution and 60 Earth days duration, and there is no discussion of rover speed.

3.2.4 Replanning

The ability to adjust existing plans may eventually be necessary throughout multiple mission phases. During mission design, plan repair can decrease the time and cost to replan, since it eliminates the need to start from scratch. Depending on how long it takes to generate a rover traverse plan from scratch, plan repair could significantly reduce the burden on mission personnel and resources when mission objectives and parameters are altered or refined. However, substantial alterations to mission objectives (e.g., choosing a new landing location or time) will likely require planning completely from scratch, limiting the value of implementing an incremental search algorithm like D* [58] or ISE [57] for pre-mission planning.

During mission operations, when the rover is executing its traverse plan, continuous replanning and plan repair at the local scale are necessary to deal with the inherent uncertainty of the environment. Mission plans generated prior to launch are based on imperfect satellite data, which is low-resolution relative to the scale of the rover and the in-situ remote sensing measurements made by the rover. Tens of meters may separate traverse waypoints, between which numerous rover-scale obstacles can be encountered. Onboard motion planning is needed to avoid newly observed obstacles and hazards and get from point to point. Because of limitations of space-qualified computing hardware, however, onboard planning and replanning will likely be restricted to local hazard avoidance over short distances and time horizons as opposed to global replanning.

It is possible that unanticipated obstacles or science discoveries are observed that have mission-level repercussions, necessitating quick replanning on a global scale. For example, a narrow ridge connecting two adjacent groupings of science targets may turn out to be impassible, invalidating the remainder of the planned route. In this case, on-ground computational resources would be needed to plan a new traverse for uploading to the rover. Here too, it is unlikely that such a dramatic change of plan would allow for effective reuse of prior planning computations. Contingency strategies should rely instead on planning methods that are fast enough to enable rapid mission-critical decisions on the ground. This further motivates the use of algorithms like Informed RRT*, which will feature rapid search space exploration and anytime solutions. Although contingency planning is beyond the specific scope of this thesis research, the presented work will contribute to solving this important problem.

3.3 Summary

Solar-powered polar roving benefits from the temporal, resource-constrained planning capabilities exhibited by TEMPEST; however, the increased size (both scale and resolution) of the problems being considered make grid-based, deterministic path planners impractical due to time and space complexity. Informed RRT* offers a fast, anytime solution in continuous (non-discretized) state space that is both probabilistically complete and asymptotically optimal, but minimizes only path length and has not yet been demonstrated to enforce resource constraints such as stored energy and drive-time communication. A aspiration this thesis research is to combine the beneficial characteristics of mission-directed path planning and Informed RRT* to produce the first randomized, nondeterministic path planning algorithm that generates anytime solutions quickly while enforcing constraints on heterogeneous states and preserving probabilistic guarantees on completeness and optimality. The remaining chapters of this dissertation begin with simplified problem statements that consider subsets of the relevant considerations and employ deterministic planning algorithms to demonstrate proof-of-concept route solutions. Generally, each subsequent chapter builds on the last by increasing the complexity of the planning problem and/or the sophistication of the solution method.

Chapter 4

Spatiotemporal Constraint Models

Chapter 2 describes the lunar polar environment and states why lighting and communication conditions are critically important considerations when planning for sustained lunar polar roving. This chapter describes in more detail the choice of gridded model representation, lunar data, and the process of how digital elevation maps are used to generate predictive models of spatiotemporal constraints.

4.1 Gridded Models

Planning traverses that satisfy constraints on ground slope, surface insolation, and communication availability requires predictive models that estimate these quantities in both space and time. Gridded models are a reasonable choice to represent the lunar environment, because surface illumination and Earth visibility are complex obstacles (or cost fields) that would be inefficient to store and query parametrically. Gridded world models are also convenient for grid-based graph search, because the model itself implicitly represents a discrete search graph [70]. Because the resolution of the world model (typically 10–20 meters) is an order of magnitude greater than the scale of the rover (1–2 meters), a trivial motion model that does not account for rover kinematics is used. The rover's state simply moves between adjacent grid elements and consecutive time steps.[1] Therefore, the same data structure can be used for both the world model and the search graph.

In this research, rovers are assumed to be quasi-static. That is, no dynamic forces or accelerations are considered. This is a reasonable assumption for the moderate speeds considered (less than 10 cm/s), even in lunar gravity. Driving at speeds approaching that of the Apollo LRV in lunar gravity can induce dynamic trajectories, which may necessitate a more descriptive motion model. Even so, the dynamic effects are relevant only locally and negligible in the context of global path planning. Because of the quasi-static assumption, rovers are effectively constrained to drive on the terrain surface. Lunar terrain is assumed to be 2.5D, meaning that they are 2D surfaces in 3D space but have no overhanging geometry that requires a full 3D representation. This assumption is generally true, with rare exceptions including lunar skylights and

[1] This is subtle variaton of the classic 8-connected grid. See Chapter 5 for more detail.

(a) (b) (c)

Figure 4.1: (a) DEM of the lunar South Pole out to 60°S derived from LOLA data (240 meters/pixel) [71]. The red box indicates the section of the terrain shown in Fig. 4.1b. (b) 3D mesh model built using the 240-meter/pixel DEM and a closer view of the region around Malapert Peak. The green box indicates the section of terrain shown in Fig. 4.1c. (c) 3D mesh model of Malapert Peak built using a high-resolution DEM produced from stereo-photogrammetry of NAC images (2 meters/pixel) [72]. Gaps were filled using 10-meter/pixel LOLA data [34].

lava tubes not considered in this thesis. Lunar terrain can therefore be accurately represented by 2D height maps. This means that only two spatial dimensions are needed to represent constraints that vary over the surface. Principal terrain slope, which is static in time, can be fully represented by a single two-dimensional gridded model implemented as a 2D array.

Unlike slope, surface insolation and communication availability vary with respect to time due to the motion of the Sun and Earth relative to the Moon. So accurate models of insolation and communication require a temporal dimension in addition to two spatial dimensions. Spatiotemporal maps of surface lighting and communication are therefore represented as three-dimensional gridded models implemented as 3D arrays.

4.2 Lunar Data

Spatiotemporal constraint models can be generated for a given region of interest using digital elevation models (DEMs) of a particular planetary body. The process for generating maps of the Moon's poles is described here, but a similar process can be used for Mercury or any other planetary body for which the necessary data exists. The process starts with high-resolution DEM data derived from orbiting satellite measurements. For the Moon, the primary source is the NASA Lunar Reconnaissance Orbiter (LRO) satellite's Lunar Orbiter Laser Altimeter (LOLA) instrument. Gridded data covering the polar regions has been compiled down to 5 meters per pixel close to the pole and 100 meters per pixel out to 45° North and South [22]. The resolution of available DEMs decreases with increasing distance from the pole due to increasingly limited coverage resulting from LRO's polar orbit. LRO's Narrow Angle Camera

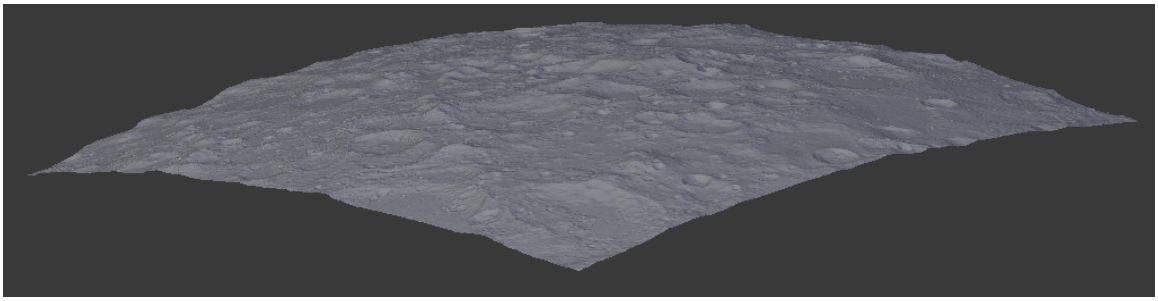

Figure 4.2: Mesh model of a large area of the Moon, seen from the side, showing the effect of the Moons curvature. This model is approximately 300 km on each side.

(NAC) data has been used to produce even higher-resolution DEMs (2 meters per pixel) via stereo image processing for select locations, such as Malapert Massif[2] near the South Pole [72]. The resolution and accuracy of this data is orders of magnitude better than what was available previous to the LRO's launch in 2009 [19]. Examples of low- and medium-resolution LOLA data and high-resolution NAC data are shown in Figure 4.1. Gridded data records and other LRO data products are accessible via NASA's Planetary Data System, specifically the Geosciences Node [73, 74].

4.3 Modeling Spatiotemporal Constraints

This section described the process used to model surface insolation, communication availability, and ground slope based on gridded data products. From the DEMs, 3D mesh models of terrain can be built for a particular region of interest. To do this, the map projection of the DEM data (typically polar stereographic) must be inverted to produce 3D points that represent the same terrain. This ensures that the terrain model will be the correct shape to interact realistically with simulated incident illumination, including effects due to the Moon's curvature. An example of a mesh model of a large patch of lunar terrain viewed from the side is shown in Figure 4.2. The Moon's curvature is clearly apparent at this scale, and capturing curvature effects is important when determining lighting and shadows.

A bounding box is selected that encompasses the extent of the region to be mapped (i.e., the exact image frame for which lighting maps will be generated). The terrain within the map's image frame does not completely determine the illumination within that frame, however. Large terrain features outside the map frame can also cast shadows into the frame. Thus, the 3D mesh model used for computing illumination needs to extend substantially farther than the map frame itself. The necessary size of the larger model is calculated considering the curvature of the Moon and the elevation of local terrain features. The immediate border of the map frame is modeled using high-resolution data that matches the resolution of the data within the frame, but the wider region outside the map frame is modeled using lower-resolution data. This is done both to reduce memory and processing requirements and also because high-

[2]Malapert Massif is sometimes referred to as "Malapert Peak."

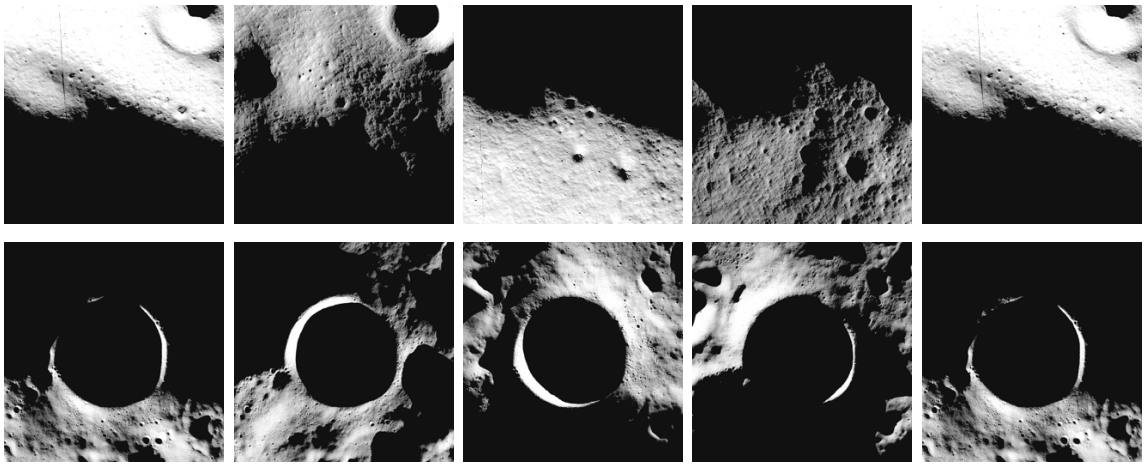

Figure 4.3: Simulated illumination maps of Malapert Peak (top) and Shackleton Crater (bottom) spanning one month (consecutive images are about 7.4 Earth days apart).

resolution data is often not available for the entire wider area, since some of it is of lower latitude. A mesh model with high-resolution and low-resolution segments is shown in Figure 4.1b. This model was created by stitching three elevation models of varying resolutions: a high-resolution stereo-generated DEM at 2 meters per pixel [75], a medium-resolution LOLA DEM at 10 meters per pixel to fill gaps in the stereo data [34], and a low-resolution LOLA DEM at 240 meters per pixel to capture the wider region [71].

4.3.1 Surface Insolation

To model solar illumination of the terrain surface, the relative position of the Sun must be known for all times of interest. This can be provided by ephemeris utilities. The SPICE toolkit [76] is used to determine the location of the Sun and the location of a point in the center of the lunar map frame at each time in the sequence of interest. From these, a Sun vector is computed in the local frame. Once the topographic terrain model and illumination angles are known, surface lighting maps are rendered using a ray tracing algorithm [77, 78], producing a 2D orthographic projection of the simulated illumination.[3] The resolution of the rendered illumination map is generally selected to be on the same order as the resolution of the original DEMs. Example sequences of surface illumination generated for Malapert Massif and Shackleton Crater are shown in Figure 4.3.

Consecutive sequences of rendered illumination maps are stacked to form 3D spatiotemporal models of sunlight. Each grid cell contains a floating point number between 0 and 1 representing the pixel intensity of a simulated orthographic camera for that

[3]All of the models used to plan rover paths presented in this dissertation were generated using the ray-tracing method. However, the models used in Section 10.1 employed a different ray-tracing utility that is more physically accurate [] and treats sunlight as an area source instead of a directional source [79].

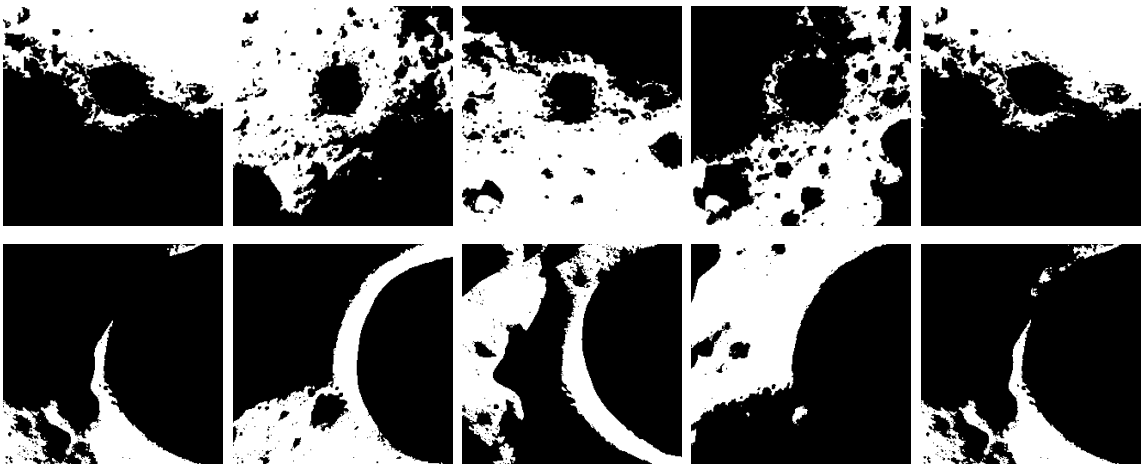

Figure 4.4: Binary illumination maps of Malapert Peak (top) and Shackleton Crater (bottom) spanning one month (consecutive images are about 7.4 Earth days apart). These images are zoomed in relative to Figure 4.3.

location–time state. For many of the routes presented, these continuous-valued illumination models are converted to binary arrays using a threshold intensity value at or below which pixels are considered unlit, or shadowed, and are set to 0. Pixels with intensities above this threshold are set to 1 and are considered to be fully illuminated by the Sun. For the examples presented in Chapters 5 and 6, the threshold used was epsilon greater than 0, meaning all pixels with nonzero illumination are defined as lit. This decision reflects an assumption that any positive amount of solar illumination on the surface indicates that a solar array above the surface will receive the full solar constant (approximately 1366 W/m^2 on the surface of the Moon). The simplest power models (used in Chapter 5) assume that a rover in a sunlit grid element is capable of capturing sufficient solar-power to maintain nominal driving speeds. This assumption implies a rover configuration with a two-degree-of-freedom (2-DOF) articulated solar array that can track the position of the Sun. It also implies that the size and efficiency of the array are sufficient to generate enough electrical energy to power all of the rover's necessary systems, including mobility. This is an obvious oversimplification of solar power and energy consumption, but it is still useful for demonstrating the concept of sustained polar exploration.

The physical quantity of key importance is the solar flux density passing through a unit area at the height of the rover's solar array. Brightness in the rendered image is a poor approximation of this for several reasons. First, the rendering software does not output this quantity directly but instead simulates the intensity of light reflected off the terrain surface back to the virtual camera. Not all light incident on the terrain is captured by the virtual camera, and the amount that is captured is a function of camera angle. The solar flux at the terrain surface is typically slightly less than that at a height of 1–2 meters above the surface. Therefore, zero flux at the surface does not necessarily indicate zero flux at the solar panel height. Second, interreflections (multiple bounces of light rays) between nearby terrain patches are not modeled, which could increase the total solar flux in some areas. Computing interreflections is

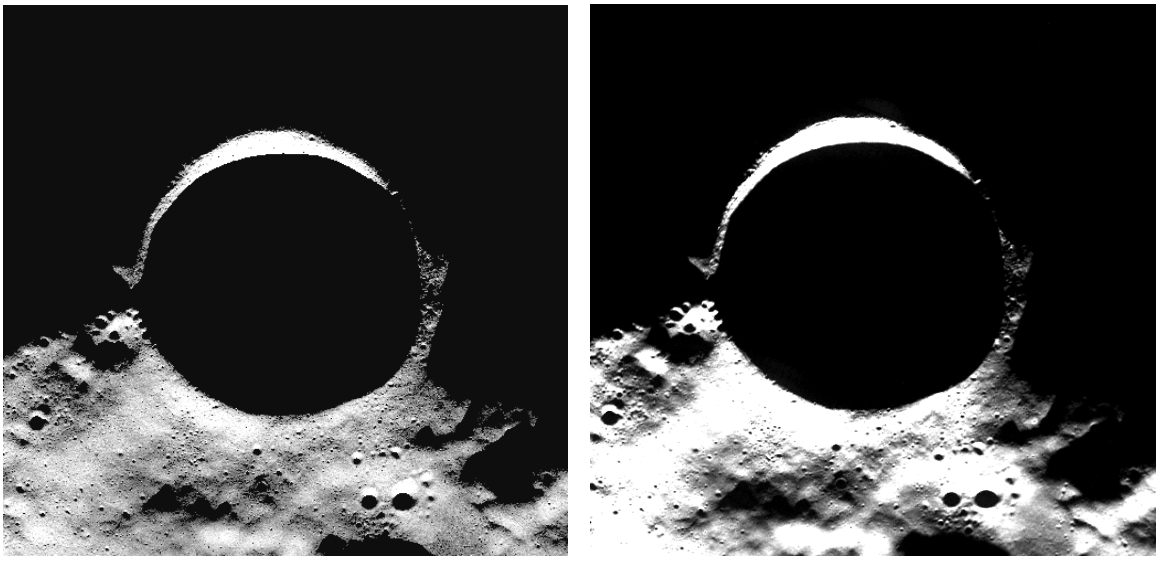

Figure 4.5: Rendered image of Shackleton Crater (left) and photographic image of Shackleton Crater taken by the LRO's Wide Angle Camera (right) [80] at the exact same time as the rendering, showing correspondence between the simulated and actual lit areas.

computationally intensive, and doing so accurately requires knowledge of the surface material's optical properties (such as color and albedo), which have been mapped only to coarse resolution. Even so, the energy gained from reflected light is typically minimal, so a conservative ignores these terms.

The greatest limitation of the method described is that incident sunlight is modeled as a directional source (equivalent to a point source at infinite distance), so rendered lighting maps do not account for partial occlusion of the Sun. Section 10.1 employs a more realistic sunlight model that treats the Sun as an area source. This produces a sunlight model of continuous values between 0 and 1 representing the portion of the solar disc that is visible from the rover's position on the surface. Multiplying these values by the solar constant yields an approximate value for the maximum flux available at each state. This difference is most noticeable at boundaries of shadows cast by distant geometry. At these shadow boundaries, the Sun is only partially obscured. These boundaries exhibit a smooth gradient from fully lit to fully shadowed (representing a penumbra) instead of a sharp delineation.

To qualitatively validate the simulated illumination maps, images were rendered of Shackleton Crater for three specific times in the past corresponding to three photographic images taken by the LRO Wide Angle Camera (WAC) [80, 81, 82]. Each image was map-projected to a polar stereographic projection using USGS's ISIS tool [83]. Some differences between rendered images and photographic data were noted, including hard versus soft shadows and differences in image intensity due to the reflectance model used for rendering, but generally the match was accurate, as shown in Figure 4.5.

A more rigorous quantitative analysis of rendering accuracy was used to verify the

accuracy of area-source models used in Section 10.1. This method proved to be more accurate both quantitatively and qualitatively, producing softer shadows as expected [79].

4.3.2 Earth Visibility

In addition to illumination for solar power, polar traverse planning considers Earth visibility for communication. Without an orbiting satellite providing relayed communication, lunar rovers will rely on line-of-sight direct-to-Earth (DTE) communication to receive commands and transmit telemetry and science data. Future missions may rely on advanced rover autonomy to execute long traverses without supervision, but initial resource prospecting missions will likely take a more conservative approach and enforce a requirement for constant communication during rover operations. With a round trip signal time delay of approximately three seconds, DTE enables near real-time supervision and teleoperation. A strict requirement for DTE during all rover operations limits exploration to the near side of the Moon and complicates sustained lunar polar roving. Despite tidal locking, the Earth oscillates in the sky slightly as viewed from the Moon, making communication visibility come and go near the poles as the Earth dips behind the horizon. Gridded, spatiotemporal communication models predict when and where on the lunar surface the Earth will be visible and therefore when and where DTE will be available. These models can be generated in exactly the same way as lighting maps except that a vector representing Earth's position (or the position of Deep Space Network antennae) replaces the Sun vector. As with the illumination maps, a nonzero intensity value indicates Earth visibility for that grid element. Communication availability is treated as binary.

Chapter 6 demonstrates methods of planning routes that adhere to strict requirements on communication for driving. Chapter 7 demonstrates the disadvantages of such an approach and suggests an alternate strategy.

4.3.3 Terrain Slope

Besides shadows and communication blackouts, rovers must avoid hazardous slopes. This necessitates the computation of surface slope maps. Small, rover- and sub-rover-scale obstacles such as rocks and craters less than 5–10 meters across are not observable by LOLA due to its sampling resolution, so these hazards cannot be explicitly planned for based on existing satellite data. However, local slopes can be calculated from the same topographic terrain models used for determining illumination and communication. The average ground slope for each pixel is the tangent of its gradient, which is computed as a divided difference over the neighboring pixels. An example of a slope map generated in this way is shown in Figure 4.6a. To treat principal slope as a constraint, a threshold is chosen based on the expected mobility performance of a particular rover, typically less than 15–20 degrees. Applying a threshold to the slope model produces a binary constraint map indicating safe and unsafe slopes. Because slope does not change over a rover mission timeline, slope maps are spatial only and two-dimensional. When both slope and constant sunlight

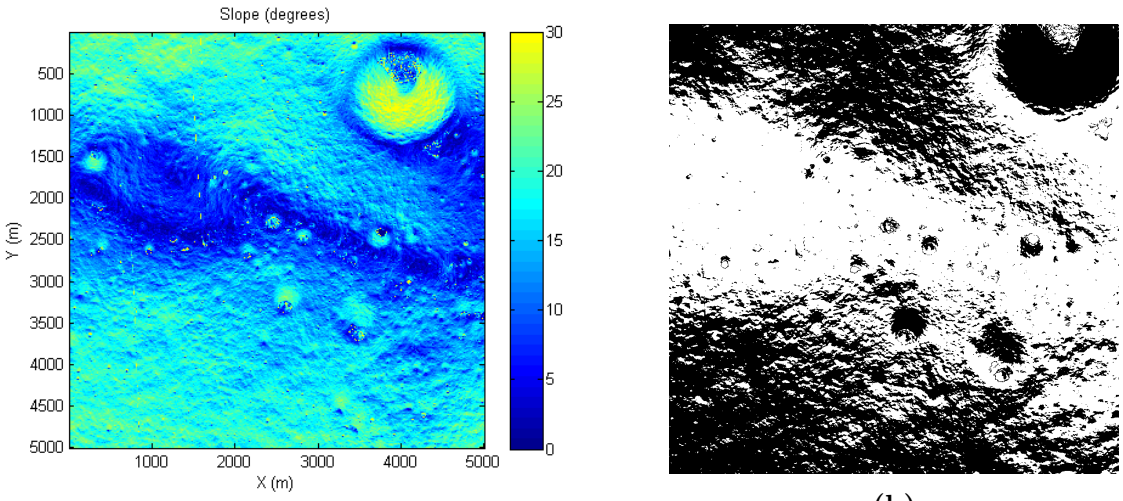

(a) **(b)**

Figure 4.6: (a) Slope map for Malapert Peak region. Color scale in degrees. (b) Map of safe slope regions around Malapert Peak. White indicates slope less than 15 degrees.

are treated as binary constraints, the slope map can be combined with each time step of the illumination model to produce a binary array representing the states that have both sunlight and safe slope, representing all permissible states. An example of this combination is shown in Figure 5.2.

Acknowledgment

The author would like to thank Heather Jones at Carnegie Mellon University and Eric Amoroso at Astrobotic Technology for helping to develop the modeling capabilities described in this section. Although the author was heavily involved in the development process, Heather and Eric are primarily responsible for implementing the ray-tracing systems used to generate the predictive models used for planning. The rendering described in this section is not itself a primary contribution of this thesis, but many of the contributions described in the remainder of this dissertation were made possible by it.

Chapter 5

Planning for Sunlight

This chapter develops and demonstrates methodology to solve a simplified version of the planning for sustained lunar polar roving problem. Specifically, the method considers only terrain slope and binary sunlight conditions without any consideration of communication. The method described in this chapter also uses trivial thermal and power models: as long as the rover stays in direct sunlight, it is assumed to stay warm and generate sufficient electrical power to operate all of its necessary subsystems, including mobility. Although these simplifying assumptions limit the relevance of the results to actual missions, the solutions presented serve to demonstrate a valuable proof of concept—that moderately paced rovers can conceivably achieve multiple lunar days of solar-powered exploration by traversing sun-synchronous lunar polar routes. This chapter also applies elements of connected component analysis to aid route selection and computation time.

5.1 Routes of Continuous Illumination

This section describes an A* graph search approach to planning for sustained lunar polar roving that treats sunlight as a hard constraint, thereby producing routes of continuous illumination.

5.1.1 Sunlight as a Hard Constraint

Lunar rovers without the benefit of RTGs or RHUs are strongly motivated to maximize their exposure to sunlight, both for heat and for power. Without sunlight, solar-powered rovers must rely on limited battery capacities to provide both necessities. Although this is feasible for short durations, it is not sustainable for durations approaching the 14 Earth days of lunar night. As a first approach to planning routes that enable multi-month exploration, a pair of simplifying assumptions can be made regarding the rover's thermal and energy states. These assumptions in turn drive a simplification of the planner's constraint on sunlight.

Instead of explicitly modeling a rover's transient thermal and electrical response to dynamic insolation conditions, consider the assumption that continuous, uninterrup-

ted sunlight automatically nullifies both issues. This assumption isn't unreasonable. Engineering an electromechanical system to operate in two vastly different thermal environments, such as lunar day and lunar night, is extremely challenging. But engineering the system to operate in either one of those environments is relatively straightforward and has been demonstrated by past lunar exploration. Energetically, a lunar rover with a solar array area of 1 square meter could generate on the order of 400 Watts if pointed normal to the Sun's rays.[1] A 2-DOF articulated array could maintain this power regardless of the rover's pose, and with this power, an efficient drive system should be able to sustain a nominal speed indefinitely.

The dual requirement to this pair of assumptions is that the rover's path must maintain continuous solar illumination. That is, the route planner must treat direct sunlight as a hard constraint that can never be violated. This is necessary to guarantee that the assumptions made regarding the thermal and electrical systems are valid. Although routes meeting this requirement are artificially limited by not being permitted to pass through shadow, these routes provide a viable means of achieving multi-lunar-day roving. Routes of continuous illumination can even be considered conservative in the sense that they represent a subset of the routes actually achievable by an identical rover, which might venture into shadows for short durations to make scientific observations. The remainder of this chapter presents planning methodology and examples of such routes.

5.1.2 Deterministic Path Planning

The discretized lighting maps described in Chapter 4 lend themselves to grid-based, deterministic path planning. Because routes of continuous illumination are sought (for now), 3D binary lighting maps are used as the basis for a graph that defines the search space. Grid cells that contain a value of 1 are lit and are therefore open, or allowable states. Grid cells that contain a value of 0 are shadowed, closed, and disallowed. So each 1-valued cell is a node in the graph and represents a state comprised of two spatial dimensions and one temporal dimension. The graph's edges are defined similarly to those of a standard 8-connected grid with one major difference. Because time must proceed in the forward direction, each node is connected to the (up to) eight spatially adjacent grid cells in the *next* time step, not its own. Including the optional action of doing nothing and staying in the same location for the duration of one time step yields a maximum of nine possible edges directed out of each node. The graph is directed such that all state transitions move forward in time. Although the maximum branching factor of the graph is nine, the typical effective branching factor is less than nine, since shadows are treated as obstacles that eliminate edges in the graph.

Waypoints are specified by array indices corresponding to (x, y, t) states. Minimum-length paths can be planned between two waypoints using standard deterministic path planning algorithms, such as breadth-first, depth-first, Dijkstra's, and A*.[2] Of these,

[1] Assuming 1366 W/m^2, zero cosign loss, and an array efficiency of about 30%.

[2] Breadth-first and depth-first search produce optimal solutions only in the special case of

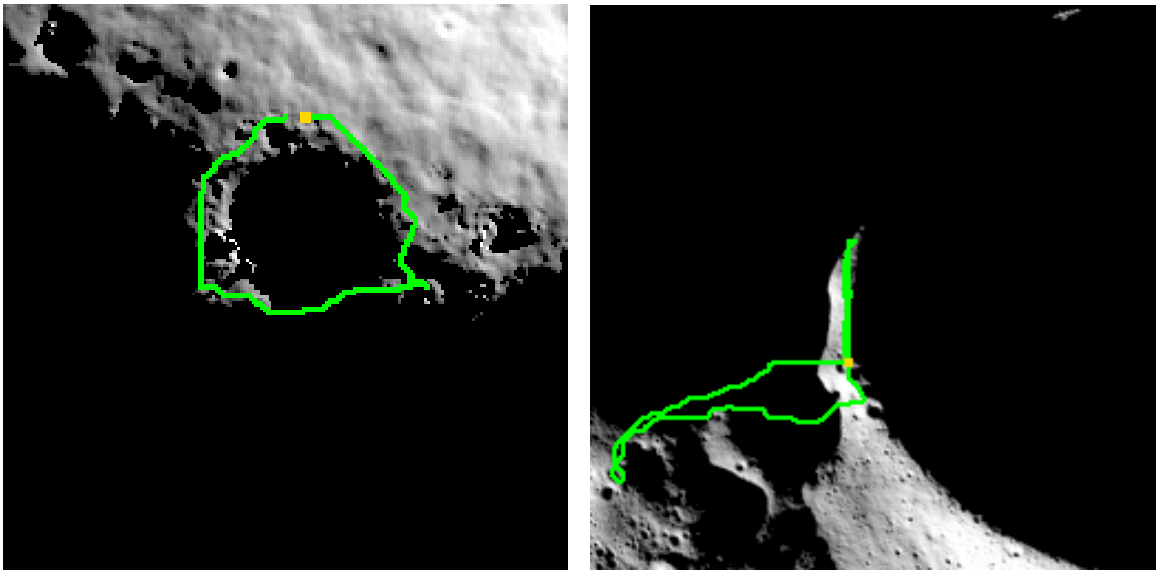

(a) Malapert Massif Route **(b)** Shackleton Crater Route

Figure 5.1: Sustained routes at Malapert Massif and Shackleton Crater near the Lunar South Pole. These static views, shown projected onto one snapshot of temporal illumination conditions, give the false impression that the routes cross shadow; however, a rover following this route (defined in x, y, and t) remains illuminated at all times. The rover's current position is indicated by a *yellow* square, and the rover's path is traced in *green*.

A* offers the best performance. Euclidean distance is used as the heuristic to estimate the cost to the goal for each (x, y, t) state, and total path length is defined as the sum of the incremental Euclidean (L^2) norm lengths of each 3-element state transition vector. Spatial distance is assumed to be uniform in x and y across the extent of the world model, meaning that elevation changes are not considered as added distance. Elevation can be accounted for by incorporating a z term in the state vector, but the effect on routes is minor.

Because the start and end times are fixed, and all allowable actions move strictly forward in the temporal dimension, the total time duration of any complete solution is fixed. Including the elapsed time in the distance calculation may therefore seem unintuitive, both because the total time duration is fixed and since it does not add to the actual distance traveled. However, including time is necessary to drive the search forward by prioritizing open nodes that are closer to the goal in time as well as space.[3] Including time in this way does not affect the final solution, but it can affect the speed of the search by expanding fewer nodes.

The Malapert and Shackleton routes shown in Figure 5.1 travel a total distance of 2.16 and 34.7 kilometers, respectively, over two full diurnal cycles on the Moon (59 Earth days), resulting in an average speed of 1.5 and 25 meters per hour, and requi-

uniform-cost search.

[3]Including time in the distance norm becomes even more important when waypoints are specified only by position, independent of time (Section 5.3.2).

ring a maximum instantaneous speed of 0.1 and 1.6 cm/s, respectively. This evidence supports the claim that feasible continuously illuminated routes lasting multiple diurnal cycles exist on the Moon. The Malapert and Shackleton routes also feature maximum dwell times, when the rover is stationary, for up to 45 and 226 consecutive hours, respectively. Long dwell times are desirable to facilitate scientific experiments and data collection at points of interest while still remaining in constant sunlight for heat and power.

Slope constraints can be easily incorporated into this deterministic path planner in one of two ways. First, at search time, the algorithm's transition function (which determines how legal edges are formed between parent nodes and child nodes) can check the binary slope map and reject all edges that result in a violation. Second, during preprocessing, slope constraints can be combined with lighting constraints using a logical `AND` operation with the slope map and each time increment of the lighting map. The result is a 3D combined lighting and slope map that is the same size as the original lighting map but only contains 1's where (and when) there is both surface lighting and traversable slope. This combined map can then be used by the search algorithm in the same way as the original lighting map. This process was used to generate the routes shown in Figure 5.1. These routes never traverse terrain with a principal slope exceeding the selected constraint of 15 degrees.

Rover Speed

In addition to sunlight and slope, routes are subject to constraints on rover speed. This constraint is enforced by allowing an integer number of "moves" or state transitions before advancing to the next time step defined by the lighting model. The result is a discrete set of effective allowable speeds. For example, if a rover's maximum allowable speed is 2 cm/s, and the world model's resolution is 20 m spatially and 2 hours temporally, then the rover is permitted to make a maximum of 5 moves per time step.[4] If the planner moves three times and remains stationary two times during a particular 2-hour time step, the rover could execute this result either by driving at 2 cm/s for 60% of the time or by driving at 1.2 cm/s for 100% of the time. Both operations achieve the same average speed and total distance traveled over the 2-hour interval, and both avoid all known obstacles resolved by the model.

Effectively, this implementation increases the temporal density of the discrete state space without increasing the temporal resolution of the discrete world model. This is a tradeoff between computational fidelity and efficiency. The advantages are that routes can be specified with more precise speed trajectories without the added computational expense of rendering higher-resolution lighting models. The disadvantage of using a less detailed, and perhaps less accurate, lighting model is lower confidence in the routes produced. Lunar polar lighting evolves only slightly, but noticeably, over 2-hour intervals. In terms of planning efficiency, this method has the advantage of directly comparing states with matching discrete times, as opposed to applying some measure of closeness to determine if two expanded nodes are equivalent.

[4] $0.02 \text{ m/s} \times 3600 \text{ s/hr} \times 2 \text{ hr} \,/\, 20\sqrt{2} \text{ m} = 5.09$

The disadvantage of allowing multiple moves per time step is that the depth of the search tree is effectively multiplied.

5.2 Connected Component Analysis

This section presents a method that applies connected component analysis to aid in planning routes that keep robots continuously illuminated and on traversable slopes while reaching one or more goal locations. The goal is to prolong polar exploration by extending the duration, range, and scientific return of solar-powered routes exploring environments with changing but predictable lighting conditions, particularly those of the Moon and Mercury. Spatiotemporal maps of lighting and ground slope are computed as described in Section 4.3, and all distinct interconnected regions that have both direct sunlight and safe slope are found using connected component analysis. These 3D connected components are pruned of roots that violate time constraints and branches that dead-end prematurely. Each component is the basis for a directed graph that encompasses all feasible routes from the beginning to the end of that component. The shortest feasible route between a pair of start and goal positions within a component is found using A* search. Malapert Massif and Shackleton Crater, both with favorable lighting conditions near the Moon's South Pole, serve as examples throughout this section.

This approach uses connected component analysis to find the largest interconnected regions in space and time that are continuously lit and have safe slope. These regions can be thought of as volumes in x, y, and t made up of gridded cells, or voxels. Using a flood-fill algorithm [84], a sorted list of the largest connected regions in the 3D sequence of combined light-and-slope maps is generated. The basic steps used to find the connected components are outlined in Algorithm 1. Connectivity is defined by a 3×3×3-element kernel of 1s and 0s, where the center element (always 1-valued) represents the cell being examined at each iteration within a flood-fill algorithm, and each neighboring element is 1-valued only if its position relative to the center element is considered connected. For example, if only the six elements sharing a face with the center element are 1-valued, then each cell is directly connected to just the six cells immediately adjacent to it (called the 6-connected neighborhood), and flood-fill adds those with value 1 to the same component as the central cell. The kernel is then applied to these newly added cells recursively until no new connected cells are found, which happens when the component has filled the volume bounded by 0-valued cells. Since the 27-element kernel must be symmetric about its center, there are 2^{13} possible definitions of connectivity for a 3D space. In the examples presented here, the most liberal definition of connectivity is used, in which all 26 neighboring elements are considered connected to the central element (also called the 26-connected neighborhood).

Each distinct component returned by flood-fill represents an undirected graph that can subsequently be searched using standard methods such as Dijkstra's or A*. By definition, no component is connected to any other component. The vast majority of components are extremely short in the time dimension, lasting only a few hours on the

Algorithm 1 Connected Components Algorithm

```
Initialize all cells in Map to unlabeled
while ∃ unlabeled 1-valued cells ∈ Map do
    c_seed ⇐ next unlabeled 1-valued cell in Map
    Set label(c_seed) ⇐ a unique label l
    C ⇐ FloodFill3D(c_seed)
    Set label(c) ⇐ l ∀c ∈ C
end while
function FloodFill3D(seed)
    return the set C of all cells connected to seed
end function
```

Moon, but, in the case of the Malapert and Shackleton examples (beginning in May 2015 and April 2018, respectively), one component spans the two full lunar cycles analyzed (Fig. 5.2). For a route satisfying the constraints on sunlight and terrain slope to exist, the start and goal state must be members of the same connected component. Although selecting start and goal states from a single component does not guarantee that a feasible route between the two exists (because connectivity does not automatically enforce a constraint on rover velocity), doing so increases the likelihood of a viable solution.

5.2.1 Connected Component Pruning

Because the flood-fill algorithm's definition of connectivity must be symmetric in all three dimensions, it produces regions that, to be reached, would require the rover to travel backward in the time dimension. This happens when two previously disconnected patches of light converge to one connected patch. If a rover starts in one of the two converging patches, it can never reach the other, despite the appearance of connectivity in three dimensions. To eliminate these features which can never be part of a feasible route, each component is pruned of branches that extend backward in time (i.e., roots) using the procedure outlined in Algorithm 2. The resulting component is a tree-like structure that only branches forward in time.

The existence of a connected component that spans from t_0 to t_n indicates that one or more routes of traversable slope and uninterrupted sunlight exist that span the entire duration. The route(s) may or may not be feasible depending of the rover's maximum speed. In other words, a rover that starts within the pruned component at t_0 can reach t_n without crossing a shadow or unsafe slope, provided that the rover has adequate speed. The absence of a pruned component that spans from t_0 to t_n indicates that no viable route of that duration exists. If a specific route duration is desired, then nothing can be gained by searching within connected components of lesser duration. By applying these insights, connected component analysis aids mission planning.

Connected component analysis can also improve planner performance. Once a goal state (location and time) has been selected, searching branches of the connected

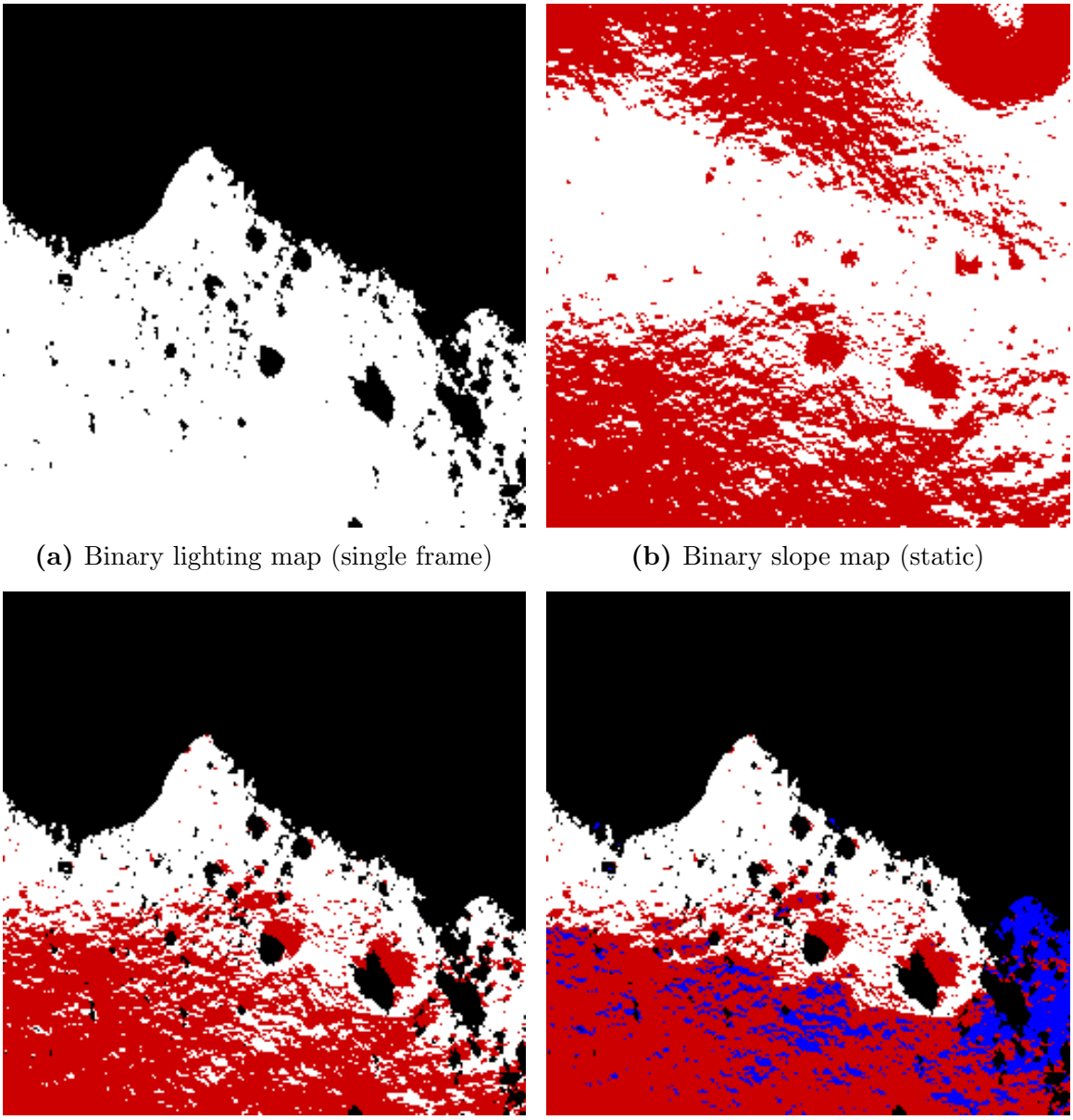

(a) Binary lighting map (single frame)

(b) Binary slope map (static)

(c) Combined lighting `AND` slope

(d) Largest connected component

Figure 5.2: From left to right: binary lighting map, binary slope map, combined slope + lighting map, and the largest connected component, all shown for just a single time step of the Malapert Peak sequence. Black is shadowed, white is lit, red is steep slope, and blue is unconnected to the largest component.

Algorithm 2 Pruning Algorithm

Let X: number of cells in Map in the x dimension
Let Y: number of cells in Map in the y dimension
Let N: number of cells in Map in the t dimension
Let $c(x, y, t)$: cell at position (x, y) and time t
Let $Map(t)$: 2D slice of Map at time t
$\{C_0^1 ... C_m^1\} \Leftarrow$ FloodFill2D($Map(t)$)
Choose $C_k^1 \in \{C_0^1, ..., C_m^1\}$
Set $label(c) \Leftarrow l \; \forall c \in C_k^1$
for $i = 2...N$ **do**
    $\{C_0^i ... C_m^i\} \Leftarrow$ FloodFill2D($Map(t)$)
    for Each component $C \in \{C_0^i ... C_m^i\}$ **do**
        if $\exists c(x, y, i) \in C \mid label(c(x, y, i-1)) = l$ **then**
            $label(c) \Leftarrow l \; \forall c \in C$
        end if
    end for
end for
function FloodFill2D($slice_t$)
    return the set of all connected components $\{C_0^t, ..., C_m^t\}$ in $slice_t$
end function

component that do not include that point is wasteful, because the search algorithm will spend time expanding search tree nodes than can never lead to a solution.[5] This can be avoided by pruning all branches but that which includes the goal state. If a goal site has not yet been selected but a target depth (duration) is desired, all branches but those that reach the target depth can be pruned. If there is no target depth but the absolute longest possible duration is desired, then all but the deepest branch(es) can be pruned. This effectively eliminates all possible dead ends that occur when sunlit surface patches diverge into multiple separate regions as time advances and one or more of these regions does not reach the goal time. Removing these dead-end branches is beneficial because it prevents the graph search from spending time exploring dead-end routes.

To implement this second stage of pruning, the result of the first pruning can be flipped in the time dimension and run through the same pruning procedure (Algorithm 2) and then flipped back. This produces a single continuous corridor through time with no roots or branches that dead-end in either direction (Fig. 5.3). It is possible for multiple branches to diverge as long as they eventually converge again prior to the goal time. As long as the rover path lies within the boundaries of this double-pruned connected component, it will reach t_n.

[5]It is important to keep clear the distinction between the connected component tree and the search tree. The connected component tree is the set of all states that can be theoretically reached by a rover with arbitrary positive speed. The search tree may or may not be able to expand every state in the connected component tree, since it is subject to the rover's maximum speed.

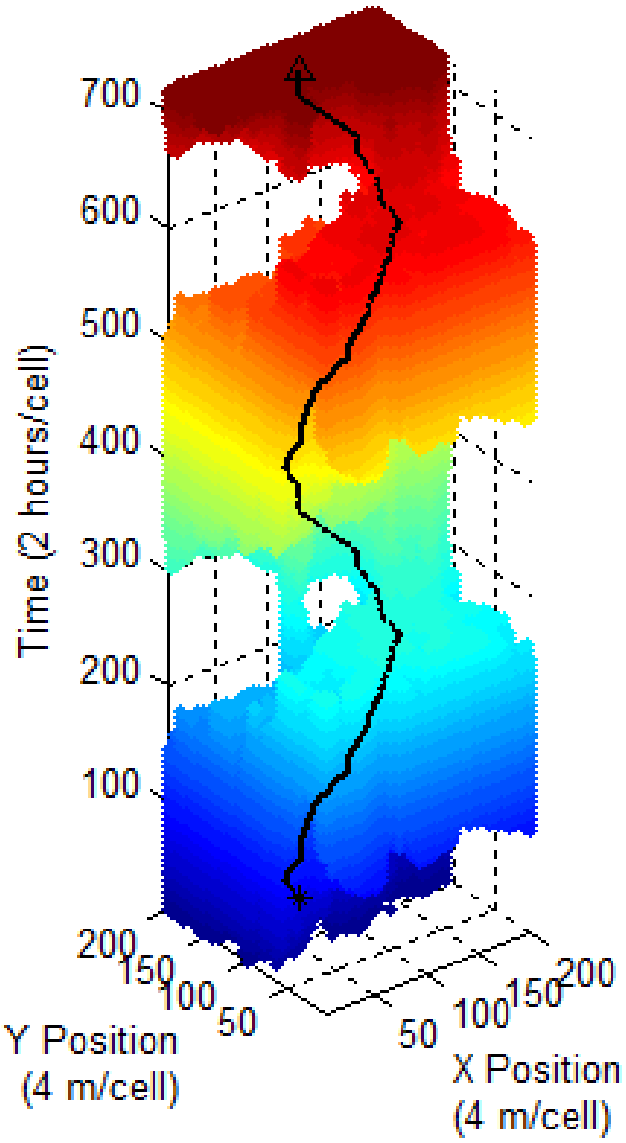

Figure 5.3: 3D representation of the largest pruned component from the Malapert Peak example and resulting shortest route. Color indicates time progression.

5.2.2 Planning within Connected Components

Once pruned, the continuously illuminated component is used as a graph for planning routes between any two points that lie within the component. Of most interest are the routes that start at t_0 and end at t_n, since the goal is to extend rover operation as long as possible. Each 1-valued cell in the pruned component represents a graph node, and edges are defined between neighboring nodes in the same sense as standard 8-connected grids except that all edges are directed forward in time. That is, each node is connected only to the 9 neighboring nodes in the following time step (the ninth representing the action to remain stationary for one time step) and is not connected to any nodes in the same or previous time steps.

For the examples in this chapter, with each action, the search algorithm moves exactly one cell forward in time and a maximum of one cell in each of the x and y directions. Utilizing a 3D gridded world model to implement a spatiotemporal graph search in this way need not be restrictive to one action per time step, however. If the constraint on maximum rover speed permits, multiple moves in $x-y$ can be made within a single time step. This is done in Chapter 6 to permit faster traverse speeds on maps of the same temporal resolution as in this chapter. An integer counter that increments with each action is added to each search node to control when the world model should advance to the next time step. This counter adds granularity to the temporal state space without adding an extra state space dimension. Although different in implementation, this produces a behavior similar to that of methods that record a continuous time value for node comparison and world model indexing, such as [68].

Standard A* search was used to find the shortest route between starting locations at t_0 and goal locations at t_n, where distance was defined by the Euclidean norm. Example routes computed in this way using several intermediate waypoints are shown in Fig. 5.4. The Malapert Massif example visits three waypoints twice each by following a nearly identical circuit on the second lunar day as the first. This route exemplifies the exceptionally slow pace that is required to achieve multiple lunar days of solar-powered roving in certain favorable scenarios such as circling polar peaks. It also demonstrates focused exploration of a small PSR for which only a modest battery capacity would be needed to make brief forays and achieve key science objectives without falling behind the pace of the Sun. The second example, at Shackleton Crater, visits five locations identified as sites of interest and does so over two lunar days. Note that unlike the Malapert example, this route does not follow the same circuit twice but instead executes two distinct legs of exploration, one on each day.

5.3 Other Improvements

5.3.1 Temporal Pruning

In addition to computing the largest connected component and pruning its roots and branches to narrow the search space, another temporal pruning technique was developed to improve algorithm efficiency. It was noticed that in cases where the

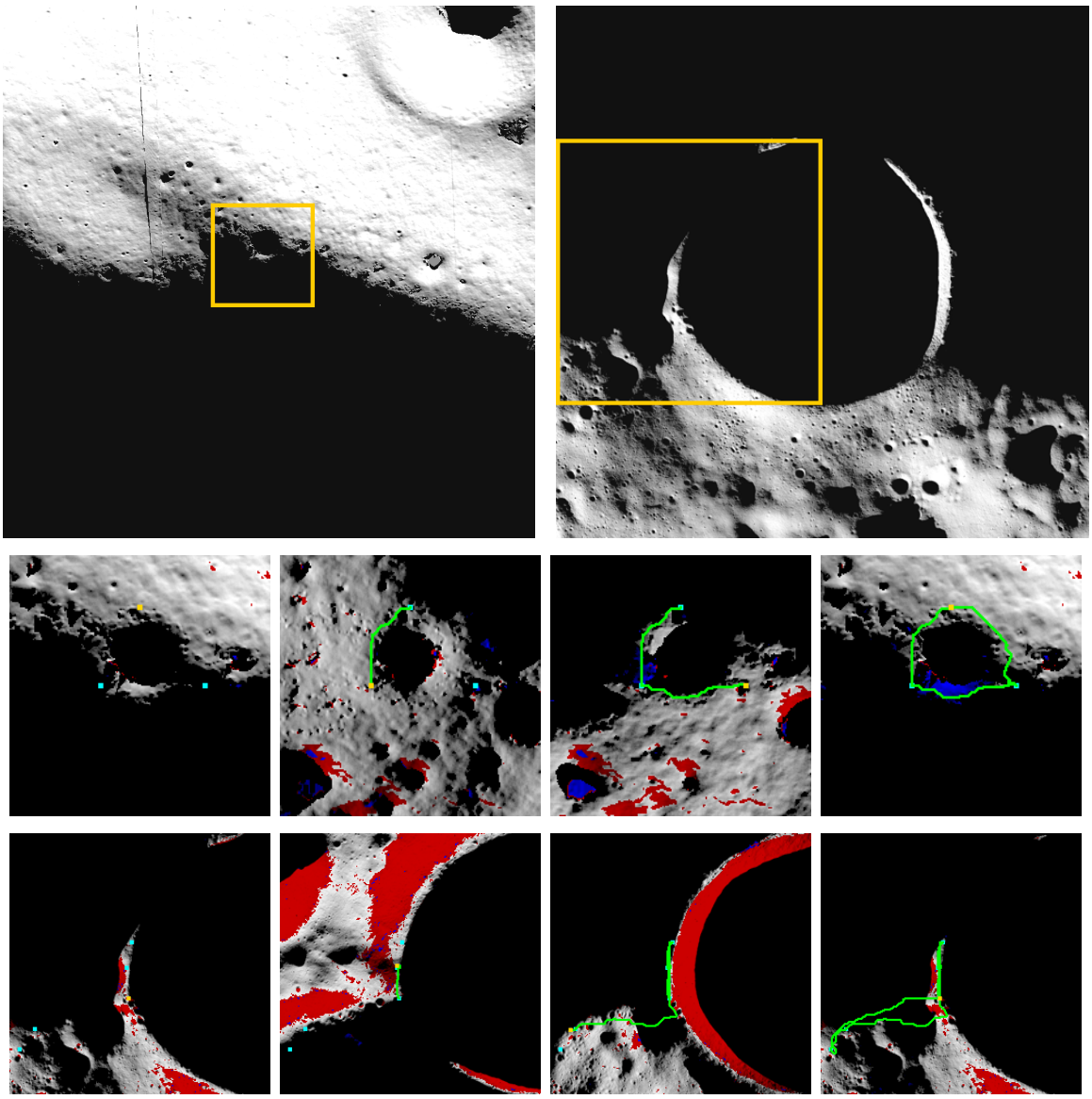

Figure 5.4: Planned route shown at several time steps during one lunar cycle for Malapert (top) and two lunar cycles for Shackleton (bottom). The leftmost image in each row indicates the area of the larger map shown in the following images. Red indicates high slope, and blue indicates disconnected regions. The route is green, and waypoints are cyan.

A* algorithm struggled to find a feasible route to the goal, the search process spent large amounts of time and resources exploring state spaces that could never lead to a solution. This was true even after connected component pruning. Because goal states include a time by when they must be reached and routes are limited by rover speed, it is possible for the search to expand states from which the goal cannot be reached in time without exceeding the speed limit. Even if there are no obstacles (shadows, steep slopes, communication outages) between the expanded state and the goal state, a rover placed at that expanded state could not reach the goal in time. As the graph search progresses, particularly if there is no feasible solution, the algorithm spends time expanding all of the remaining states until they are exhausted even though none of them can possibly be part of a viable route.

It is possible to prune away these states in one of two ways. The first method occurs at search time when a state is popped from the open list. Before the state transition function is used to generate the state's children, a simple check can be made to ensure that the parent state falls within a certain radius of the goal state, such that a route could reach the goal state in the time remaining. If the goal could theoretically be reached in time by driving in a straight line at top speed from a given state, then its children can be added to the open list; if not, no children are generated and the state is placed on the closed list. Doing this prevents additional "out of bounds" states will be added to the open list or expanded later. As the search proceeds, more of these boundary states are encountered. Once every state on this boundary has been checked and the frontier has been exhausted, the search terminates and returns failure.

The second method occurs during preprocessing before search time. In three dimensions, the boundary representing the maximum speed of the rover looks like a cone extending backward in time with its point at the goal state. The angle of the cone depends on the maximum speed. The goal state can be (potentially) be reached from states within this cone, but it is impossible to reached the goal state from outside this cone. Therefore, all state outside this cone can be pruned away prior to search. This can be done by constructing a binary array representing the shape of the cone and either passing it to the search function as an additional binary constraint or by performing a logical AND with another binary constraint map (e.g., slope and/or lighting). This will have the same effect as the first method, which is to prevent the search from spending time expanding futile states.

The portion of states that can be pruned in this fashion can be substantial depending on the relative dimensions of the search space and the maximum allowable rover speed. Observed speedups have been up to a factor of 50x; however, it should be noted that the speedup produced by this pruning technique is greatest in cases when there is no feasible path to be found. Its primary effectiveness is in reporting failures faster. In cases where a valid path exists, the speedup is typically marginal.

5.3.2 Time-Independent Waypoints

Specifying waypoints and goals with single, unique time values is both impractical and suboptimal. Typically, it is desirable to reach a location as soon as possible

so that science activities can be completed and the rover can move on to the next target. Trying to guess when to set a goal time is almost always flawed. If the time is set later than necessary, valuable time is wasted waiting for the goal state to arrive. If the time is set too early, it will be impossible to reach the goal in time even if that location is reachable at a later time. To prevent these outcomes, a method of specifying time-independent waypoints was implemented.

The method relies on two separate extensions to standard best-first search approaches such as A*, referred to here as "multi-goal" and "time-independent goal," the later of which builds on the former. Accommodating multiple goals is a common extension of A* that can be applied to achieve more flexible goals such as getting to high ground, where high ground might be defined by a large set of possible states. The first step is often to implement the search backwards, such that the goal becomes the start and the start becomes the goal. This makes defining a heuristic function that directs the search toward the goal simple, since there is now just a single goal state (the rover's starting state) instead of many. The search begins by initializing all of the goal states to the open list and then proceeding in the usual way toward the single start state. In cases using 3D spatiotemporal grids, this behavior can be achieved simply by inverting the discrete state space (world models) prior to calling the search function, passing to the search function the set of goal states in place of the starting state(s) and the start state in place of the goal state. After the search function returns an output, the output path is reversed to produce the actual path.

The role of the second extension, time-independent goal, is to take a single goal state as input and construct the complete set of allowable goals to then be passed to the multi-goal function. The set of allowable goals is defined to be all valid states that have the same position as the original goal state and a time less than or equal to that of the goal state. In this way, the time specified by the original goal state is treated as a deadline, or the last allowable time by which to reach the goal position. The original goal is a member of the time-independent goal set, since it meets the definition. All other states in the set represent reaching the same position at an earlier time than originally specified. These goal states are checked against the binary constraint maps (e.g., lighting and slope) to ensure they are valid states before being passed to the multi-goal function, which in turn calls the main A* search function.

Employing both of these extensions enables mission designers to specify a sequence of waypoints without having to specify timing requirements. Although specifying last allowable arrival times is an option, this can be omitted if desired by setting all goal times to the last time in the lighting map data being used. Not only does this approach provide more flexibility, but it also tends to produce routes that reach the goal locations sooner than if exact times had been specified. The primary drawback of this approach is one characteristic of greedy approaches: it generally produces suboptimal global solutions and may even fail to produce a feasible solution even if one exists. This can happen due to an unintended ripple effect that leads to routes failing to reach later waypoints due to becoming trapped in a dead end after greedily arriving early at previous waypoints. In some instances, a later arrival time at the previous target would have avoided this outcome.

5.4 Summary

This chapter presents a route planning method that uses connected components to enforce spatiotemporal constraints, specifically lighting and slope. As a specific example, connected component analysis was applied to 3D illumination and slope maps of the Malapert Massif and Shackleton Crater regions near the Moon's South Pole to plan multi-lunar-day routes that are continuously illuminated and of traversable slope. Sun-synchronous circumnavigation eliminates the need for hibernation through the lunar night, and constant solar power increases the amount of exploration, science, and utility that is possible. A solar-powered rover exploring environments like the lunar poles with dynamic but predictable lighting must consider not only where it needs to be to achieve its mission but also when it needs to be there. Planning capabilities that exploit dynamic sunlight enable sustained roving and exploration of the lunar poles.

Conclusions

- The South Pole of the Moon features numerous examples of multi-lunar-day sunlight routes, some of which are achievable with maximum sustained rover speed of less than 1 cm/s. Many more are possible with speeds of less than 10 cm/s.
- Deterministic grid-based graph search methods such as A* are sufficient to plan paths of moderate spatial and temporal resolution that avoid steep slopes and maintain uninterrupted sunlight for multiple lunar days.
- Connected component analysis can aid mission planning by informing the selection of waypoints that are likely to be reachable from a given starting state and eliminating a large subset of unreachable states.
- Connected component analysis can improve planner performance by pruning spatiotemporal branches of sunlit states that cannot lead to a valid solution and/or do not reach a goal mission duration.

Chapter 6

Planning for Communication

Remote communication between lunar rovers and mission operators on Earth is essential for sending and receiving commands, telemetry, and scientific data. All planetary rovers, even those with robust autonomy systems, will require periodic communication links for transmitting the data they were designed to collect. Early lunar prospecting rovers will likely feature less autonomy and will rely heavily on persistent communication for highly supervised operation if not strict teleoperation.

Although broad communication coverage could one day be provided by signal relay via assets in lunar orbit, early missions will rely on direct-to-Earth (DTE) communication, which requires line-of-sight to Earth. Lunar DTE communication coverage is limited to the near side of the Moon due to tidal locking; however, the 1.5°-axial tilt of the Moon combined with its motion around the Earth induces slight oscillations in DTE communication coverage near the poles. These conditions preclude equatorial and mid-latitude circumnavigation by rovers requiring teleoperation but enable persistent DTE communication for some polar routes.

Adding constraints on communication is only slightly more complicated than for sunlight. Performing a logical `AND` between the communication and lighting maps would leave only the states with both sunlight and Earth visibility, thus constraining routes to maintain both continuously. This turns out to be very restrictive, since the Sun circles the pole but Earth remains almost fixed in the sky due to tidal locking. Instead, routes are only required to have communication when the rover is moving. This type of constraint cannot be preprocessed and must be enforced at search time. The state transition function simply rejects all edges for which position changes without communication at both the parent and child states and keeps the rest (subject to lighting and slope constraints).

This chapter builds on the planning methods introduced in Chapter 5 by adding a constraint for constant DTE communication when the rover is in motion. Such a constraint reflects a "conservative" approach to lunar polar roving that does not permit autonomous driving. A 74-Earth-day route near Nobile Crater on the Lunar South Pole serves as a proof of concept that there exist multi-month routes that satisfy hard constraints on both sunlight and DTE communication simultaneously, *assuming* the topographic maps used to generate predictive models are sufficiently accurate. It will then be observed that such routes are potentially susceptible to

errors present in these models and that their existence may not be guaranteed. This sensitivity to model error will be addressed in Chapter 7.

6.1 Supervised Teleoperation

This section describes a common concept of operations that uses a mix of highly supervised autonomy and teleoperation referred to here as *supervised teleoperation*[1]. An example route is presented as a baseline for later comparison with a route demonstrating the concept of *strategic autonomy* (see Chapter 7).

The default concept of operations is loosely modeled after those used by NASA's Mars rovers, albeit at an accelerated cadence. The Mars Science Laboratory "Curiosity" and the Mars Exploration Rover "Opportunity" (and prior to 2010, "Spirit") are each actively managed by a team of rover operators that upload a sequence of commands no more than once per day based on previously returned telemetry and science data. Upon receiving the command sequence, each rover executes the actions (if possible) with the aid of a limited set of semi-autonomous navigation capabilities geared primarily toward hazard avoidance, transmits new data back to Earth, and awaits further instruction. This cyclical process generally repeats every 24 hours. The pace is dictated by the 20-minute average communication delay, limited solar flux to generate electric power for driving, and the length of a Martian sol. Real-time teleoperation is prohibited by high latency due to the large distance between Earth and Mars, but rover movement is highly supervised in that traverses are limited to the previous day's horizon. If the rover encounters an obstacle or situation that it deems unnavigable, it stops and awaits further instruction.

A similar approach could be used for lunar exploration but at a far more rapid cadence enabled by the Moon's proximity to Earth, greater solar flux, and lesser gravity. Command cycles could iterate every few hours or minutes instead of once per day. This pace approaches that of pure teleoperation, which is possible at slow driving speeds and with the low Earth-Moon-Earth latency of about 3 seconds. In this strategy, no unsupervised rover autonomy would be required nor permitted. The rover would operate under constant supervision with humans in the loop ready to intervene if necessary.

6.1.1 Constraints

The supervised teleoperation ("teleop") concept of operations imposes the following constraints on sunlight, communication, and terrain slope. Note that the constraints on sunlight and terrain slope are identical to those imposed in Chapter 5, with the exception of differing maximum slope values.

[1]For brevity, this document will sometimes abbreviate "supervised teleoperation" as "teleop."

Sunlight

The rover must remain in direct sunlight at all times and cannot enter or be overcome by shadow.

This constraint is constant and unconditional. Although a rover's onboard battery, depending on its size, could enable it to operate, drive, and possibly even heat itself for a limited time in the absence of sunlight, it is simpler, safer, and more conservative to impose a strict constraint to always remain in sunlight. This constraint guarantees consistent power and heating and leverages the unique character of polar lighting to extend operational life. For the work presented here, being in shadow is defined as being at any state (location and time) for which the ground is shadowed. Extensions that account for the height of the solar array above the ground are possible; however, the definition used here provides a reasonable and conservative approximation. Prior related work also indicates the benefit of elevating a solar array may be relatively minor, even at a height of 10 meters [33], which is impractical for mobile robots.

Communication

The rover must maintain an unobstructed view of Earth at all times during which it is driving.

This constraint is conditional, as it is only active when the rover is moving. The proximity of Earth and the Moon enables a level of control not possible for Mars. The opportunity for near real-time communication invites a seemingly prudent approach that not only takes advantage of constant supervision but mandates it. Direct line-of-sight to Earth is treated as equivalent to DTE communication availability. The models used here represent the states for which the Earth's center point is visible, but this can be easily extended to specific locations of Deep Space Network (DSN) antennae, LEO assets, or other communication infrastructure.

Slope

The rover must remain on terrain of principal slope not exceeding 20 degrees.

This value was chosen such that it would not dominate route planning in the following examples. In practice, this constraint is dependent on the mobility platform and could be higher or (most likely) lower. A mild Gaussian smoothing function was applied to the lunar DEM before computing slope to mitigate the negative effects of obvious artifacts in the data. The use of principal slope instead of directional slope is justified by the 20-meter resolution of the models. Because rover-scale obstacles are not visible at this resolution, side-sloping rovers may occasionally be required to traverse in the direction of maximum slope to avoid a hazard. Limiting principal slope instead of directional slope is therefore conservative.

6.1.2 Planning Method

The gridded lunar model representations described in Section 4.1 are conducive to grid-based planning methods. The distinctions of sunlight, communication, and slope

yield a planning problem with heterogeneous constraints. Enforcing a constraint on slope is the simplest, since it is defined by a static 2D map of binary go/no-go conditions. Enforcing a constraint on sunlight is similarly simple, with the only difference being that the map is dynamic, represented by a 3D binary array composed of stacked 2D maps for each time step. The communication condition must be enforced at planning time, since it is conditional on whether or not two consecutive rover states share the same spatial position. For two graph nodes of differing positions to be legally connected by an edge, both must have communication coverage (and sunlight). Sunlit nodes of identical position are connected along the time dimension, regardless of communication coverage, since it is permissible to remain stationary without communication as long as sunlight persists. This conditional constraint is straightforward to implement in the state transition function (which generates child nodes) of any standard heuristic graph search algorithm.

To generate the following example route, a starting point was selected based on favorable landing site criteria, and several major waypoints were manually selected such that the rover would visit numerous sites of scientific interest near PSRs. A minimum distance path passing through all waypoints was generated using A* graph search on a 3D adaptation of an eight-connected grid (see Chapter 5 for details). This was done first at a resolution of 80 meters to generate a coarse route. Then the coarse route was refined to a resolution of 20 meters using the 80-meter route sequence as waypoints for a second iteration of A*. This hierarchical approach was used to reduce computation time.

6.1.3 Example Route

The baseline teleop route is illustrated by a series of snapshots in Fig. 6.1. Each frame represents only a single instant in time; however, each path represents the full route history up to that point. Hence, *green* path overlaid on top of *black* or *blue* ground does not indicate that the rover passed through shadow, only that a visited location later became shadowed. The route covers approximately 63.5 kilometers in 74 Earth days without exceeding 10 centimeters per second. It returns to its starting point after each of three laps, or drives, to wait out the communication blackout. Dwelling at this local peak, dubbed a *singularity*, is the only apparent means of achieving three lunar days of solar-powered exploration under the given constraints.

6.2 Route Analysis

This section utilizes the visualization technique introduced in Chapter 4 to help analyze the supervised teleoperation route and draw conclusions about its actual feasibility given limitations of model accuracy.

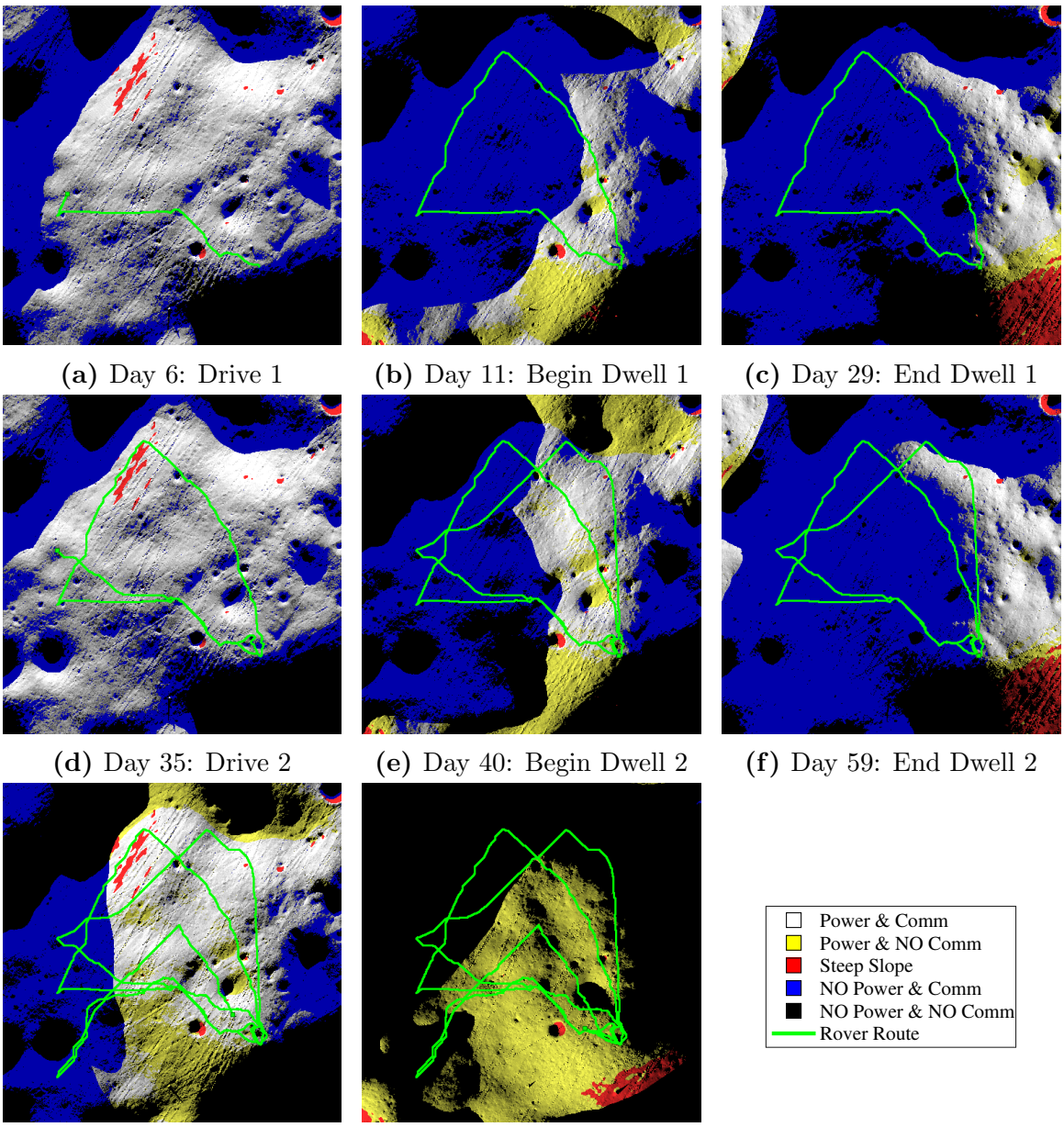

(a) Day 6: Drive 1 **(b)** Day 11: Begin Dwell 1 **(c)** Day 29: End Dwell 1

(d) Day 35: Drive 2 **(e)** Day 40: Begin Dwell 2 **(f)** Day 59: End Dwell 2

(g) Day 67: Drive 3 **(h)** Day 74: End Route

Figure 6.1: *Supervised Teleoperation*: This sequence of snapshots illustrates a 3-lunar-day route near Nobile Crater. The triangular shape of each circuit is due to intermediate waypoints placed at the vertices of the triangle. The route starts in the bottom-right quadrant and proceeds in a clockwise fashion with a long dwell period at a singularity near the starting point between each of the three drives. The rover is stationary from Day 11 (**b**) to Day 29 (**c**) and from Day 40 (**e**) to Day 59 (**f**) due the communication constraint. It theoretically maintains uninterrupted solar power near the edge of the terminator while dwelling, but this is uncertain. The terrain is color-coded by constraint conditions.

6.2.1 Visualizing 3D Route Constraints in 2D

This section revisits a novel method for visualizing three-dimensional spatiotemporal routes in two dimensions. The route's spatial proximity to an ordered set of dynamic constraint conditions is viewed as a function of time. This 2D projection is useful for visualizing, analyzing, and comparing routes, particularly where 3D formats (e.g., videos) are not possible. Furthermore, this technique reveals the risk associated with dwelling at singularities.

This 2D graphical representation was inspired by weather radar history graphs and can be explained using that analogy. A video playback of weather radar can be condensed from three dimensions to two by plotting the distance from a given location (e.g., a city center) to the nearest storm front in any direction for all times. An even richer representation can be constructed by plotting the most severe weather condition that occurs a specific distance away (in any direction) for all distances with a given range and for all instants over a span of time. Essentially, this type of graph displays the minimum distance to the worst case conditions as a function of time. A similar graph can be constructed for a moving vehicle instead of a static point, where distances are relative to the vehicle's instantaneous position. Rover constraints (e.g., sunlight, communication, slope, and combinations thereof) can be substituted for weather conditions as long as they are ordered by severity.

Applying this concept to the teleop route yields the graph shown in Fig. 6.2. The y-axis represents time and advances downward like a strip chart. The x-axis marks distance from the rover's instantaneous position, which is indicated by a vertical green line. Distances are relative and can be in any direction. Each row of the plot represents a snapshot of the dominant constraints at each distance from the rover's position at that instant in time. To the right of the green line is the worst-case condition at every distance, analogous to the distance outside the storm's edge. To the left of the green line is the best-case condition at every distance (distance inside the storm's edge). The precedence of the color-coded conditions match that of Fig. 6.1 and are in order of increasing severity: white (power & comm), yellow (power & no comm), red (steep slope), blue (no power & comm), black (no power & no comm).

6.2.2 Computational Method

The graph is computed one row at a time. Distance is discretized into uniform bins, each defined by two radii. For example, at a distance of $d = 100$ meters with a resolution of 20 meters, $r_1 = 90$ meters and $r_2 = 110$ meters. All unique constraint conditions lying within the ring formed by the two radii are isolated. The most severe condition within that subset is plotted at distance d, and the least severe condition is plotted distance $-d$. This is repeated for every distance to complete the first row and for every row to complete the graph.

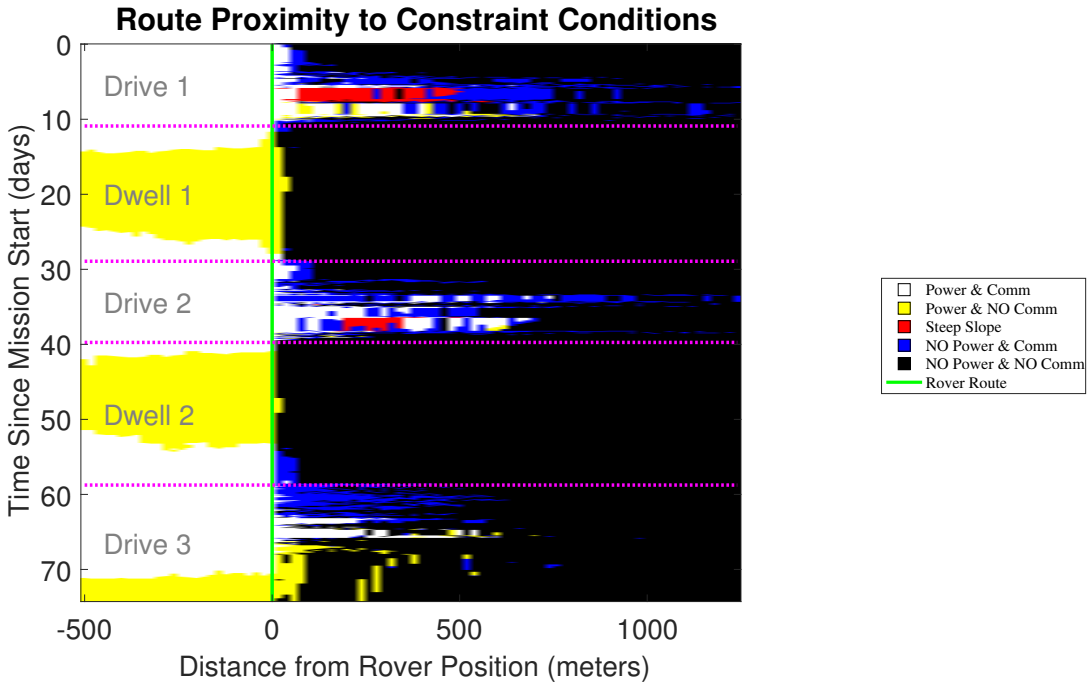

Figure 6.2: This graph shows the proximity of the teleop route to the best- and worst-case constraint conditions as a function of time. The vertical *green* line at 0 represents the relative position of the rover's planned path. On the right side of the *green* line is the most dominant constraint at every distance from the rover's position. On the left side is the least dominant constraint. The horizontal *magenta dotted* lines mark when the rover arrives at and departs from the singularity. See Fig. 6.1 for color-coding.

6.2.3 Interpretation

The proximity graph efficiently conveys useful information about the route plan and reveals potential concerns. By examining Fig. 6.2, it is clear that rover spends two periods of nearly 20 days each within 10–30 meters of total blackout from sunlight. This happens when the rover is parked at a singularity as the terminator rotates about the peak. During this time, the rover is not permitted to move due to communication denial. The accuracy of individual LOLA ground points is approximately 10 meters radially and 50–100 meters spatially [20], and gridded LOLA DEMs contain a myriad of visible artifacts. Because the DEM contains errors of up to 50–100 meters, the location of this single point of light may vary significantly, or it may not even exist. Either case could strand the rover in darkness and cold for weeks, likely ending the mission before communication is restored.

6.3 Summary

This chapter extends the method of planning for sunlight to also plan for communication. Spatiotemporal models of DTE communication availability are generated in a similar fashion to models of sunlight. Enforcing a strict constraint for 100% communication coverage simultaneously with 100% sunlight is overly restrictive and eliminates the possibility of sustaining polar roving for multiple lunar days. Instead, a communication constraint is enforced only when the rover is in motion, and the rover is permitted to remain stationary without view of Earth so long as it retains uninterrupted sunlight. This combination of constraints is implemented using an A* graph search approach.

The combination of constraints on continuous sunlight and drive-time communication tends to force routes to local peaks to wait out extended communication blackouts. These peaks are dubbed *singularities* due to their apparent rarity, small size, and pivotal effect on route planning. Although proof-of-concept routes can be generated that achieve three lunar days of mobile exploration, they do so by dwelling at singularities for weeks at a time within 10–30 meters of total darkness. Model error on the order of 50–100 meters suggests that dwelling at these singularities in an unreliable means of sustaining lunar polar roving.

Conclusions

- There exist on lunar South Pole spatiotemporal routes lasting multiple lunar days that maintain uninterrupted direct sunlight and feature a direct line-of-sight to Earth at all times when the rover is in motion.
- Polar routes that enforce hard constraints on both sunlight and direct-to-Earth communication when moving tend to dwell at local peaks for weeks at a time due to a lack of autonomous driving capabilities.

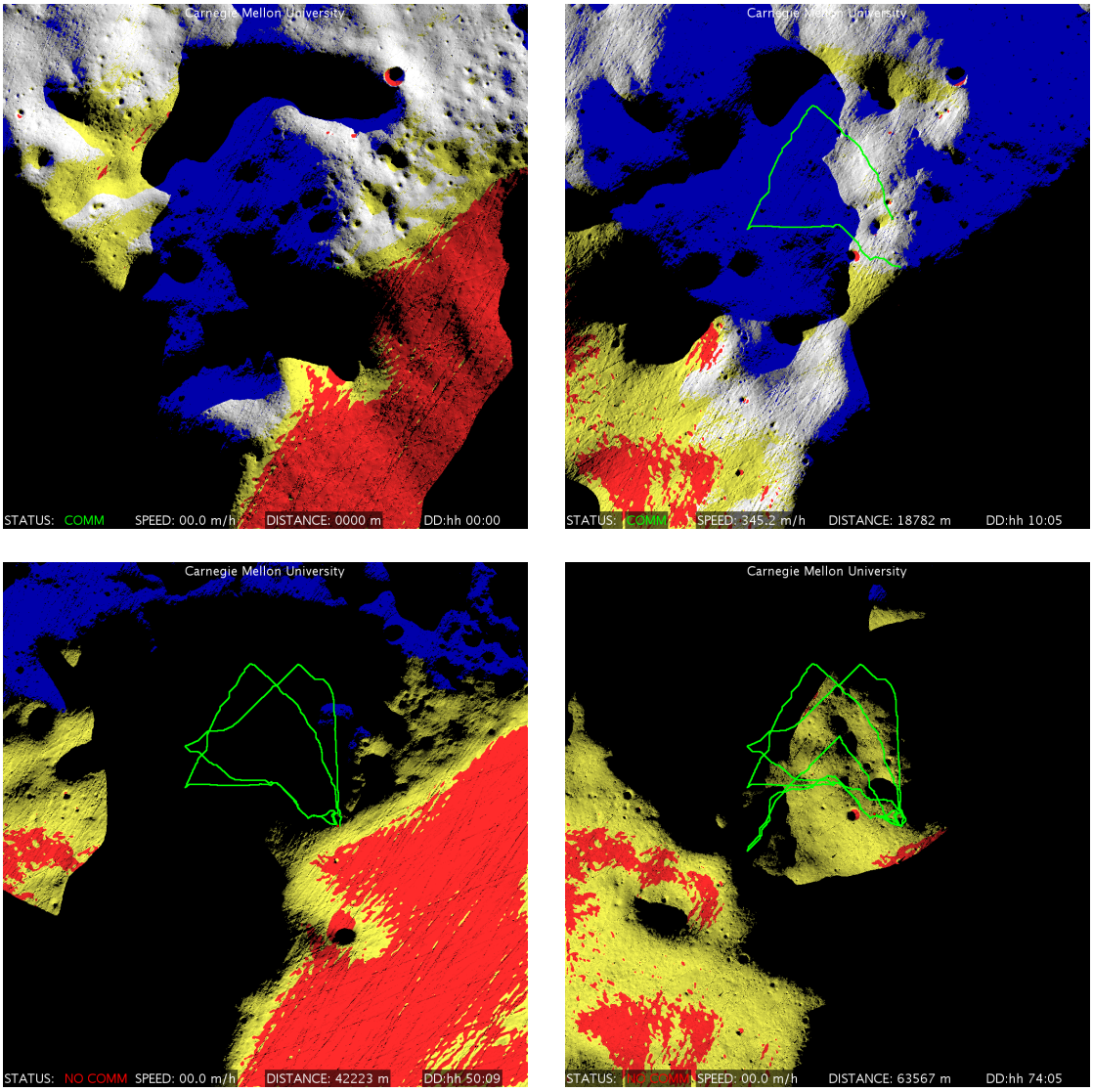

Figure 6.3: *Nobile route.* This route on the Nobile Crater rim near the South Pole of the Moon demonstrates a prolonged solar-powered traverse that spans 74 Earth days (2.5 lunar days) and features continuous sunlight, drive-time communication with Earth, and a maximum slope of less than 20 degrees. The terrain is colored as follows: **White** = sunlight and communication, **Yellow** = sunlight only, **Blue** = communication only, **Black** = neither sunlight nor communication, **Red** = slopes steeper than 20 degrees, **Green** = rover traverse. From left to right, top to bottom, the times relative times shown are 0, 10, 50, and 74 Earth days from the route's initial state.

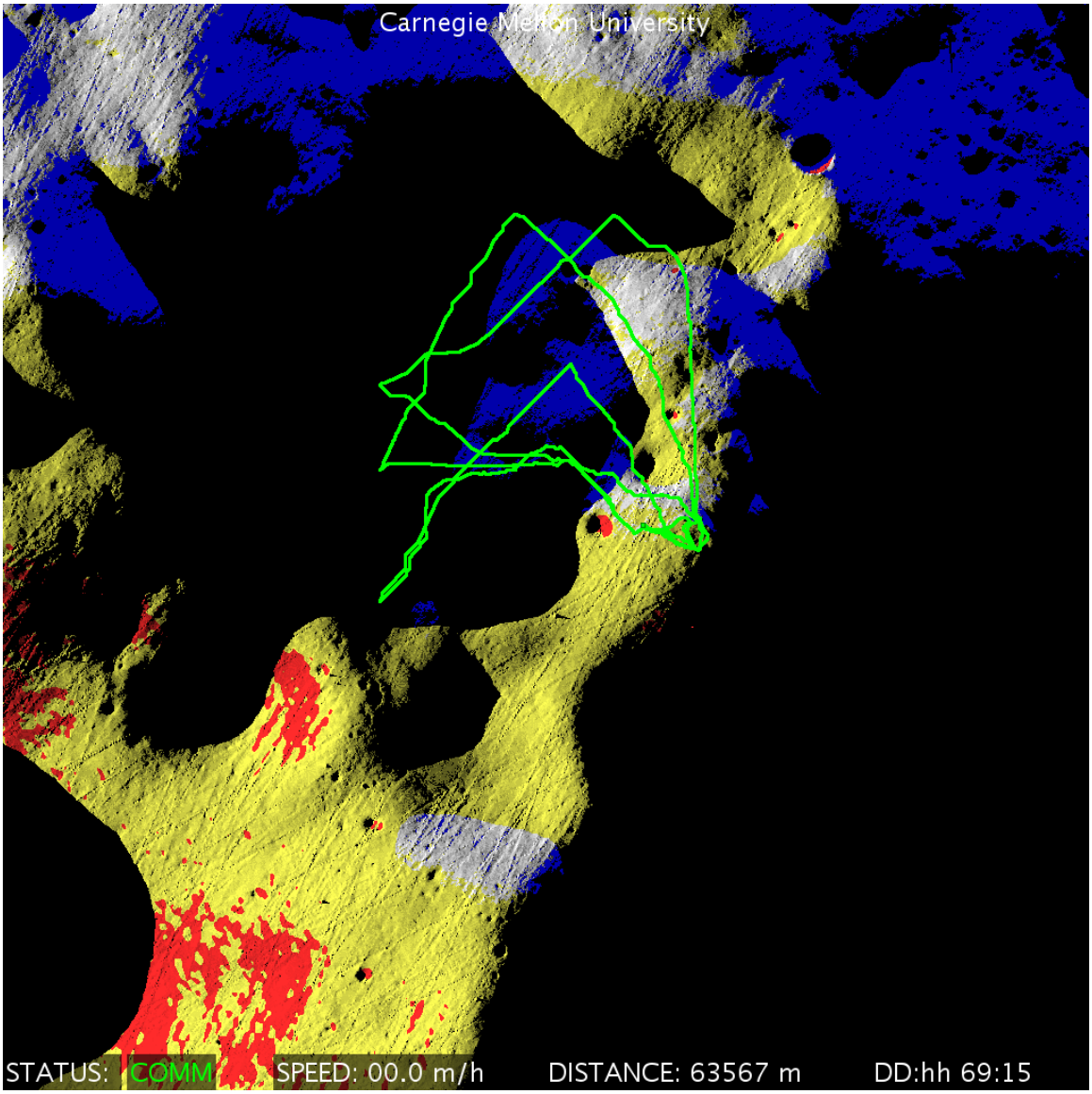

Figure 6.4: This is a larger view of the same Nobile route shown in Figure 6.3 with the same color-coding of terrain. The time shown is Earth day 69 out of 74. The route begins and ends near the farthest bottom-right corner of the path indicated in green and completes three full circuits over three lunar days in a clockwise direction. The rover dwells in sunlight during communication outages at the local peak located near the start and end points.

Chapter 7

Planning for Uncertainty

The combination of polar sunlight and direct-to-Earth communication coverage makes supervised teleoperation especially susceptible to lunar model uncertainty. Teleoperated sun-synchronous rovers are constrained to drive only when in direct view of both the Sun and Earth. The temporality of DTE communication coverage at the lunar poles is more subtle than that of Sun coverage, but it is still consequential. Due to tidal locking, only one hemisphere (the "near side") of the Moon ever faces Earth; however, lunar libration induces subtle dynamic effects most apparent at the poles. Whereas the Sun clocks around the lunar poles as the Moon rotates about its axis, the Earth oscillates just above and below the horizon as the Moon wobbles. Metaphorically, polar sunlight spins while polar communication ebbs and flows. This distinction creates a disparity between the angular distributions of sunlight and Earth view over time, illustrated in Fig. 7.1.

As the Earth sets below the horizon, teleoperated sun-synchronous rovers are forced to dwell, sometimes for weeks, at local peaks of persistent sunlight while waiting for the Earth to rise again. Prominent locations where this is possible—dubbed *singularities* in this research—are small and rare. Predicting the existence, size, and precise locations of singularities is highly sensitive to uncertainty in predictive models of sunlight and communication coverage. This uncertainty stems from measurement error in LOLA ground points as well as artifacts present in lunar DEMs based on LOLA data.

This chapter highlights some specific sources of error and uncertainty in lunar models and proposes a new mission concept called *strategic autonomy* as a means of planning for this uncertainty. Unlike supervised teleoperation, strategic autonomy permits rovers to execute short, slow, preplanned drives autonomously during communication blackouts. The major benefit of these autonomous drives is that they increase the rover's distance from predicted shadow boundaries and increase confidence in sustained solar power. In this way, the objective of strategic autonomy is to reduce overall risk for sun-synchronous lunar polar missions. Beyond the special case of avoiding singularities, Section 7.3 suggests potential approaches to quantify risk and route sensitivity to address planning for uncertainty in lunar models more generally.

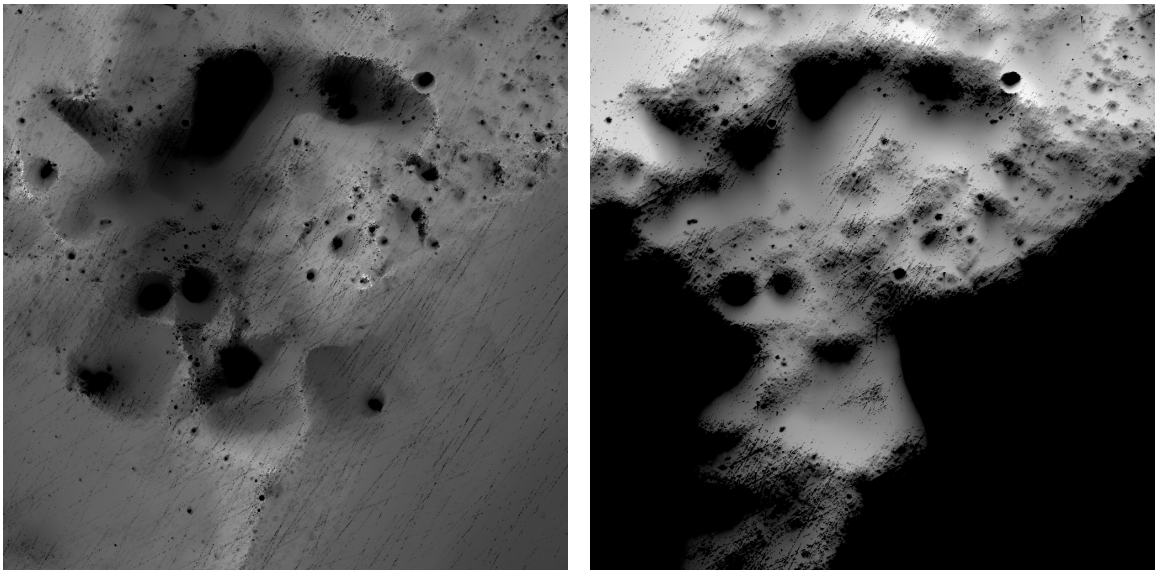

(a) Average Sunlight Exposure **(b)** Average DTE Communication Coverage

Figure 7.1: Average illumination (**a**) and communication (**b**) coverage over a 4-month period of a 20-by-20-km area on the rim of Nobile Crater near the Lunar South Pole. Brighter values indicate greater cumulative exposure: *white* indicates 100%, *black* indicates 0%. Note the omnidirectional distribution of sunlight, which clocks around the pole, compared to the unidirectional distribution of DTE communication, which is only available on Earth-facing slopes. These conditions contribute to polar *singularities*.

7.1 Sources of Error and Uncertainty

This research uses predictions of future lighting generated using lunar DEMs, lunar and solar ephemeris data, and ray-tracing software. The DEMs are a data product of LRO's LOLA instrument.[1] The highest resolution LOLA DEM that covers the South Pole out to 85°S (including the Nobile Crater region studied in this chapter and Chapter 6) is 10 meters per pixel [22]. This 2.5D elevation model, shown in Fig. 7.2, was converted into a 3D mesh model in Cartesian coordinates, and a simulated Sun[2] was positioned according to the SPICE toolkit [85]. Ray-tracing software renders an orthographic map of lighting conditions for each time in a predefined sequence. The result is a 3D binary array that defines each (x, y, t) state as either lit or shadowed. The same process was used to estimate communication coverage by substituting the Earth's position for the Sun's.[3] Principal ground slope was computed by applying divided difference to the DEM. The models used in this chapter (and the last) have a spatial resolution of 20 meters and a temporal resolution of approximately 2 hours.

The resolution and accuracy of LOLA data is orders of magnitude better than what was available prior to LRO [19]; however, uncertainty remains an issue. The

[1] LRO data products are accessible via NASA's Planetary Data System Geosciences Node [73, 74].

[2] The Sun can be approximated as a directional or area light source. The latter yields a range of solar flux values, which can be thresholded to produce a binary output for planning purposes.

[3] Since radio waves behave differently than visible light, this yields a slightly optimistic estimate.

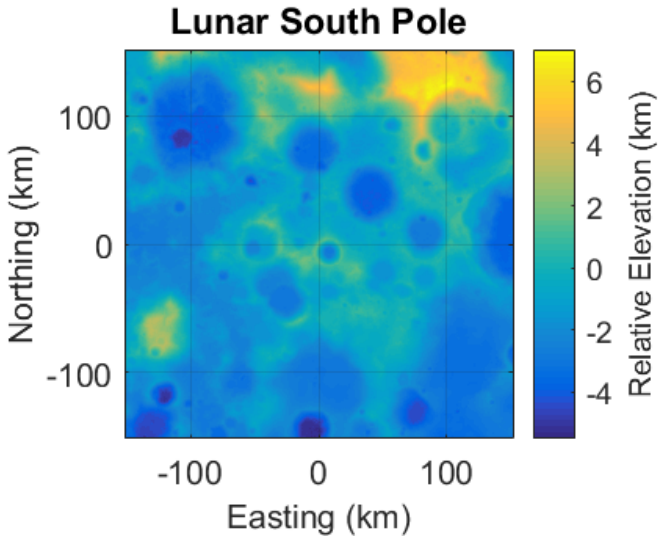

Figure 7.2: This 10-meter LOLA DEM covers the Lunar South Pole out to approximately 85°S (at the map sides' midpoints). The Nobile Crater rim is among the peak elevations. The area studied is located at approximately 90 km Easting and 110 km Northing in this projection.

accuracy of individual LOLA ground points is approximately 10 meters radially and 50–100 meters spatially [20], and gridded LOLA DEMs contain a myriad of visible artifacts. In low-angle lighting, these errors are magnified, resulting is substantial uncertainty about the exact location of sunlight–shadow boundaries. This uncertainty makes operating, and especially dwelling, near shadow boundaries risky.

7.2 Strategic Autonomy

The concept of strategic autonomy is motivated by concerns of dwelling at uncertain singularities, a side effect of supervised teleoperation constraints (see Chapter 6). This new operational concept seeks to reduce overall mission risk by distancing the rover from singularities (akin to the way robotic manipulators avoid kinematic singularities) and shadow boundaries. This comes at the cost of some accepted added risk related to unsupervised autonomy during communication outages. This thesis asserts that this tradeoff is beneficial.

7.2.1 Singularities

Solar-powered lunar rovers can achieve months of exploration by following sun-synchronous polar routes to maintain continuous sunlight for power and heating while avoiding prolonged exposure to extreme cold. These routes favor peak elevations at high latitudes and could be accomplished with slow driving speeds as low as 0.1 cm/s, as shown in Chapter 5. Such routes are intriguing because of their extended durations and their proximity to areas of scientific and commercial interest. Planning reliable

sun-synchronous routes prior to launch requires detailed predictive models of future lighting conditions based on lunar elevation models. The resolution and accuracy of predictive insolation models is limited by error in the underlying elevation models. The inherent uncertainty of lunar topography data leads to uncertainty that rovers following preplanned sun-synchronous routes will actually remain in continuous sunlight. The magnitude of this uncertainty is a function of the planned route's proximity to shadow boundaries, which is strongly influenced by the strictness of a mission's requirement for rover-to-Earth communication.

An ostensibly conservative strategy permits rovers to drive only when in direct communication with ground controllers to facilitate teleoperation and/or highly supervised autonomy (see Chapter 6). Sans satellite relay, rovers would be required to maintain an unobstructed view of Earth when driving. This strict requirement severely constrains rover movement and can force rovers to dwell motionless near the day–night terminator for weeks at a time to achieve multiple lunar days of operation. Locations of enduring sunlight must be reached prior to losing Earth communication, which must later be reestablished before driving can resume.

At the Nobile Crater rim, such locations are so small and rare that they effectively behave as single points or *singularities*, through which all valid routes must pass. It is reasonable to expect similar characteristics at other polar sites because of the common patterns of DTE communication coverage and polar sunlight. Whereas the Sun repeatedly circles the lunar pole illuminating all longitudes evenly, the Earth oscillates only a few degrees along a single longitude. This results in extended periods with little to no overlap between sunlight and communication coverage. If rovers are not permitted to move without constant DTE communication, then they are forced to dwell at a peak of persistent sunlight.

Due to the uncertainty of predicted insolation maps given current lunar orbital data, the existence of reachable singularities where communication blackouts can be safely waited out in continuous sunlight cannot be guaranteed. A mission dependent on dwelling at a presumed singularity that turns out not to exist will almost certainly terminate prematurely. Although real singularities might enable solar-powered missions with a strict requirement for communication when driving to achieve multiple lunar days of operation, the uncertainty of such phenomena makes them unreliable as a means to that end. Rather than reducing overall mission risk, this "conservative" strategy may ultimately increase the odds of failure.

This chapter proposes an alternative strategy for achieving sustained lunar polar rover missions. In the absence of DTE communication, *strategic autonomy* permits short, slow, autonomous drives following preplanned paths in areas adjacent to singularities to improve the probability of continuous sunlight. Under this new mission concept, the majority of a rover's distance traveled could still be teleoperated and highly supervised. The key difference is that in situations where a communication blackout is inevitable, the rover would be liberated to drive autonomously to increase its predicted distance from shadow and thus increase its expectation of solar power. While the limited use of unsupervised autonomy does incur some additional risk, it is outweighed by improved confidence in uninterrupted sunlight. The adoption of strategic autonomy for sun-synchronous lunar polar roving could substantially reduce

overall risk and enable greater mission durations and returns.

7.2.2 Constraints

Strategic autonomy is defined by the following constraints. Constraints on sunlight and and principal terrain slope are identical to those enforced by the supervised teleoperation concept (Section 6.1.1).

Sunlight

The rover must remain in direct sunlight at all times (same as teleop).

Communication

The rover must maintain an unobstructed view of Earth when driving except when doing so would cause the rover to dwell at a singularity for a period of time exceeding 24 hours. In this case, the rover is permitted to drive autonomously without communication at 20% of the nominal maximum drive speed.

This is the key distinguishing feature of the strategic autonomy concept of operations. This modified constraint prevents the rover from dwelling motionless at a singularity for long periods of time. Instead, the planner is free to maximize the rover's distance from shadow and thus confidence of sunlight.

Slope

Principal terrain slopes must not exceed 20 degrees (same as teleop).

7.2.3 Planning Method

The planning method begins by generating a baseline route using the supervised teleoperation constraints and modifies discrete route segments according to the strategic autonomy communication constraint. For the example provided, the baseline is the route presented in Section 6.1.3. Singularities are identified manually with the aid of the 2D constraint proximity graph (Fig. 6.2), but in the future this step could be automated. Each route segment that dwells at a singularity is defined by two timestamps representing the first and last time steps of the dwell.

At the instant the rover reaches an identified singularity, the altered constraints are activated. A small set of new waypoints are selected (manually for this example; but again, this could be automated) to approximately maximize distance from darkness and steep slopes such that the new route segment splices into the original route at the instant the original dwell would have ended. Minimum-distance paths passing through all new waypoints are computed using the same A* method as in Chapter 6 but with reduced maximum drive speed (from 10 to 2 centimeters per second) and while suspending the requirement for communication.

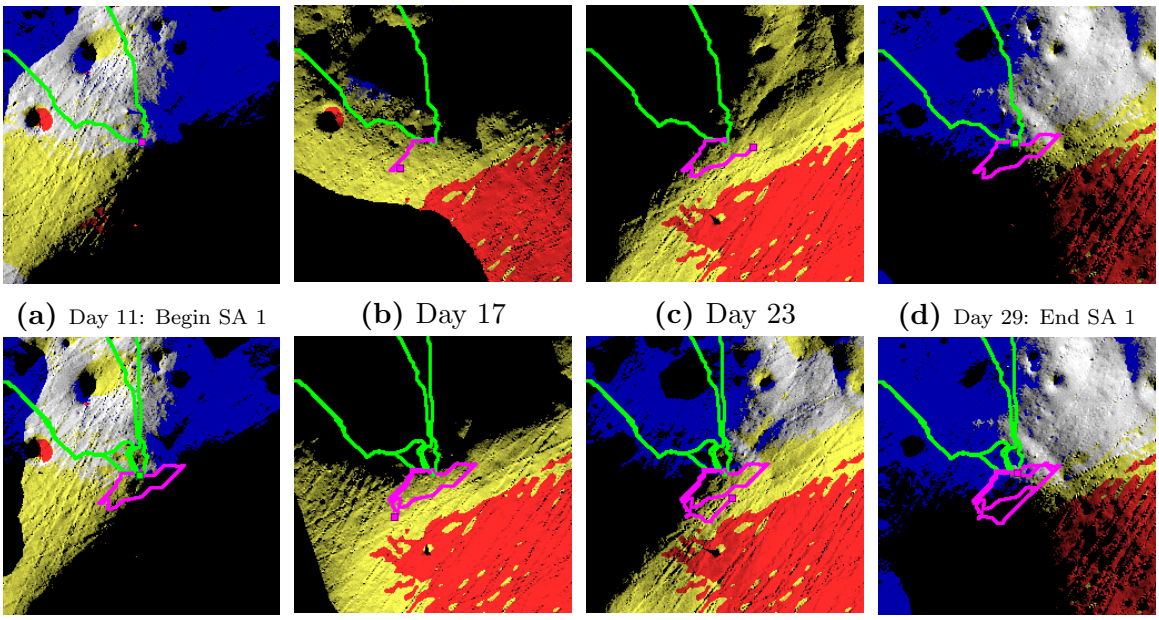

(a) Day 11: Begin SA 1 **(b)** Day 17 **(c)** Day 23 **(d)** Day 29: End SA 1

(e) Day 40: Begin SA 2 **(f)** Day 50 **(g)** Day 55 **(h)** Day 59: End SA 2

Figure 7.3: *Strategic Autonomy (SA)*: This sequence of snapshots (zoomed in relative to Fig. 6.1 and centered at the route's starting point/singularity) illustrates the two autonomous route segments that differ from the baseline teleop route. The top row (**a**–**d**) replaces first teleop dwell period, and the bottom row (**e**–**h**) replaces the second teleop dwell period. The autonomous drive segments are drawn in *magenta*, whereas unaltered route segments are *green*. See Fig. 6.1 for terrain color-coding.

7.2.4 Example Route

Using this method, two instances of dwelling at singularities were identified in the baseline route. These were replaced with two new route segments. The altered route segments, which exhibit strategic autonomy, are shown in Fig. 7.3. All other route segments remain unaltered and are identical to those in Fig. 6.1. Note that the first autonomous segment occurs between the first and second drive segments of the baseline route, and the second autonomous drive segment occurs between the second and third drive segments of the baseline route. Like the teleop baseline, the full strategic autonomy route spans 74 Earth days but covers a greater total distance of 71.8 kilometers, an 11.5% increase compared to the teleop route. The resulting constraint proximity graph is shown in Fig. 7.4.

7.2.5 Discussion

Notable differences between the supervised teleoperation and strategic autonomy routes are shown in Table 7.1. Most notable is the increased mean distance to shadow. Whereas the teleop route dwells approximately 10 and 30 meters from the nearest shadow (the day–night terminator) the corresponding strategic autonomy route segments achieve a mean separation of approximately 180–190 meters. On a 20-meter

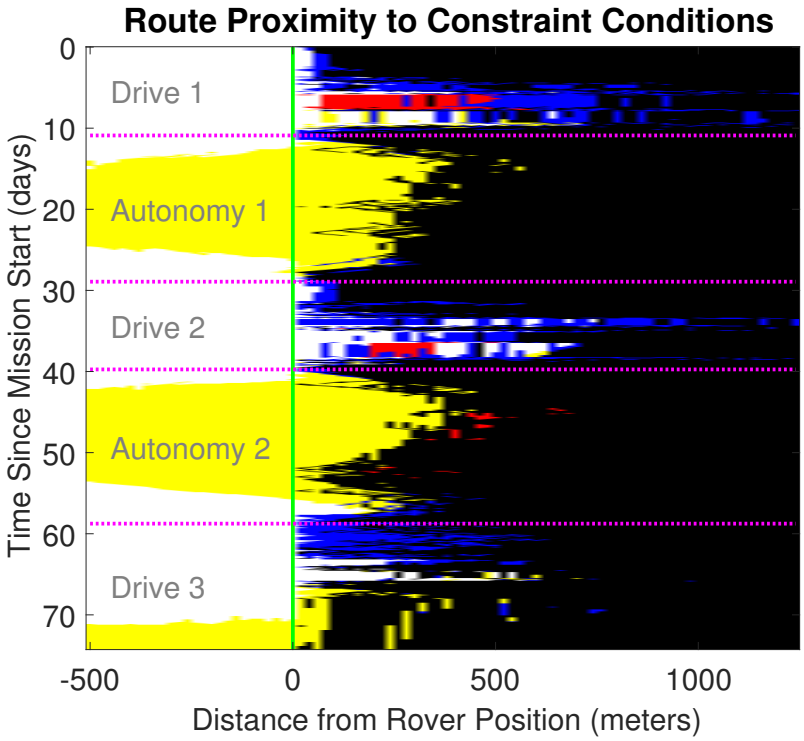

Figure 7.4: This visualization shows the proximity of the strategic autonomy route to the best- and worst-case constraint conditions as a function of time. The vertical *green* line at 0 represents the position of the rover as it traverses the planned path. This plot should be interpreted in the same manner as Fig. 6.2. Likewise, constraints are color-coded as in Fig. 6.1. The large *yellow* areas to the right of the *green* line indicate a wide margin of predicted sunlight in all directions around the rover.

lighting model, this is the difference between 1–2 pixels and 9–10 pixels. This difference becomes even more significant when considering that the LOLA topography models have an estimated spatial accuracy of 50–100 meters. If this translates to an error of up to 100 meters, the supervised teleoperation route is problematic, whereas the strategic autonomy route should still retain a safety margin of almost 100 meters. Compared to dwelling at uncertain singularities, this added buffer substantially increases the likelihood of maintaining solar power and continued exploration.

Strategic autonomy is not without drawbacks. Its reliance on unsupervised autonomous driving, even at very slow driving speeds, incurs some added risk. The total magnitude of this risk depends on numerous complex factors related to the rover's perceptual, computational, and mechanical design and is not easily estimated or quantified, particularly without rigorous practical testing of the actual systems. However, the high level of risk inherent to dwelling at an uncertain, unverified singularity the size of which is less than the estimated error of the models used to predict such a point likely exceeds that of short, slow, autonomous drives preplanned to favor regions of almost certain sunlight. Quantifying this tradeoff is left as a suggested

Table 7.1: Route Segment Comparison

Route Segment	Total Time (days)	Dwell Time (%)	Distance Traveled (km)	Max Speed (cm/s)	Mean Speed (cm/s)	Min Dist. to Shadow (m)	Max Dist. to Shadow (m)	Mean Dist. to Shadow (m)
Dwell 1	18	100	0	0	0	10	50	29
Dwell 2	19	100	0	0	0	10	30	12
Autonomy 1	18	36	4.1	1.5	0.26	10	390	191
Autonomy 2	19	38	4.2	1.6	0.26	10	370	178

Dwell: supervised teleoperation dwell segment; **Autonomy**: strategic autonomy drive segment

avenue of future work.

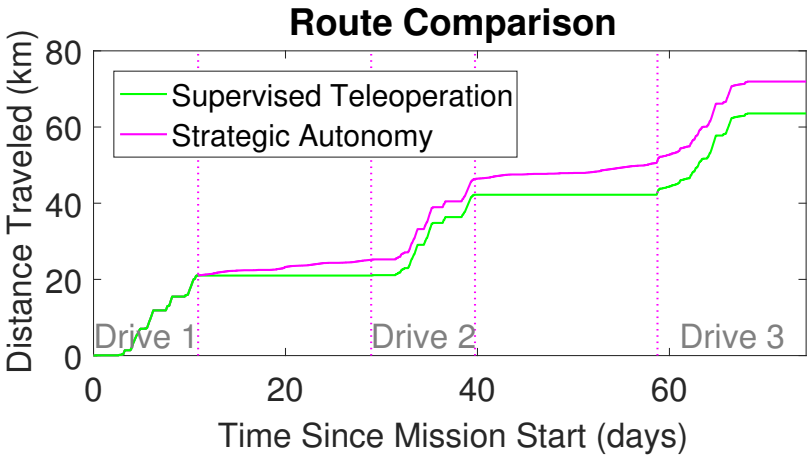

Figure 7.5: The supervised teleoperation route dwells statically at singularities while the strategic autonomy route continues driving to avoid them. Vertical lines mark the start and end of the two dwell/autonomy segments corresponding to Table 7.1. The three segments labeled "Drive" are identical between the two routes.

7.3 Quantifying Risk and Route Sensitivity

Robotic missions to extraterrestrial environments exercise extreme caution and prioritize risk reduction and safety. To this end, it is important to estimate risk when planning rover traverses and, if possible, minimize that risk. Rovers following preplanned routes that are low-resolution relative to the scale of the rover (for example, routes defined on a 10–20 meter grid relative to a 1–2-meter-long rover) are at risk of encountering unanticipated obstacles and hazardous terrain that force the rover off its intended course. In most cases, the rover's onboard hazard avoidance and autonomous motion planning should be able to circumvent local hazards and return the rover to it planned route. It is possible, however, that seemingly small perturbations to the rover's path cascade into catastrophic missteps from which the rover cannot recover. For example, this could happen if the rover unexpectedly cannot cross a

narrow ridge between two steep slopes to gain access to another region, if circumventing numerous small obstacles causes cumulative delays that prevents the rover from staying ahead of the shadows, or if a planned dwell at an predicted singularity turns out to be nonviable. Such scenarios indicate that the preplanned route is sensitive to uncertainty. Although it is a goal of this research to plan polar traverses that are robust to this kind of uncertainty, this thesis stops short of quantifying risk and route sensitivity due to uncertainty. This topic is instead suggested as a compelling avenue of future work.

A possible next step in addressing planning for uncertainty is to develop a means to estimate the robustness, or sensitivity, of planned routes to uncertainty caused by the limited resolution of terrain maps and measurement errors they may contain. A Monte Carlo simulation approach could be used to estimate route robustness. Monte Carlo simulations estimate an unknown quantity by simulating an event many times and then using the cumulative results to derive an estimate that converges to the true value as the number of iterations approaches infinity [86] (provided that the simulation accurately reflects reality). For estimating risk associated with sustained lunar polar roving, high-resolution terrain maps must be simulated. This could be done by applying bicubic interpolation to an LRO DEM to upsample to the necessary resolution, adding Gaussian noise to this DEM, and then applying a statistical model to distribute small rocks and craters on top of the DEM. Alternatively, a fractal terrain generation algorithm could be employed [87], using the LRO DEM as a seed. The result will be a simulated high-resolution representation of what the actual lunar terrain along the rover's path might reasonably look like. A simulated executor could then attempt to "drive" a simulated rover along its planned traverse, circumventing hazards whenever necessary. Each instance of the simulation will either succeed (if the rover accomplishes all planned activities and reaches the final goal state) or fail (if it does not). This process can then be repeated, each time using a new simulated version of the same terrain. Each time the process is repeated, the result is recorded. As the number of iterations grows, the fraction of total attempts that are successful should converge to some value between 0 and 1. This value can be interpreted as a measure of that particular route's robustness to terrain map error. Executing a procedure like this for a sufficiently large number of iterations will likely require implementation of a distributed cloud computing platform.

Once route sensitivity/robustness has been estimated for a variety of different routes, it may be possible to apply lessons learned to improve planning for uncertainty. Heuristics might be developed that can be incorporated into the traverse planning system. These might be applied directly to resource maps (e.g., lighting maps) prior to plan time or incorporated into the path planning algorithm(s) in the form of altered constraints or cost functions. For example, to decrease the risk of the rover falling behind the Sun and being overtaken by shadow, it is possible that either the lighting map could be altered to provide an added buffer to shadows in the time dimension, or an added constraint could enforce the same added buffer at plan time. Such a buffer is likely to improve robustness and decrease sensitivity of planned routes, thereby reducing overall mission risk, but a naive solution may also be overly restrictive in terms of capability.

In addition to uncertain surface geometry, solar-powered traverses planned on the ground prior to launch may be sensitive to errors in simulated sunlight and communication availability. A simplistic way to estimate this sensitivity is to add noise directly to the lighting maps by expanding shadows and shrinking lit areas and then conducting a Monte Carlo experiment in a fashion similar to that already described. However, this oversimplification does not account for the nonlinear nature of polar lighting and shadow. Because of the constantly low Sun angles, a small change in terrain height can produce a large change in the shadow it casts. The magnitude of the effect also varies according to the relative inclination and surface shape of the surrounding terrain upon which the shadow falls. A more accurate way to simulate this effect might be to apply the interpolation, noise, and rock distribution to the raw DEM before lighting maps are rendered. This requires substantially more computing power than the simpler approach, and a highly efficient implementation of the entire render-plan-simulate pipeline would likely be needed to facilitate adequate Monte Carlo simulations.

7.4 Summary

Mission concepts that prohibit autonomy and enforce a strict requirement on constant communication for teleoperation inevitably force rovers to dwell stationary for weeks at small peaks of predicted sunlight; however, the existence and exact locations of such singularities cannot be confidently predicted due to limitations of lunar topographic data. This thesis asserts that the risk associated with dwelling at uncertain singularities exceeds that of driving autonomously with guaranteed solar power.

Strategic autonomy maintains continuous exposure to sunlight by permitting short, slow, autonomous drives during periodic communication blackouts—a natural consequence of sun-synchronous routes. These drives follow preplanned paths and distance rovers from the day–night terminator where sustained insolation is uncertain. Strategic autonomy ultimately reduces overall mission risk while enabling sustained lunar polar roving.

Conclusions

- Rovers constrained by a requirement for supervised teleoperation are susceptible to errors present in lunar topography models, since long, stationary dwells in sunlight are not guaranteed.
- Rovers that are permitted to selectively deploy limited use of autonomous driving capabilities during unavoidable communication blackouts may reduce overall mission risk by guaranteeing continuous solar power.

Chapter 8

Planning for Longevity

This chapter describes the application of a generic RRT path planing approach to the problem of sun-synchronous planning and presents a resulting route that sustains uninterrupted direct sunlight for 6 months on the South Pole of the Moon.

8.1 Introduction

A key motivation and benefit of planning sun-synchronous polar routes is the ability to increase rover longevity beyond a single lunar day. The planning methods described thus far are capable of generating sun-synchronous routes that last multiple lunar days at temporal resolutions of hours and spatial resolutions approaching that of the best available lunar DEMs. However, due to computational complexity, generating these routes often requires the use of one or more undesirable speedups, such as decreased model extent and/or resolution, hierarchical planning, or manual selection of intermediate waypoints. At best, these techniques introduce suboptimality (in addition to that inherent to grid-based planners) and significant manual labor. At worst, these techniques limit the scope of achievable routes or prevent viable solutions from being found altogether.

These issues are inherent to deterministic grid-based planners like A* because of their computational complexity. As the size of the state space grows, particularly in depth, path planning problems quickly become intractable for even efficient implementations of algorithms in the class of A*. The irony of planning for sun-synchronous routes is that the deepest possible solution is desired, but in the worst cast, the time complexity of A* search is exponential in the depth of the solution [88, 89]. Without sacrificing resolution, A* methods are inefficient and often insufficient for planning sun-synchronous routes exceeding a few months.

An alternative method is the use of randomized sampling-based approaches, such as the rapidly-exploring random tree (RRT) [61] and its descendants. Although RRT* and more recent variants provide conditional guarantees on route quality and algorithm performance [62, 63, 64, 65], the most basic RRT path planner gives up the optimality of the route generated in favor of a much faster solution (or any solution). The result is essentially a random walk that connects two or more waypoints while

avoiding obstacles in the search space. Although RRT does not produce optimal paths, it provides a valuable proof of concept that long-duration sun-synchronous routes are possible, even at slow speeds.

As the extent and dimensionality of the search space grows, so too does the speed advantage of randomized sampling-based planners over deterministic grid-based planners. The method and results presented in this chapter demonstrate the utility of sampling-based approaches for planning sun-synchronous lunar polar routes that improve rover longevity.

8.2 Method

This section describes the data model, preprocessing steps, and planning method used to plan 6-month routes.

8.2.1 Model

One of the benefits of sampling-based approaches is the ability to efficiently search expansive state spaces. To demonstrate this aspect of RRTs, the study presented in this chapter uses the largest spatiotemporal model (in terms of grid size) of any presented in this thesis. Although the planner is not constrained by the grid, the gridded world model is still a natural and efficient representation of the environment. The dataset extends 12 km horizontally (x) and 9 km vertically (y) with a spatial resolution of 10 meters per pixel. The dataset extends 6 months (January 1, 2020 to July 1, 2020) or 182 Earth days in the temporal dimension (t) at a resolution of 1 hour per time step. This yields a $1200 \times 900 \times 4368$ grid with over 4.7 billion elements.

Like chapter 5, this study enforces constraints on sunlight and terrain slope. The principal terrain slope for every pixel of the 12×9-km area is shown in Figure 8.1. This area is a subset of the Nobile Crater Rim region studied in Chapters 6 and 7, but the model is double the resolution of the Nobile model used in previous chapters. Slope is treated as a static binary constraint with a maximum permissible terrain slope or 20 degrees as indicated in Figure 8.1.

Unlike the models used in previous chapters, which approximate the Sun as a directional source, this dataset treats the Sun a uniform area source. This produces models representing the percent of the solar disk visible from the surface at every (x, y, t) state. This improves accuracy, and multiplying these values by the solar constant ($\sim$1366 W/m^2) closely approximates the maximum solar flux available at each state. Instead of hard shadow edges, this method produces gradient shadow boundaries, or penumbras, when the occluding geometry is distant from the shadowed surface (see Figure 8.2). These soft shadow edges represent the states for which the Sun is partially occluded. Shadows cast by nearby terrain still appear hard.

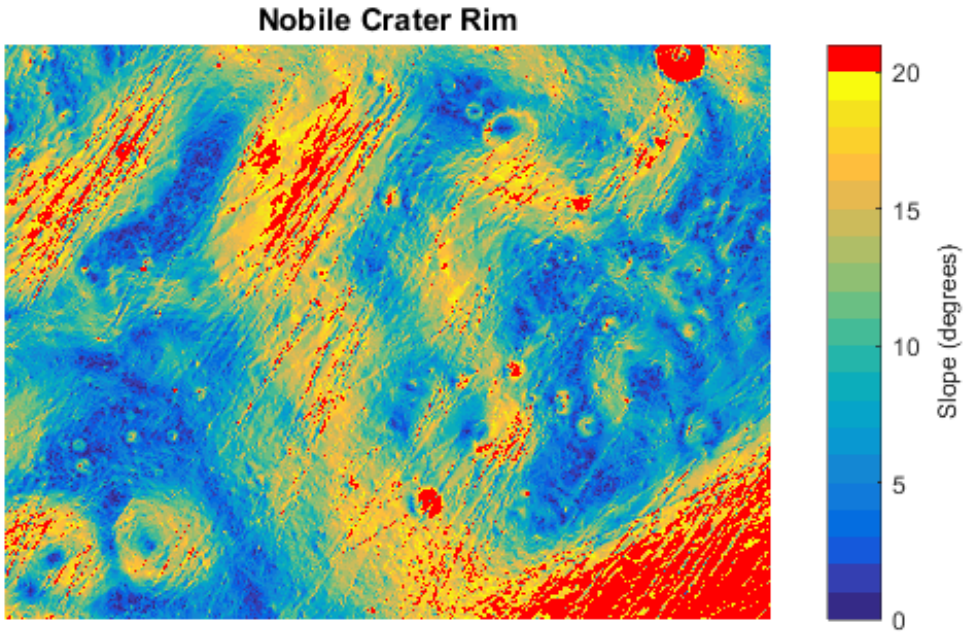

Figure 8.1: The dataset studied in this chapter extends 12 km horizontally and 9 km vertically with a spatial resolution of 10 meters per pixel. Principal terrain slope is represented here. Slopes greater than 20 degrees are indicated in *red*.

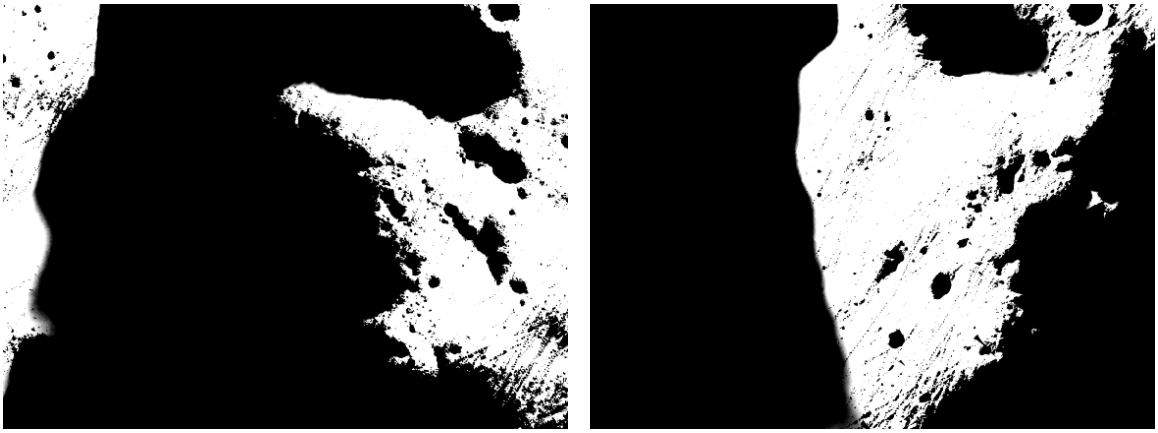

(a) January 6, 2020 **(b)** January 14, 2020

Figure 8.2: These images represent two time frames from the 6-month Nobile dataset. Each pixel value represents the percent of the solar disk that is visible from the surface, which corresponds approximately to solar flux. 100% of the solar disk is visible from *white* areas; 0% of the solar disk is visible from *black* areas. *Gray* pixels indicate where the Sun is partially occluded by surrounding geometry. Soft shadow boundaries can be seen on the left side of **(a)** and at the bottom center of **(b)**.

8.2.2 Preprocessing

Before planning, several preprocessing steps are executed to prepare the model for sun-synchronous constraints, evaluate sensitivity to thresholding solar flux, and select points with which to seed the planner.

Sensitivity Analysis

Although modeling the Sun as an area source enables more accurate explicit modeling of solar battery levels, the method demonstrated here applies the same simplifying assumption as previous chapters by treating sunlight as a binary constraint. Two natural questions are at what value should the solar flux (solar disk visibility) model be thresholded and to what degree is the planner sensitive to changes in the specific threshold value.

These questions are addressed in two ways. First, the relative frequency of solar disk visibility for all discrete grid elements in the model, shown in Figure 8.3a, is examined. Virtually all grid elements are valued at either 0 or 1, indicating that very few states in the spatiotemporal model are partially occluded. This stands to reason, since most shadows are cast by nearby geometry and therefore have hard boundaries with little to no gradient. Soft shadows are relatively rare, and they are small both spatially and temporally relative to the size of the model. This observation suggests that sun-synchronous routes are fairly robust and insensitive to changes in the flux threshold. For example, changing the solar disk visibility threshold from 50% to 90% does not substantially alter the resulting binary model of sunlight. Small changes to the threshold on terrain slope, however, does produce a significant change in the binary slope constraint model as evidenced by Figure 8.3b.

The second way that threshold sensitivity is addressed uses connected component analysis to bound the longest possible route for a series of possible flux thresholds. Connected components are used in this preprocessing step because this analysis is faster than simply running the RRT planner for each possible threshold. The method of identifying the single longest component is the same as that described in Chapter 5. It turns out that in the case of this Nobile dataset, the longest connected component that satisfies constraints on both sunlight and 20-degree slope is unaffected by the the solar flux threshold (Figure 8.4). The longest component spans the full 182-Earth-day model regardless of if the requirement for Sun visibility is set to 50% or 100%. This provides further evidence that the specific threshold value has little to no effect on the longevity of the longest route possible with this dataset, although it is not a guarantee, since connected component analysis does not account for limited rover speed. Due to the apparent insensitivity of route length to solar disk visibility, the threshold used to generate the results presented in this chapter was set to 100%.

Seed Point Selection

Another benefit of performing connected component analysis prior to planning is to aid the selection of one or more seed points. The temporal length of each component represents an upper bound on the maximum duration of routes that start within the

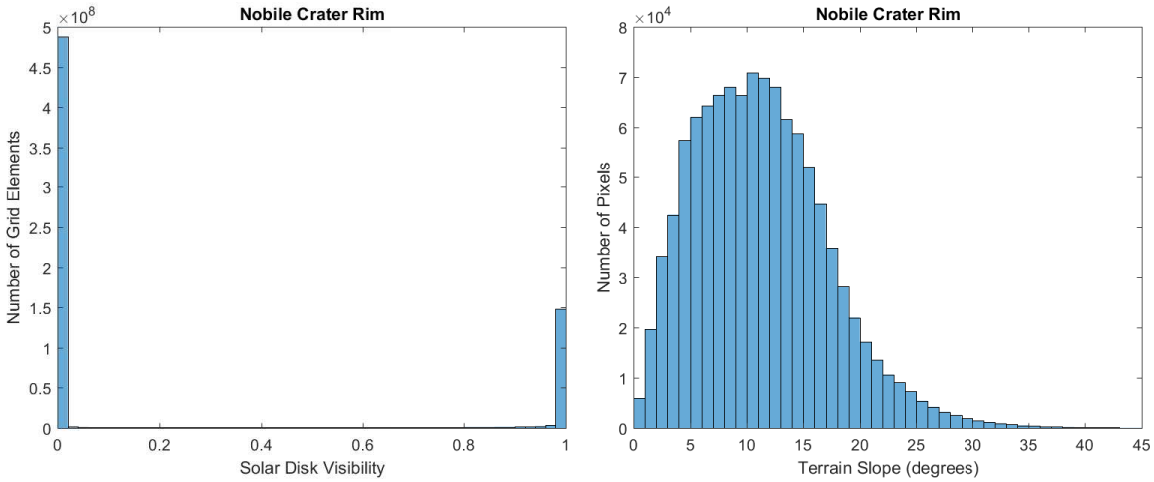

(a) Histogram of solar disk visibility **(b)** Histogram of terrain slope

Figure 8.3: **(a)** The relative frequency of solar disk visibility for all 3D grid elements in the spatiotemporal model. A value of 1 indicates that 100% of the Sun is visible at the surface. Solar disk visibility can approximate the maximum solar flux available at each state by multiplying by the solar constant ($\sim$1366 W/m^2). **(b)** The relative frequency of principal terrain slope for all 2D pixels in the model.

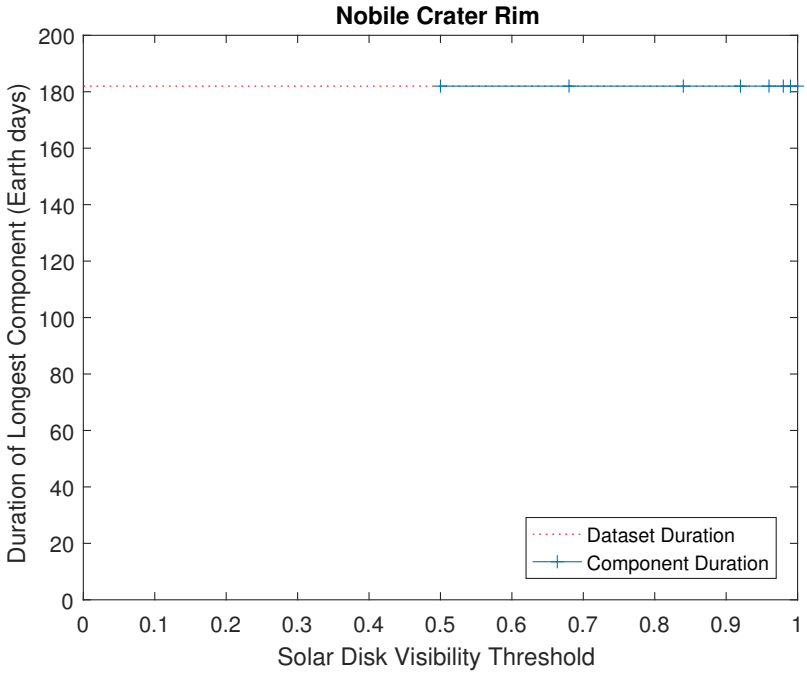

Figure 8.4: Connected component analysis was performed on a combined model of lighting and slope for eight different solar disk visibility thresholds between 50% and 100%. In all cases, the single longest duration connected component that satisfies both Sun visibility (as defined by the threshold) and mild slope (less than 20 degrees) spans the full 182 Earth days of the dataset.

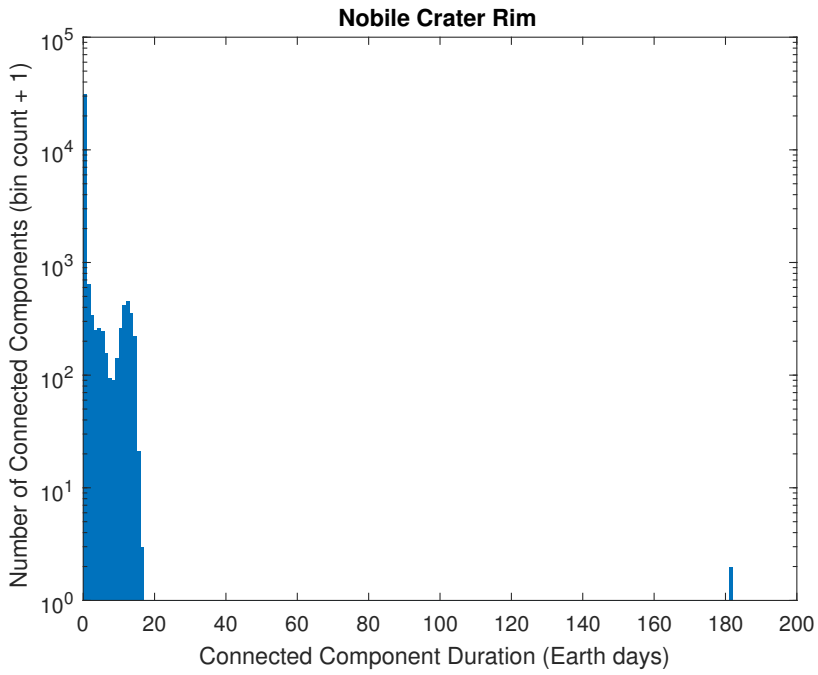

Figure 8.5: Connected component analysis produces a list of all distinct regions in the spatiotemporal model as defined by a 26-connected kernel. The relative frequency of these components' time durations is shown here. Note that the y-axis is log scale and that the all bin counts were incremented by 1 so that frequencies of 1 are visible above the x-axis. Only a single connected component spans the temporal extent of the solar flux model, and the next largest component is less than 20 Earth days in duration.

first time step of that component. In the case of this study, only one component extends the full 6 months of the model (Figure 8.5), so any 6-month route must start within that single component, specifically at the first time step.

The first time step of the longest connected component provides a subset of possible staring points. Selecting a single (x, y) point arbitrarily runs the risk of initializing the RRT such that it cannot reach the final time step given a constraint on rover speed. Instead, a random sample of all possible starting points is generated, as shown in Figure 8.6a. The RRT planner will naturally grow multiple search trees in parallel from many or all of these points as the search space is randomly sampled.

8.2.3 Route Planning

Once starting points are selected and initialized, route planning proceeds in typical RRT fashion. First, a single point within the bounds of the gridded model is sampled randomly, and the single nearest neighbor out of all graph nodes (just the staring points in the first iteration) is identified. A graph edge not exceeding a predetermined length (in this case, 100 meters) is generated from the nearest neighbor in the direction of the random sample. The speed required to traverse this edge is checked to verify that it is both non-negative and less than or equal to the maximum allowable rover

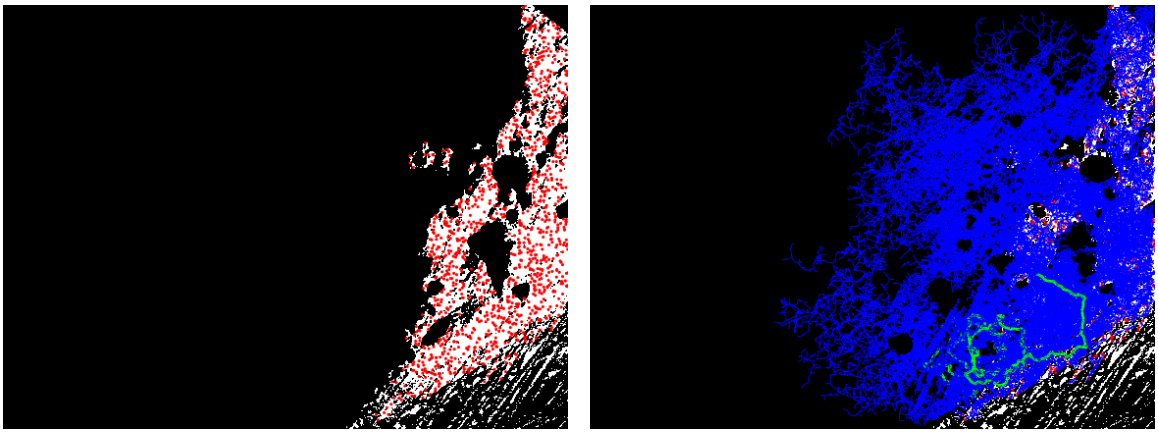

(a) RRT starting points **(b)** RRT graph structure and solution

Figure 8.6: **(a)** *Red* dots represent starting points used to seed the RRT planner. Points were randomly sampled from the area shown in *white*, which represents the first frame of the longest connected component of 100% solar disk visibility and less than 20 degrees slope. The random sample contains 1% of all possible starting points. **(b)** *Blue* lines represent edges of the RRT graph structure explored by the planner before finding a solution. The *green* line represents the solution from one of the starting points to the final time frame.

speed (10 cm/s). Then the edge is checked against the gridded world model for collisions with obstacles (shadows or steep slopes). If the edge is obstacle-free, it is added to the graph tree structure along with the corresponding node.

This process is repeated until a node is generated which satisfies the goal condition, which in this case is any state at the final time step (182 Earth days). Then the path through the graph tree structure is traced back and returned as a solution. If no solution is found before a predetermined number of iterations has expired, no solution is returned.

8.3 Results

Given sufficient runtime, the route planning method generated routes lasting the full 6 months of the dataset. One such route is shown in Figures 8.6b–8.10. The route is summarized in Table 8.1.

Table 8.1: RRT Route Summary

Total Distance	39.8 km
Total Duration	182 days
Average Speed	0.25 cm/s
Maximum Speed	9.31 cm/s

Notable is the way the route circles a peak elevation counterclockwise in sync with the Sun. This is an emergent behavior accomplished without any heuristics

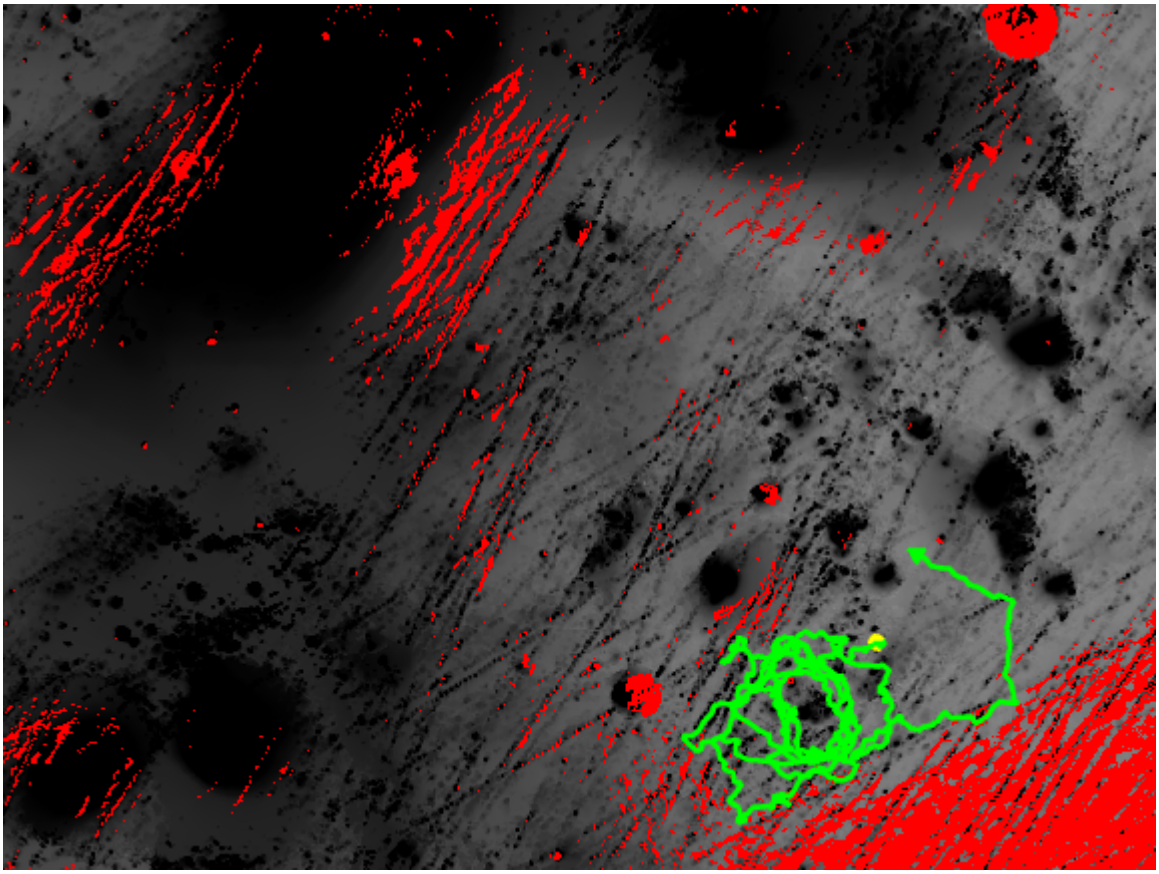

Figure 8.7: The *green* line represents the path generated by the RRT planner. It starts at the *yellow* circle and moves counterclockwise around a local peak for 182 Earth days, or 6 months, until ending at the *green* arrow. The *grayscale* background represents the average illumination over the 6-month time span, with lighter areas receiving more sunlight and darker areas receiving less. The *red* areas indicate terrain slopes steeper than 20 degrees.

or intermediate waypoints. This general behavior is most apparent in Figure 8.10. The entire RRT graph structure tends to spiral around the peak elevation as the sun circles the pole each lunar day, a pattern characteristic of sun-synchronous routes.

8.4 Summary

A 6-month route was generated without any intermediate waypoints on a model resolution of 10 meters per pixel spatially and 1 hour per time step temporally. This demonstrates the computational advantage of sampling-based approaches over grid-based approaches, which are ineffective at the scale of this model. More importantly, this route and others demonstrate the existence of sun-synchronous routes that feature uninterrupted sunlight for power and heating for durations of up to 6-months on the South Pole of the Moon. Although basic RRT planners do not produce optimal shortest-distance routes like A*, RRT* [62] and more recent extensions such

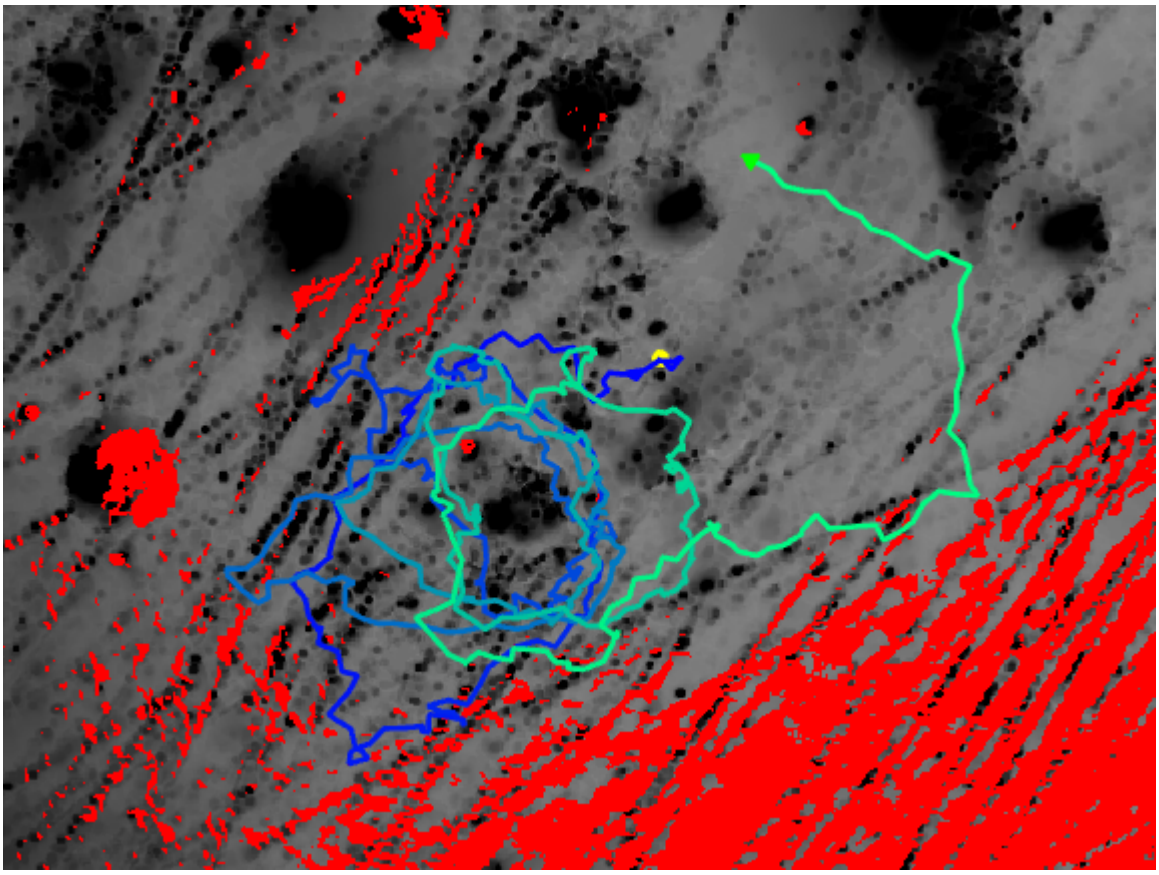

Figure 8.8: This zoomed-in view better shows the detail of the RRT solution. The *blue*-to-*green* gradient line represents the path generated by the RRT planner. It starts at the *yellow* circle and moves counterclockwise around a local peak until ending at the *green* arrow. The *grayscale* background represents the average illumination over the 6-month time span. The *red* areas indicate terrain slopes steeper than 20 degrees.

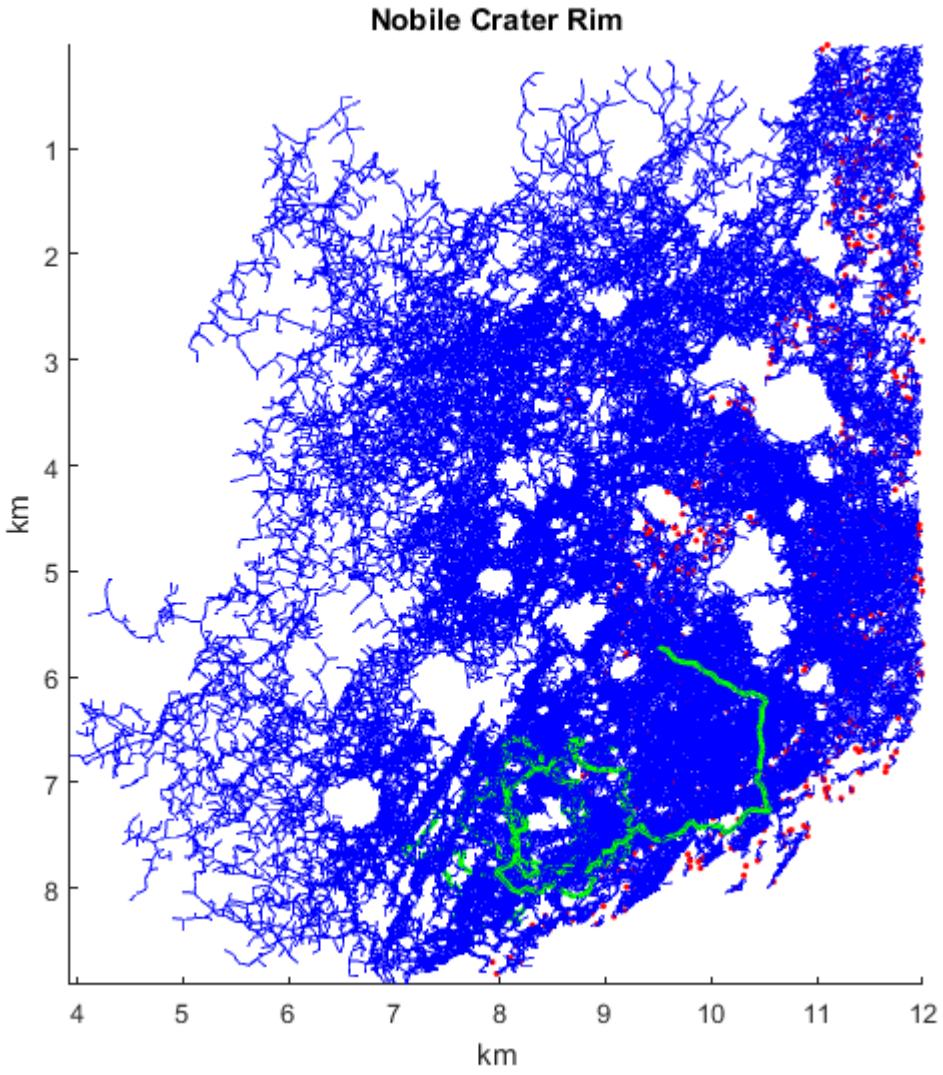

Figure 8.9: The isolated top view of the graph structure illustrates the extent to which the RRT planner expands beyond its starting states while avoiding permanently shadowed craters and steep slopes. *Red* dots represent starting points used to seed the planner. *Blue* lines represent edges explored by the planner. The *green* line represents the solution path connecting the starting point to the ending time. Every state explored by the RRT can be reached from one of the starting points given the constraints on uninterrupted sunlight, mild slope, and maximum rover speed.

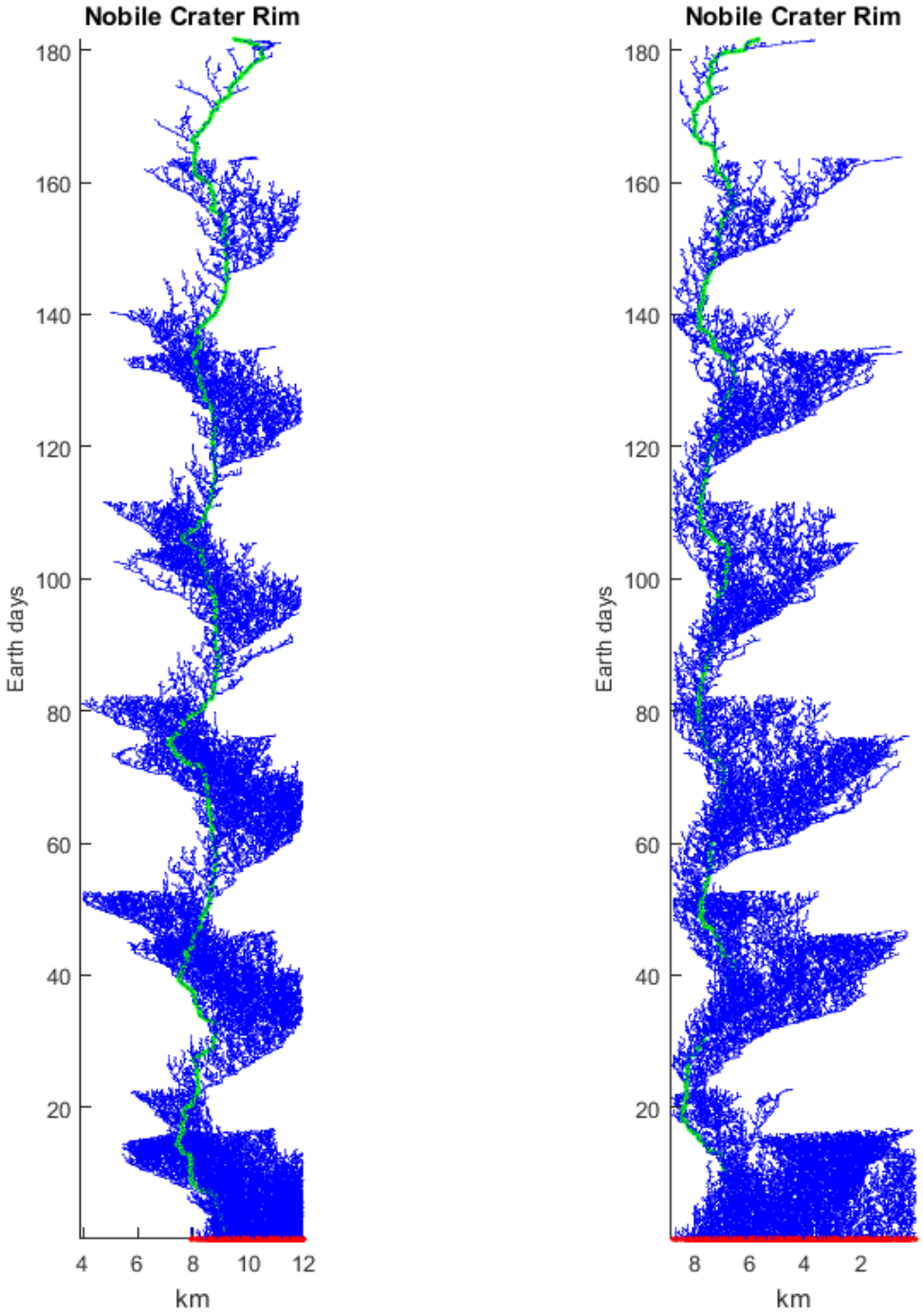

(a) X-T view of RRT

(b) Y-T view of RRT

Figure 8.10: The side views of the RRT reveal the periodic structure that emerges from polar sunlight. *Red* dots represent starting points used to seed the RRT planner. *Blue* lines represent edges explored by the planner prior to finding a solution. The *green* line represents the solution path connecting the starting point to the ending time at 182 Earth days. Every state explored by the tree can be reached from one of the starting points given the constraints on uninterrupted sunlight, slope, and rover speed.

as Informed RRT* [63], BIT* [64], and RABIT* [65] are asymptotically optimal and increasingly efficient. Applying these methods to sun-synchronous planning is a promising area of future work.

Conclusions

- Randomized sampling-based planning methods, such as RRT, facilitate the generation of longer-duration routes on larger models with higher spatial and temporal resolution than is possible with deterministic grid-based planning methods, such as A*.
- On the South Pole of the Moon, there exist sun-synchronous routes that satisfy constraints on terrain slope, rover speed, and uninterrupted sunlight for up to 6 months. Six months of sun-synchronous lunar polar roving is achievable at speeds of less than 10 cm/s.

Chapter 9

Planning for Landing

Routes of sustained lunar polar roving are useless if they cannot be accessed by a lunar lander. Lunar ambitions such as pursuit of ice, habitation, lunar observatories, establishment of solar grids, and rover routes of persistent sunlight compel polar destinations. Subtleties of lighting and terrain unique to the poles are the conditions that accreted the ice and also yield the favorable power, siting, and rover scenarios. However, these same subtleties, combined with requirement of direct-to-Earth communication, impose profound constraints on sites that are amenable for landings, missions, and long-term presence.

This chapter presents methodology for evaluating landing site amenability. The method is applied to Malapert Massif as an exemplar where prominent elevation, lighting, Earth-view, and traversable slopes combine to illustrate the principles of the method. The work identifies promising sites and regions for landing at Malapert that grant access to multi-lunar-day rover routes. This same procedure can be applied to other polar sites to seed and validate routes planned for sustained lunar polar roving.

9.1 Data

This chapter relies on the same style of predictive models (Chapter 4) as does route planning (Chapters 5–7). Specifically, the method incorporates models of terrain slope, dynamic DTE communication, and dynamic solar illumination. The particular models used to generate the results reported in this chapter are generated by a ray-tracing renderer that models the Sun as a uniform area light source and simulates the portion (0–1) of the solar disk that is visible from the surface at each state [79]. This value can be used to roughly approximate the solar flux at the surface by multiplying by the solar constant ($\sim$1366 W/m^2). The dataset spans 6 months, from January 1 to July 1, 2019 at 2-hour increments, and covers a 16-by-9-km area at 10 meters per pixel, centered at 86°S, 0°E.

Figure 9.1 shows the cumulative illumination (or average flux) at every grid element during the 6-month span. This 2D compression of spatiotemporal lighting lacks important temporal information and is therefore not used as part of the method presented; however, it does provide some context. Local peaks appear as the brightest

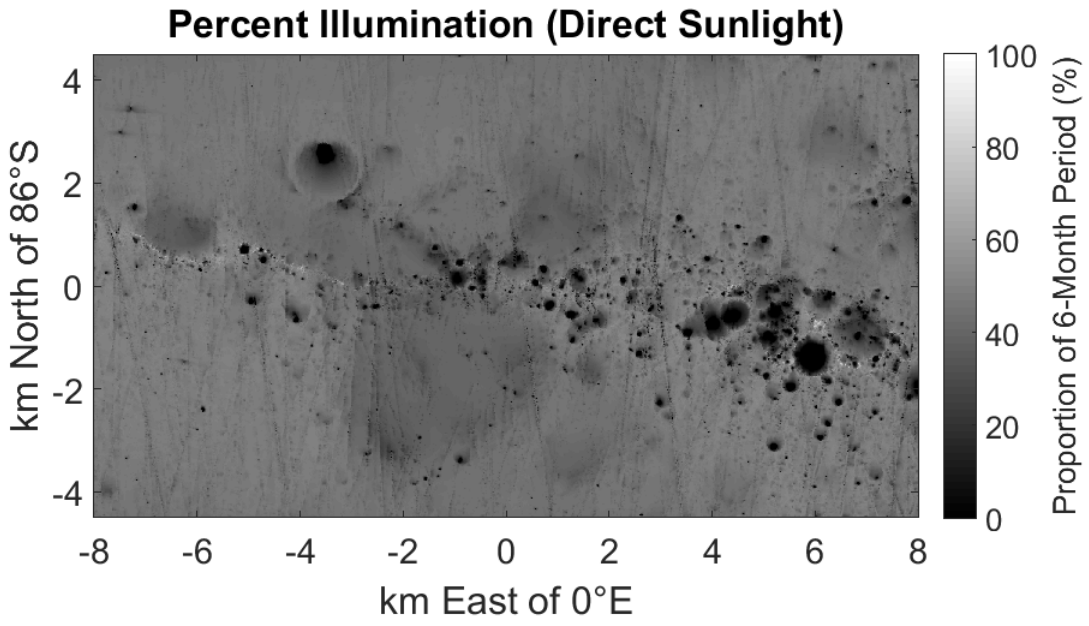

Figure 9.1: Total percent illumination over 6-month period. This region feature two local peaks (on the left and right halves of the image) separated by a saddle-shaped valley (in the center of the image). A multi-lunar day route identified in Chapter 5 circles one of the small craters near the western (left-most) peak.

locations in the average illumination map, and regions that receive zero sunlight during this 6-month span appear totally black. True PSRs are a strict subset of the black regions. The method described in Section 9.2 makes use of spatiotemporal lighting models to compute for each location the single longest period of uninterrupted sunlight. Even though all static landing sites are eventually shadowed, maximizing this period is beneficial for rover deployment, checkout, and radio relay.

The local terrain slope of the Malapert Massif region, derived from LOLA DEMs [22, 20] and computed using a divided difference method, is shown in Figure 9.2a. These values represent the principal slope, which corresponds to the maximum gradient at each grid element. The steepest slopes exceed 25 degrees to the north and south of the ridge that stretches east-to-west. Although ambitious rovers might be capable of traversing slopes approaching 15–20 degrees, landers favor milder slopes, which are available along the ridgeline. Figure 9.2b masks all slopes greater than 10 degrees and rescales the color map for slopes less than 10 degrees.

The cumulative duration of surface-to-Earth visibility (as percentage of the full 6 months) is shown in Figure 9.3. On the Earth-facing side of the Moon's South Pole, the Earth hovers in the northern sky near the horizon. Due to its latitude of 4 degrees off the pole, elevation, and slope orientation, the vast majority of the northern slopes of Malapert Massif maintain a constant line-of-sight to Earth for the entire 6-month period studied. From the surface of southern slopes, which face away from Earth and are obscured by the higher elevations to the north, the Earth is never visible.

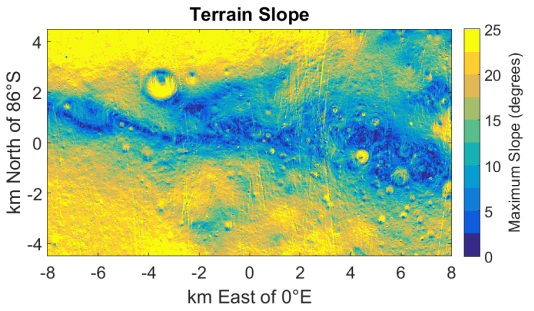

(a) Principal terrain slope (max gradient)

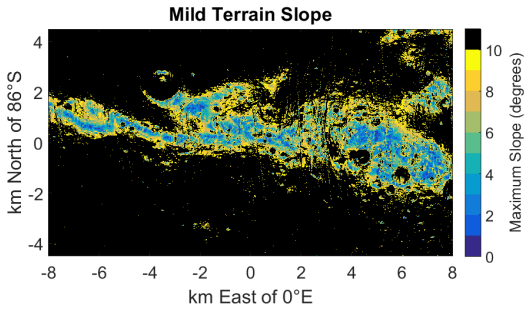

(b) Principal slopes $\leq 10°$ (black $> 10°$)

Figure 9.2: Malapert Massif (**a**) local principal terrain slope computed from maximum gradient and (**b**) region with principal slope no greater than 10 degrees (slopes greater than 10 degrees are masked in *black*). Note that the color maps of **a** and **b** are scaled differently.

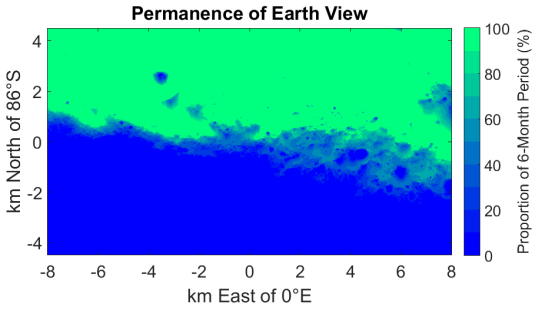

(a) Earth view for DTE communication

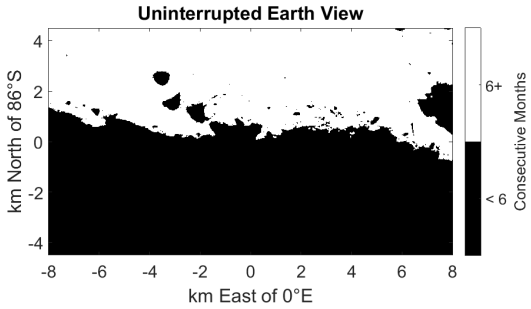

(b) 100% DTE communication for 6 months

Figure 9.3: Malapert Massif direct-to-Earth communication conditions. **a**: Earth view for DTE communication as a percentage of the 6-month period studied. **b**: *White* indicates all positions where Earth view is unobstructed for the full 6 months; *black* indicates where Earth view is occluded at least once during the 6 months.

Only along the east–west ridgeline does Earth view come and go with lunar libration, causing the narrow gradient band apparent in Fig. 9.3a. Figure 9.3b highlights the region of Malapert Massif for which Earth view is uninterrupted. A stationary lander anywhere in this region would have access to continuous DTE communication for at least 6 months and likely much longer.

9.2 Method

The maximum number of consecutive Earth days for which each location will receive uninterrupted direct sunlight is computed algorithmically. First, the 3D illumination model is made binary by thresholding such that, for each grid element, if less than 50% of the solar disk is visible, then that surface element is considered unlit at that time. This is equivalent to thresholding at a flux value of approximately 683 W/m^2.

Then, Algorithm 3 is applied to the resulting 3D binary lighting map. For each pixel in the 2D spatial extent of the map, the algorithm loops through the time series while keeping track of the maximum count of consecutively lit (1-valued) elements. Multiplying the incremental *count* variable by the value of the i^{th} time step has the effect of resetting the count whenever an unlit (0-valued) element is encountered. This serial process in the temporal dimension is performed in parallel for all pixels in the two spatial dimensions using matrix operators for efficiency. The maximum count of consecutively sunlit 2-hour time steps is converted to the equivalent number of Earth days by dividing by 12.

Algorithm 3 Compute Maximum Uninterrupted Sunlight Algorithm

for each pixel p **do** (in parallel)
    $count = 0$
    $maxCount = 0$
    for each time step t **do** (in series)
        $count = (count + 1) \cdot binaryLightMap(p, t)$
        $maxCount \Leftarrow \textsc{Max}(count, maxCount)$
    end for
end for
$maxConsecutiveDays = maxCount/12$

The result of Algorithm 3 is shown in Fig. 9.4a. As expected, the longest spans of continuous sunlight occur near local peaks. Large regions of Malapert Massif receive at least 14 consecutive days of sunlight (41.3% of the area shown), and many smaller regions receive at least 16 consecutive days of sunlight (1.8% of the area shown). Exceptional sites (the top 0.11% of all 1,440,000 shown) receive uninterrupted sunlight for greater than or equal to 21 consecutive Earth days. Although no sites provide perpetual solar-power for landers, selecting a landing site that offers uninterrupted sunlight at the beginning of surface operations facilitates rover deployment, system checkouts, and radio relay during a critical mission phase. Figure 9.4b indicates all sites that receive at least 10 consecutive Earth days of uninterrupted sunlight. This value is relatively low but was selected to filter out heavily shadowed regions without being overly restrictive. Ultimately, all stationary landers will succumb to lunar night. The primary objective is to successfully deploy sun-synchronous rovers.

Once models of terrain slope, Earth view, and sunlight have been processed as described, the results can be combined to filter out potential landing sites with unfavorable conditions. The method presented here enforces the following conditions as necessary criteria for acceptable "safe" landing sites:

1. local principal slope no greater than 10 degrees

2. 100% uninterrupted Earth visibility for 6 months

3. at least 10 consecutive Earth days of uninterrupted direct sunlight

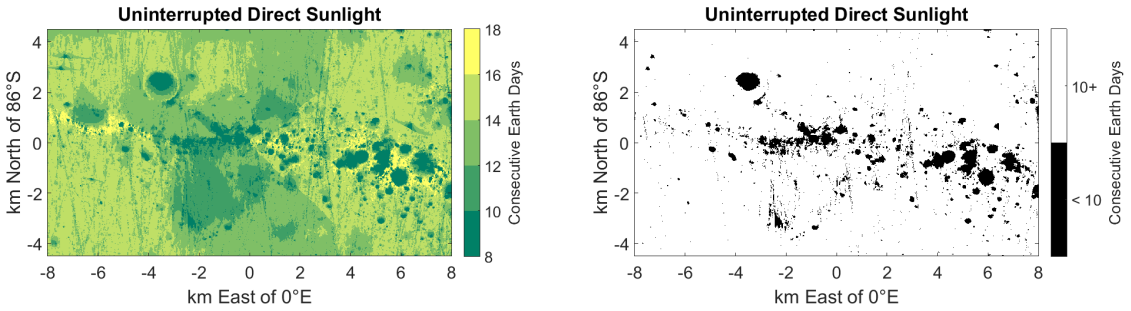

(a) Longest period of uninterrupted sunlight **(b)** 10+ days of uninterrupted sunlight

Figure 9.4: Malapert Massif longest local period of uninterrupted direct sunlight. **a**: The single longest period of uninterrupted sunlight for every site. **b**: Filter indicating all sites featuring at least 10 consecutive Earth days of uninterrupted direct sunlight.

Filters for meeting individual criteria on slope, Earth visibility, and uninterrupted sunlight are shown in Figures 9.2b, 9.3b, and 9.4b, respectively. These three filters are combined to produce the set of all theoretically viable landing sites shown in Fig. 9.5a. Examining these sites reveals two distinct problems. The first problem is that many of the smallest viable landing regions appear to be the result of small data artifacts. This is evident by visible satellite track lines, particularly on the northern Earth-facing slope. The second problem is that even if a 10-by-10-meter site is truly safe for landing, it is unlikely that a lander targeting the center of that site can execute a landing with precision better than $\pm$ 5 meters. This means not all "safe" landing sites should be considered safe landing *targets*.

These two problems can be addressed in similar fashions to increase confidence in landing targets. First, the set of all sites meeting the three safe landing criteria are passed through a majority filter. This filter sets a pixel to 1 if a majority of the pixels in its 3-by-3 neighborhood are 1s; otherwise, it sets the pixel to 0. This effectively removes isolated false-positive sites that are likely caused by data artifacts and are too small to be reliable landing targets. It also adds back some small regions previously considered unsafe in cases where the surrounding area is generally considered safe. This can be beneficial, since in the same way that data artifacts can cause false positives, they can also cause false negatives, and the majority filter corrects this. The downside is that some true negatives may become false positives. Although undesirable, this effect is not catastrophic. Because landers are imprecise, their actual landing spot can be thought of as a probability distribution over the surface, so including a small number of false-positive "safe" landing sites only slightly increases the probability of actually landing on one. Also, advanced perception, navigation, and control technologies are designed to adapt and avoid unexpected hazards, so as long as a region is generally safe for landing, it may be a viable landing target.

The second step to addressing problems with data artifacts and landing precision is to require a sizable radius of safe landing sites around the selected landing target. If the actual landing error is less than the radius used as a buffer, then the lander will remain within the region of safe landing sites. The radius, or safety buffer, is

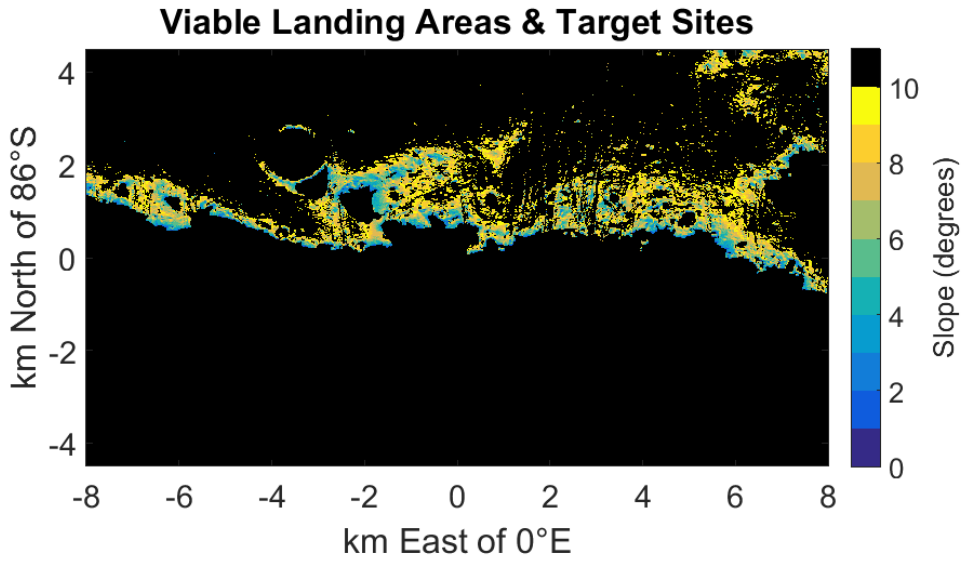

(a) Safe landing targets given a landing radius of 10 m

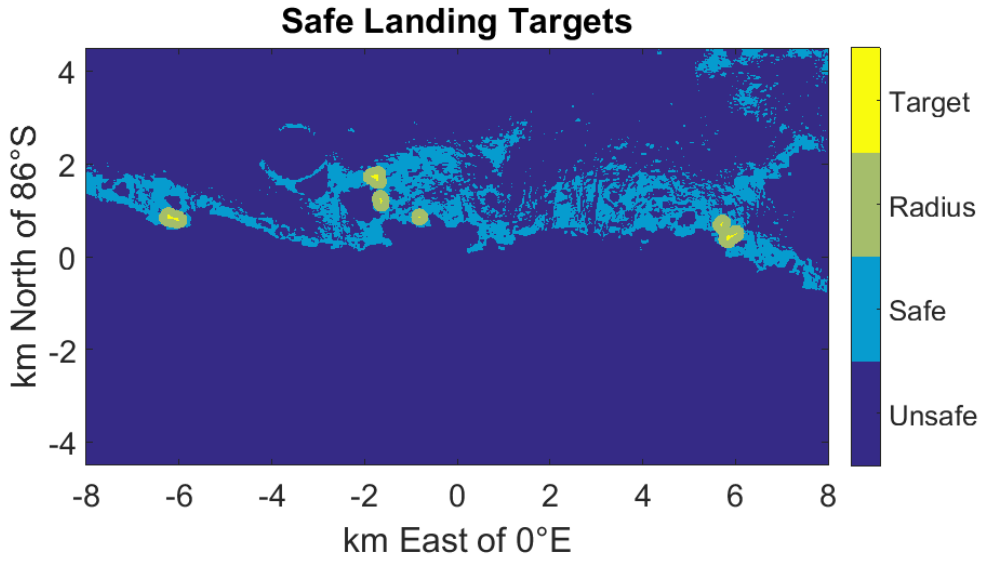

(b) Safe landing targets given a landing radius of 150 m

Figure 9.5: (**a**): All colored grid elements represent areas that would be safe to land. (The safety criteria are mild slope, uninterrupted DTE communication, and 10+ Earth days of uninterrupted sunlight.) These sites are all viable landing targets for landers with a landing accuracy radius of 10 meters or less. Colors indicate terrain slope. Black indicates unsafe landing areas. (**b**): The yellow "target" grid elements represent sites that are viable landing targets for landers with a landing accuracy of 150 meters or less. The green "radius" represents the extent of the where a lander targeting a yellow target site might actually land. The cyan "safe" areas represent all sites that meet the safety criteria (same as **a**). The indigo "unsafe" areas do not meet the safety criteria.

characteristic of the lander system's precision. The example presented demonstrates a landing radius of 150 meters, which requires the lander to hit a landing circle 300 meters in diameter. Although this level of precision is so far unprecedented (except on Earth), it may soon be possible. The Moon's lack of atmosphere eliminates aerodynamic effects that increase uncertainty and landing ellipse size, and recent advances in terrain relative navigation (TRN) and propulsive landing technology may soon enable high-precision lunar landings. Enforcing the 150-meter landing radius is accomplish by applying a morphological operator to erode the set of safe landing sites by fifteen 10-meter pixels. This produces the six distinct landing target regions shown in Fig. 9.5b.

9.3 Results

The six distinct safe landing target regions were reduced to six target points located at the centroids of individual target regions. These six target sites are indicated by their 300-meter landing circles in Fig. 9.6. The entire surface area within these circles meet all three criteria on terrain slope, DTE communication, and uninterrupted sunlight. A lander that targets the center point of one of these sites with an error less than 150 meters in any direction will land at a site deemed both safe and amenable for deploying solar-powered lunar rovers. Dozens more such target sites are viable given 100-meter landing accuracy.

9.3.1 Route Validation

At least one of the six target sites identified is located in close proximity to a sun-synchronous route lasting multiple lunar days (see Chapter 5). The west-most landing target shown in Figure 9.6 lies within a few hundred meters of the 2-lunar-day route shown in Figure 5.1a. This demonstrates the ability the landing target identification method to validate already-planned routes.

9.3.2 Route Seeding

More powerful than route validation, is route seeding. Instead of planning a route and then checking if a viable landing site exists nearby, all viable landing sites in a given region of interest can be identified and then used as starting points for route planning. The six landing targets were used to seed the RRT-generated route shown in Figures 9.7–9.10. This route traverses 19.1 km over 5 lunar days (148 Earth days) of uninterrupted sunlight without exceeding 2 cm/s drive speed or 15 degrees slope.

9.4 Summary

At Malapert Massif, six sites are identified as viable landing targets given a landing accuracy radius of 150 meters. These meet criteria for mild terrain slope, uninterrupted DTE communication, and sustained direct sunlight. One such site is within

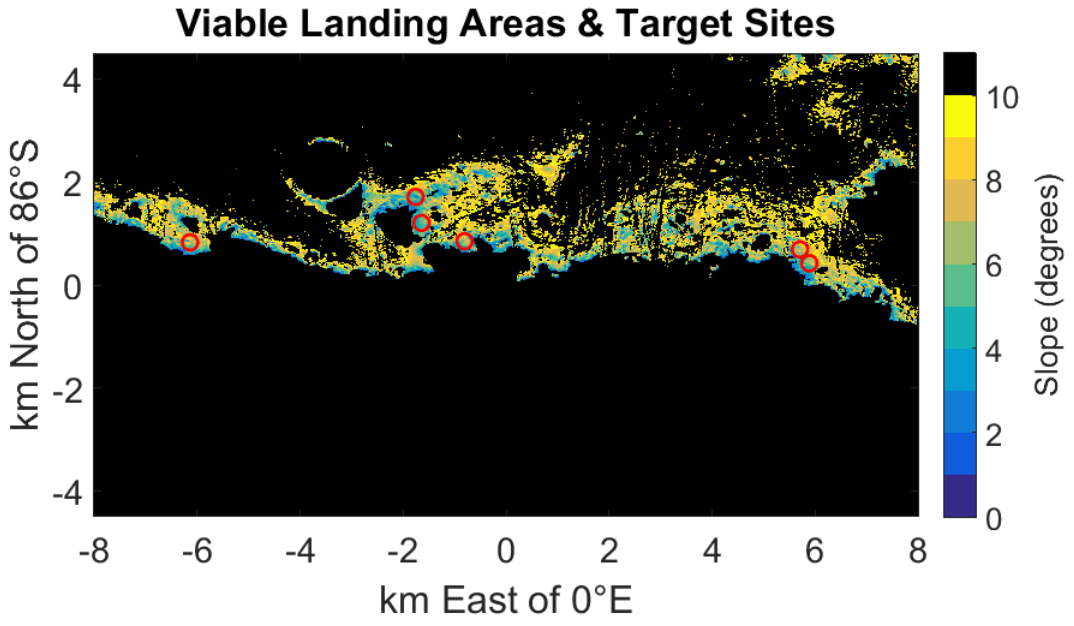

Figure 9.6: This figure shows in greater detail all area that are considered safe for landing, that is, all area with mild slope (no greater than 10 degrees), uninterrupted DTE communication for 6 months, and at least 10 days of uninterrupted sunlight. Areas masked in black are unsafe. Terrain is colored by principal slope. Six target site featuring radii of at least 150 meters of safe landing area in all directions are circled in red (red circles are 300 meters in diameter).

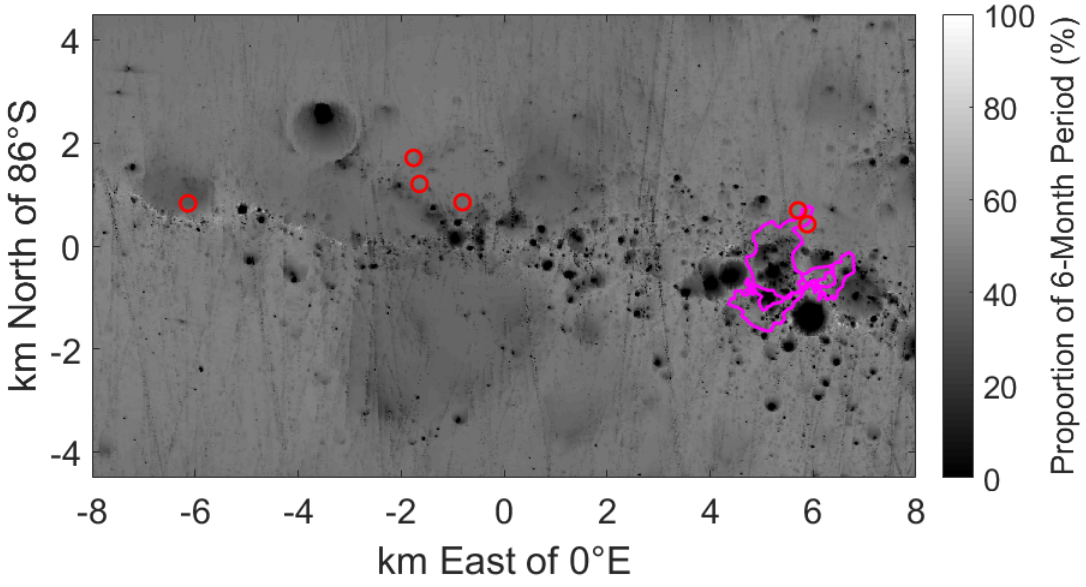

Figure 9.7: The 5-month route shown in *magenta* begins and ends at one of the safe landing targets circled in *red*. The route travels 19.1 km at an average speed of 0.15 cm/s and a maximum speed of 1.72 cm/s. The background gradient represents average solar illumination over a 6-month period.

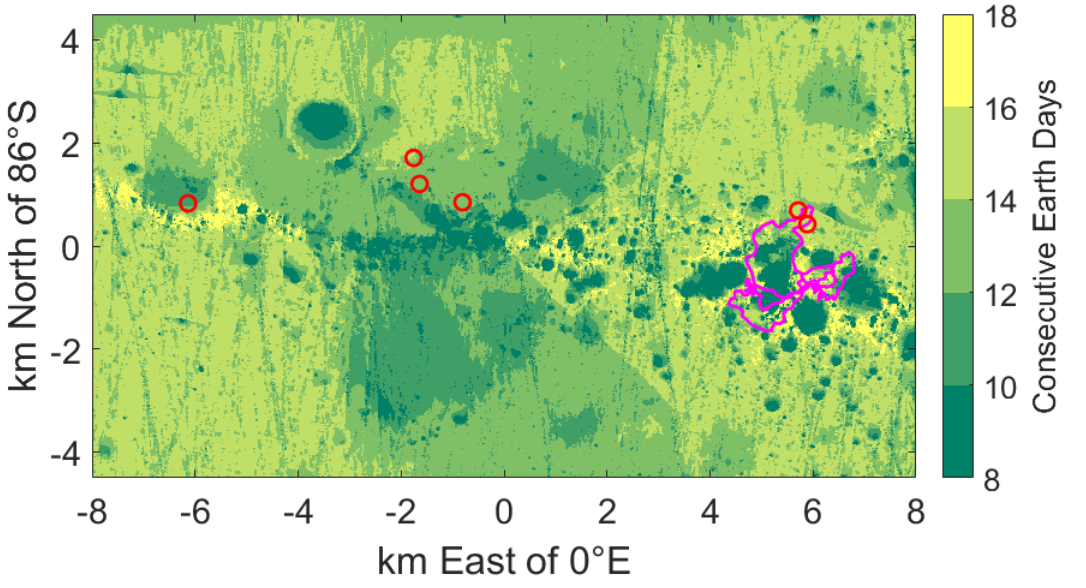

Figure 9.8: The 5-month route shown in *magenta* is maintains continuous sunlight for 148 Earth days. The background gradient represents the maximum duration of continuous sunlight at every location during a 6-month period.

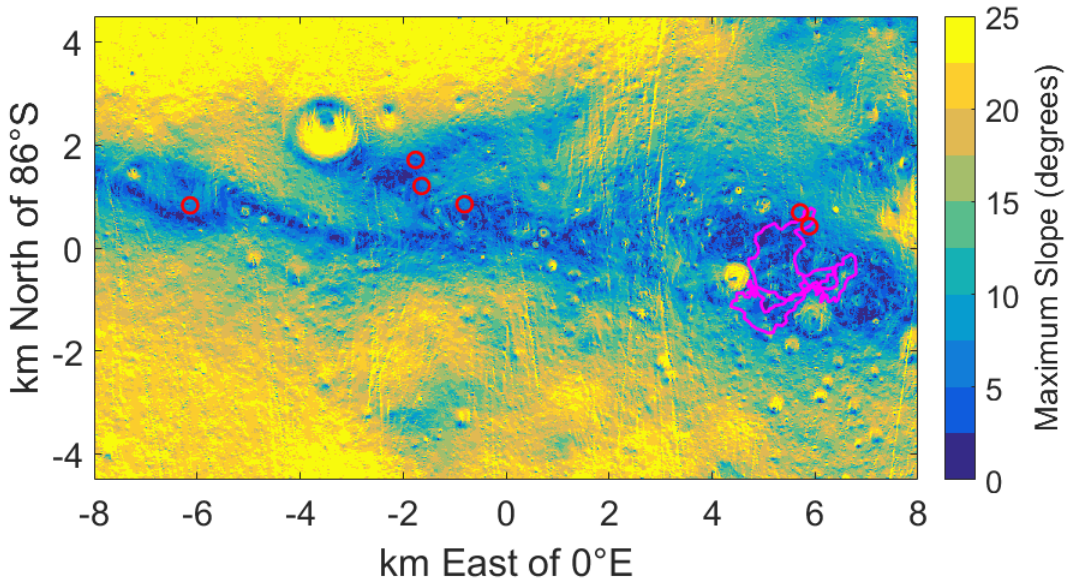

Figure 9.9: The 5-month route shown in *magenta* avoids terrain slopes exceeding 15 degrees. The background gradient represents principal terrain slope.

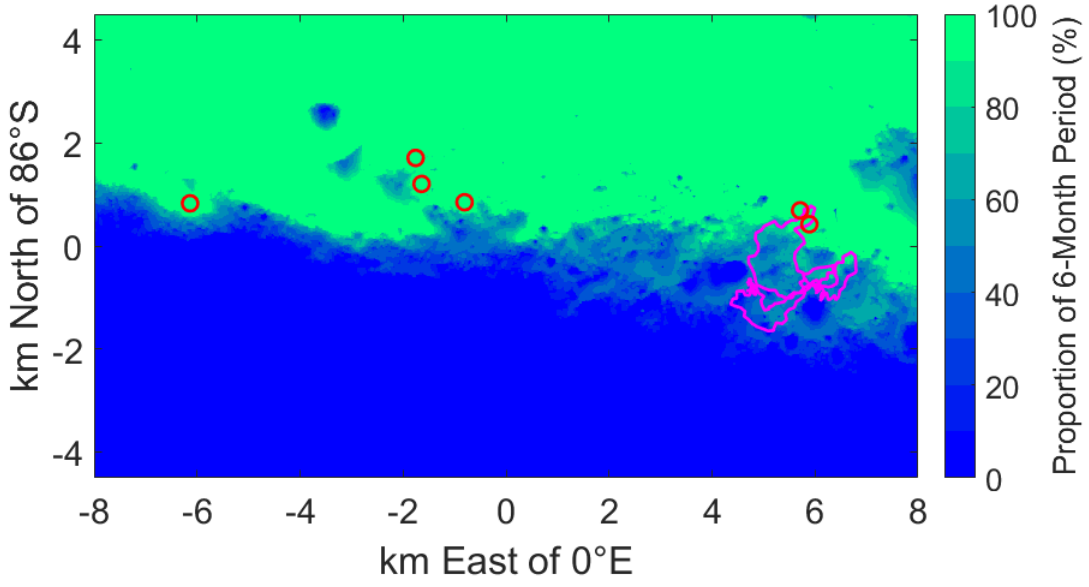

Figure 9.10: The 5-month route shown in *magenta* experiences approximately 60% DTE communication coverage. The background gradient represents cumulative DTE communication coverage over a 6-month period.

100 meters of a multi-month continuously lit rover route. The combination of elevation, topology, latitude, and longitude combine to make Malapert a premier polar landing destination with numerous promising landing sites. Additional sites can be identified by applying this method to other lunar polar regions. Planning for landing sites generates compelling starting points for planning routes of sustained lunar polar roving.

Conclusions

- Within close proximity to examples of multi-lunar-day rover routes, there exist numerous feasible landing sites that feature mild slope, sustained sunlight and Earth view, and a landing radius of at least 150 meters. These sites are important for successful deployment of lunar polar rovers and can be used to validate and seed sun-synchronous routes.

Chapter 10

Planning for the Future

Future research must achieve advances on several key fronts to fully enable sustained lunar polar roving. These include but are not limited to: handling the complex interaction of constraints and resources characteristic of polar exploration; enforcing global constraints on the rover's stored energy state given an arbitrary solar panel configuration; enhancing routes to maximize mission-level objectives; estimating and improving route robustness to terrain map error and resolution; and performing all of these computations tractably. Additional avenues of future research include: enforcing global constraints on the rover's thermal state; adding mixed-initiative human input; identifying the minimum viable route that enables multiyear solar-powered exploration; and identifying the minimum viable solar power grid for a given planetary body. Together, these capabilities will enable mission planners to generate safe, reliable traverses that ensure mission requirements are met and dramatically expand the scope of solar-powered polar exploration. These advancements represent the primary goals of the suggested future work.

The following sections discuss several suggested topics of future work in greater detail and propose potential approaches.

10.1 Planning for Shadow

To complete certain key science objectives, rovers will be required to enter PSRs and potentially other shadowed areas for brief periods of time to acquire samples and instrumental data. Although strictly sun-synchronous routes can be manually altered post hoc to include short battery-powered forays into shadow, planners that forbid shadowed roving cannot plan for these scenarios automatically. This extension is outside the scope of this dissertation but is suggested as an important avenue for future work.

10.1.1 Rover Stored Energy State

The research presented in Chapters 5–7 demonstrated the feasibility of extended solar-powered exploration through examples of routes that maintain continuous, un-

interrupted sunlight for multiple diurnal cycles on the Moon. This work provides a valuable proof of concept, since those routes represent viable missions, but it falls short of the ambitions of this thesis in several respects. For example, enforcing a hard constraint that requires continuous solar illumination is overly restrictive, since all rovers are equipped with batteries, which store electric energy. The stored energy capacity can vary greatly based on system design, but even relatively small batteries provide a buffer of energy that can be used to operate and drive the rover without continuous solar power for a finite time and distance. In some cases, this stored energy will be enough to cross a gap in surface lighting (i.e., a shadow) to reach an otherwise unconnected region of lit terrain. Doing so can greatly expand the total reachable area and enable prolonged routes that cover more ground. In other mission scenarios, rovers will pursue science targets located in permanently shadowed regions (PSRs). Because they are never exposed to sunlight, PSRs act as cold traps, where the temperature never exceeds the sublimation point of frozen volatiles. The highest concentrations of water ice and other valuable resources are expected to be found within PSRs, making them high priority targets for science sampling. Obviously, a rover entering a PSR will not receive continuous solar power and must instead rely on its batteries. So while treating exposure to direct sunlight as a hard constraint does produce viable routes, doing so fails to take advantage of battery power and artificially limits polar exploration.

Instead, either sunlight must be treated as a soft constraint or battery level must be added as a global constraint. A planner that treats sunlight exposure as a soft constraint would penalize route segments that occupy unlit states, or conversely, reward route segments that occupy sunlit states. This can be done using weighted cost functions that define a combined path cost as done in [90], but this solution is unsatisfactory for several reasons. First, merely penalizing routes for crossing unlit terrain does not guarantee that a rover's stored energy will not drop below zero at some point when traversing the route, because battery level is not explicitly modeled. The only way to make this guarantee is to set the penalty to infinity, in which case the soft constraint on lighting degenerates to become a hard constraint. Second, there is no straightforward or principled way of tuning the numerical weights to balance path length and path lighting. It is difficult to accurately predict the effect these numerical weights have on the generated path, and the weights have to be hand-tuned in a trial-and-error fashion. Even then, one set of weights might not always produce desirable results. Third, while implementing a weighted cost function is straightforward for deterministic path planners like A*, it is less so for a randomized path planner like RRT*, since distances are measured in the state space, and binary illumination is not part of the rover's state.

Instead, the rover's stored energy state can be treated as a global constraint in a manner similar to that of Stentz and Tompkins Incremental Search Engine (ISE) algorithm [57], which specifies individual global constraints and plans paths that satisfy all constraints. This approach has distinct advantages over those that require hand-tuning numerical weights of a combined cost function. It guarantees that the stored energy level does not drop below zero, it requires no hand-tuning of numerical weights that have no physical meaning, and it can be implemented in both deterministic

planners, like A*, and randomized planners, such as RRT*.

10.1.2 Maximizing Solar Array Configurations

An important addition is developing a power model that can handle arbitrary solar panel configurations. This thesis does not account for the orientation of a rover's solar panel relative to the sun angle. It instead assumes that the solar array receives 100% of the solar flux passing through a surface area normal to the sun vector (minus photovoltaic efficiency losses). This simplified model is only true for the case of fully articulated solar arrays that can use three degrees of freedom to always point the solar array directly toward the Sun, regardless of Sun position, surface normal, rover suspension, or heading. This assumption is unrealistic for most rover configurations, especially those designed for planetary missions, for which the solar panel might have zero or one articulated degree of freedom (e.g., yaw only).

This section suggests a method to plan for arbitrary solar panel configurations while maximizing solar gain through route planning. This could be done by computing the minimum angle between the solar panel's normal vector and the Sun vector using a kinematic representation of the rover's solar panel configuration, the rover's heading, the ground surface normal as a function of location, and the Sun angle as a function of time. The minimum angle between the Sun vector and solar panel normal corresponds to the maximum solar flux for a given configuration and state. It is assumed that the rover's solar panel can track the Sun subject to its configuration during route execution. Rover suspension could also be considered; however, because the finest polar DEMs available have a spatial resolution an order of magnitude larger than the scale of a typical planetary rover wheelbase and track width ($\sim$10 meters versus $\sim$1 meter), terrain geometry affecting a rover's suspension cannot be resolved. This limits the usefulness of modeling rover suspension when planning global routs. Instead, a small constant efficiency loss might be assumed to account for small variations in rover suspension.

10.2 Planning for Efficiency

Global path planners must generate solutions quickly and efficiently to be useful, and doing so becomes increasingly challenging as the temporal extent of models and routes increases in pursuit of rover longevity. Even during early stages of mission planning, when real-time path planning is unnecessary, efficient route generation is important because it reduces the resources—time, money, computation, personnel—that must be spent. As the size, resolution, and dimensionality of the planning problem increase to facilitate better plans, the search space becomes intractable for grid-based planners like A*. This thesis began to address this issue through novel use of connected component analysis and other temporal pruning techniques (see Chapter 5). Additional efficiency mechanisms should be implemented to further speed up deterministic path planning. These might include dynamic state generation, resolution equivalence pruning, and state dominance in a manner similar to [57]; however these techniques

will likely not be enough to make a full-featured version of an A*-based planner viable at the greatest resolutions and scales. This motivates faster, sampling-based, asymptotically optimal methods due to their speed advantages.

Whereas this thesis work focused on the development of a deterministic, grid-based path planner, the future work might emphasizes the development of a randomized, non-grid-based planner. The primary motivation for this is to address run speed performance concerns related to the time complexity of the A* algorithm, which does not scale well with increasing dimensionality and range. Rapidly-exploring random tree (RRT) algorithms use a stochastic sampling-based approach, which avoids discretizing the state space and generates a search tree that explores the state space much more rapidly than do algorithms like A* [61]. The tradeoff is that because RRTs are not deterministic, they do not produce optimal plans (i.e., they do not minimize path length or path cost), and the paths they generate tend to "wander" through the environment before arriving at the goal.

RRTs are also only probabilistically complete, meaning that the probability of finding a solution approaches unity as time approaches infinity. This completeness guarantee is weaker than that of A*. More recently, the RRT* algorithm addressed the suboptimality of RRTs by introducing an iterative anytime approach that is asymptotically optimal, meaning that over time, the solution converges to the optimal solution (that which minimizes path length) [62]. RRT* works by constantly updating the search tree's parent-child relationships as uniform samples are generated, effectively finding the optimal path to every sampled point in the state space. Because only a single path to a single query is needed, much of the computation is wasted effort. The amount of time it takes for the algorithm to converge grows arbitrarily large with increasing dimensionality of the state space.

Another drawback is that, like standard RRTs, RRT* tends to have trouble exploring narrow passageways due to the reduced probability of randomly sampling these areas. A new, recently published algorithm, Informed RRT* addresses both of these issues by directly sampling from the n-dimensional ellipsoid that can theoretically improve the current best solution [63]. This modification improves performance compared to RRT* by an order of magnitude in complex environments.

The Informed RRT* algorithm as presented in [63] may serve as the basis for a randomized polar path planning algorithm, referred to here as "Polar RRT*." Development of Polar RRT* could begin by implementing Informed RRT* in the same three-dimensional spatiotemporal state space (x, y, t) as described in Chapter 5 and with the same constraints on sunlight, communication, and slope described in Chapter 6. Polar RRT* can use the same discretized maps representing surface lighting, communication access, and steep slope, but constraints on these quantities can be enforced as collision checks along continuous straight-line arcs connecting the nodes of the algorithm's search tree. The random sampling step can be modified to generate search tree edges that represent positive time increments only to prevent physically impossible paths that require the rover to travel backward in time. State generation can also be constrained by rover velocity limits. That is, newly sampled states that would generate an edge to an existing node that exceeds a maximum velocity parameter should be thrown out. This way, all paths through the randomly generated search

tree are guaranteed to be executable by the rover. Ideally, it could be shown that even with these modifications, Polar RRT* retains the completeness and optimality guarantees of Informed RRT*.

Initial comparisons of algorithm performance and solution quality might include just the three state space dimensions and three environmental constraints already prototyped for "Polar A*." A corresponding version of Polar RRT* ought to first be prototyped, and then both algorithms should be implemented in an efficient coding language to facilitate effective testing and evaluation. Experiments may include comparisons of several metrics, including the average time to generate solutions of a certain path cost and the path cost of the best solution given a fixed duration of computation time. Once this baseline testing and comparison have been completed, functionality can be added to both planners in parallel followed by additional testing. Development should occur in cycles of prototyping, implementation, and testing.

Additional constraints and parameters can be added to the planner as necessary to achieve the primary and stretch goals described in this chapter. Added constraints could include limits on the rover's stored energy state (battery level) and the rover's thermal state. These must be treated as global constraints over the entire planned path because they are dependent on both the current and previous sequence of states. Battery energy and thermal state need not be added dimensions of the state space being searched, since these state are solely dependent on other states and parameters. For example, battery energy is a function of the entire history of position and time along with parameters that include rover heading, Sun angle, surface normal, and solar panel configuration. It would be inappropriate, therefore, to randomly sample these states in the same fashion as the x, y, t states, which are independent parameters. The treatment of these states, parameters, and constraints could follow that of the Incremental Search Engine and TEMPEST planner described in [57].

These additions should be implemented in both Polar RRT* and Polar A* to provide a valid comparison of algorithm performance and route quality. This can be done as a parallel development in which the objectives of the two planners are the same, but the approaches are different. The primary motivation for developing Polar RRT* is to overcome the time complexity issues of Polar A* by taking advantage of Informed RRT*'s focused state expansion. Parallel development of Polar A* is needed primarily to provide a basis for evaluating performance and quality. Both developments seek to retain guarantees of completeness and optimality, which are stronger for A* than RRT*. As the dimensionality and range of the planning problem are increased, it is expected that Polar A* will become impractical or even intractable from a run time perspective and will be outperformed by Polar RRT*, leaving randomized methods as the only viable approach.

10.3 Planning for Thermal

Thermal state is an important consideration for any spacecraft, especially rovers exploring polar regions where day–night temperature swings are extreme. It is virtually impossible to design a rover that can passively survive both the hottest and coldest

temperatures recorded at the lunar poles, which is a large part of the motivation of sun-synchronous routes. When rover traverses are planned in a way that maximizes electric solar power, near-continuous thermal solar energy is a convenient side effect. For this reason, it may not be necessary to explicitly enforce constraints on the rover's thermal state at plan time. It may instead be enough to compute the thermal state as a function of time over the planned path post hoc (after planning is complete) to check for violations. This can be done using simple transient models of thermodynamics. If this strategy turns out to be insufficient, leading to regular violations of temperature limits, then thermal state must be added to the planner's set of constraint parameters. This addition should not add dimensionality to the search space, since thermal state is a function of other states and dependent parameters. It will merely serve to reject certain transitions from existing states to new states upon node expansion. It is effectively just additional collision checking. For routes that include short forays into permanently shadowed regions, it may be necessary for the rover to heat itself using battery energy for short durations of time. In this case, interdependencies between thermal state and battery state must be modeled.

10.4 Planning for Science

10.4.1 Mission Enhancement

The path planning developed so far by this research is limited to point-to-point planning. It assumes that a start location and goal location, or a longer sequence of waypoints, are provided by human mission planners. The planner then plans the shortest distance and duration path from the first waypoint to the second, from the second to the third, and so on until the final goal has been reached. Waypoints are specified in space and time as (x, y, t) tuples. The planner interprets the waypoint time as a constraint on the latest acceptable time and is capable of finding shorter-duration routes to the same point at earlier times if they exist. When it is possible to arrive at a point early, the planner also allows the route to leave that point early to head to the next waypoint. In this way, waypoint sequences can sometimes be condensed in the time dimension, resulting in early arrival at the final goal. When this happens, the rover's position remains stationary for any remaining time. The advantage of this strategy is that when the rover is ahead of its required pace, it is generally less susceptible to losing sunlight and being overtake by shadow. The disadvantage is that because traverse segments between waypoint pairs are planned serially, it is possible that by altering the timing of early waypoints it becomes impossible to reach later waypoints that would otherwise have been feasible. This can happen if the early arrival of the rover at a waypoint leads to it being trapped a shadow sweeping across that location that a later-arriving rover would have avoided. This behavior is undesirable, and future work should attempt to resolve this issue.

A bigger problem is that the requirement for waypoints to be explicitly expressed as input to the planner severely limits its utility. The purpose of the suggested research is to enable planners to identify prolonged routes that are unintuitive or

impossible to plan manually. A human mission planner cannot be expected to seed the planner with exact waypoints that facilitate this. Additionally, the order in which the waypoints are visited may not matter, so an ordered sequence of points as input may be inappropriate. Future research should seek to address these issues to enhance missions with respect to their science objectives. The remainder of this subsection describe some possible approaches.

The first approach to improve human mission planners' ability to plan a prolonged feasible path is a repurposing and extension of the connected component analysis described in Chapter 5. Connected component analysis with temporal pruning yields a representation of future location–time states that can be reached from a given starting point without crossing shadowed terrain. So, given a single landing location and time, connected component analysis can be used to indicate a set of valid states that can be reached. It does not provide the complete set of reachable states, since it does not account for battery-powered driving in darkness. It does, however, offer useful data that can inform waypoint and science target selection. Once a first goal location has been chosen, the connected components can be reanalyzed to update the set of reachable states, and the process can be repeated. The strategy will not produce globally optimal mission plans and requires a human in the loop, but it may lead to better, longer, more efficient rover traverses. This idea is related to the mixed-initiative planning discussed in Subsection 10.4.2.

When trying to maximize scientific discovery, human mission planners often generate a (sometimes prioritized) list of candidate locations for specific experiments, measurements, and samples, but the order in which these science targets are visited may not matter. The list of candidate science targets may even contain duplicate science activities in several different locations, only a subset of which are possible or necessary. In this case, it would be useful to have a traverse planner that can consider all possible combinations and orderings of science targets. For small problems with few permutations, it may be feasible to compute routes for every possible permutation by brute force, but in general, this will not be possible. This problem is similar to the Traveling Salesman Problem (TSP), which has been studied at length, yielding many approaches that produce approximate solutions. The problem of solar-powered exploration is unique in that it must enforce constraints in dynamic environments, meaning the edge costs of the TSP change as a function of time. Some edges will even disappear when the constraints make an edge infeasible or of infinite cost. Still, some TSP solvers might be adapted to enhance polar mission planning.

Another enhancement that addresses the problem of specifying waypoints is related to an inherent property of RRTs. The primary reason so many waypoints were needed to plan multi-month missions on the Moon (as in Chapter 6) was to reduce computation time by limiting the maximum search tree depth. In the worst cast, the time complexity of A* search is exponential in the depth of the solution [88, 89]. Doubling the number of waypoints doubles the number of searches that must be executed but halves the average search depth, resulting in a dramatically reduced overall time complexity.[1] Adding additional waypoints between science targets exacerba-

[1]For example, adding a single waypoint midway between a start and goal separated by 20 time

tes the problem of manually determining a viable (much less, optimal) placement of those waypoints. The speed advantages of Informed RRT* ameliorate this problem, since intermediary waypoints are not needed for the algorithm to be tractable. Polar RRT* should explore the full depth of the search space rapidly, and the only necessary waypoints will be those representing specific science targets.

Finally, it is sometimes the case that targeting exact locations for science activities to a precision of just a few meters is not only impractical but also unnecessary, when getting close will suffice. This is the case in prospecting for native resources on the Moon, since the hydrogen concentration maps that indicate evidence for water ice are coarse in resolution. Science targets can then be expressed as a certain radius around a center point: any sample within that circle is acceptable. This representation adds slack to the planning problem, since route might be shortened by visiting points just within the target area before changing direction. Adding multiple goals, or a set of goals comprising a circular region of space, is simple. For A* algorithms, the entire set of goals can be used to initialize the frontier list, and the search can run backward to the start location. In RRT algorithms, the goal state check can include a radius around a central point goal state. However, when this behavior is used to plan a sequence of traverses between a series of waypoints in a greedy, serial fashion, the resulting route will in general not be globally optimal. Future research might pursue algorithmic enhancements to make better use of allowable slack.

10.4.2 Mixed-Initiative Planning

Planning feasible routes and activity schedules manually is expensive, time-consuming, error-prone, and suboptimal. For problems with large, high-dimensional state spaces and complex constraints, humans are often incapable of generating viable solutions, much less optimal ones. Automation can greatly reduce the cost and time to generate plans that are both correct and optimal (with respect to some cost function and map resolution); however, these plans do not always reflect high-level human intent. For example, standard path planning algorithms can quickly compute the shortest obstacle-free path between pairs of pre-defined waypoints, but a human must first supply an ordered sequence of manually selected waypoints. Each waypoint might be the location of a science activity, but this is a poor representation of the humans intent to maximize the number and diversity of science targets. Furthermore, poorly selected waypoints may invalidate the entire plan. This challenge is even greater in the case of solar-powered polar rovers, which must navigate dynamic, unintuitive lighting and communication environments.

Future research may seek to automate rover traverse planning in a way that naturally incorporates human input at the mission-objective level to improve plans and reduce the burden on mission personnel. Instead of specifying exact coordinates where specific activities should be executed, a user will define the types of activities that can be performed (including logistical parameters such as the amount of time, energy,

steps reduces the time complexity from $O(b^{20c})$ to $O(2b^{10c})$ where b is the branching factor and c is a constant related to the search heuristic. For $b = 9$ and $c = 0.5$, this reduces the worst case number of nodes expanded from 3.48 billion to 118 thousand.

and memory required), the target quantity of each activity, and a corresponding set of regions in which activities should occur. The initial activity plan can be ordered, unordered, or partially ordered, and the size and shape of each region can vary between a single point and the entire globe. The planning algorithm will then return a feasible solution that prevents conflicts and violations if one exists. If not, the algorithm will return an approximate solution. The user will then provide feedback by altering initial conditions or manually editing segments of the plan, and the algorithm will replan to reflect that input. This process can continue until the user is satisfied with the result, which is optimal given the users constraints.

Tompkins TEMPEST planner shares this ambition for mission-directed path planning with dynamic lighting but requires fully ordered sequences of goals and actions [57]. Existing mixed-initiative planning and scheduling tools for planetary rovers such as MAPGEN [91] require excessive hand-editing and lack fully integrated path planning and dynamic resource constraints. Future research could improve upon these approaches by combining elements of spatiotemporal path planning and mixed-initiative activity planning and scheduling.

10.5 Planning for Perpetual Exploration

Minimum Viable Multiyear Route

This thesis suggests that solar-powered routes can be divided into three distinct classes: sub-day, multi-day (sub-year), and multiyear. Sub-day routes are those that last less than one diurnal cycle on a particular planetary body. For example, one lunar day lasts approximately 29.5 Earth days, so a sub-day route on the Moon would last less than one month before the solar-powered vehicle is overtaken by shadow. Without sunlight, the vehicle would lose power, deplete its battery energy, and succumb to extreme cold temperatures, likely ending the mission. These are conservative routes that linger near a single location anywhere on the globe until nightfall. They require no particular driving speed. The only way to extend these missions is to choose locations with greater than average Sun exposure near the pole. In the case of the Moon, no single site is lit continuously for a full diurnal cycle.

Multi-day sub-year routes are those that endure more than one diurnal cycle but less than one annual cycle. For the Moon, this is between 30 and 365 Earth days (one lunar year is equivalent to one Earth year). This is the class of route already demonstrated to exist by this research and with which the primary goals of the future work are concerned. To execute a multi-day route, solar-powered vehicles must be in close proximity to the geographic pole and circle either the pole itself of a region of high elevation to remain predominantly in sunlight. These routes require slow to moderate driving speeds depending on the size of the planetary body, its rate of rotation, and the latitude and local geometry of the terrain being explored (often less than 10 cm/s on the Moon). This is only possible during local summer if the body's axis of rotation is inclined relative to the ecliptic plane (the Moon's axis is tilted approximately 1.5 degrees). During local winter, the globe's roughly spherical

shape will shadow the entire polar region, eliminating access to solar power. Without leaving the polar region, vehicles are likely limited to about half a year of solar-power. The actual maximum duration is an unknown quantity that the future work should seek to determine.

Multiyear routes are those that last longer than one annual cycle (more than 365 Earth days for the Moon). The only way for a solar-powered vehicle to accomplish this is to migrate away from polar latitudes. Because of the Moon's 1.5-degree tilt, lunar rovers would have to descend below about 88.5 degrees North or South, since the region above this latitude experiences extended periods of seasonal darkness. For a hypothetical perfectly spherical body, this approximation is exact, but the eccentricities and local surface features of actual planets and moons make determining this line nontrivial. This leads to the idea of computing the minimum viable multiyear route, which is the shortest path that enables solar-powered exploration for at least one full year. Solving this minimization problem is important because it indicates what maximum drive speed is required to achieve indefinite solar-powered exploration.

One possible method of finding the minimum viable multiyear route for a particular planetary body is to first find the highest line of latitude that, if followed with proper timing and speed, provides continuous sunlight to the vehicle for the full year. This could be done using a binary search process that begins with an upper and lower bound that bracket that sought latitude and then narrows the gap based on whether or not continuous illumination at the bounds is possible. This of course assumes that the illumination test behaves like a sorted list with respect to latitude, which it may not. In other words, the result of the check as a function of latitude must be a step function. Once the approximate maximum latitude of continuous illumination is found, the total path length might be honed iteratively as follows. First place along the circle a set of points connected by straight line segments (actually curved segments of great circles). Then remove one point at a time, connect the two adjacent point with a straight line, and check if that arc violates the lighting constraint. If the constraint is violated, replace the removed point; if not, move on to the next point. Repeat this process until no points can be removed without violating the constraint. Then, add a midpoint between each of the original points and start the process over. Eventually, the segmented route should converge to the shortest viable multiyear route.

This iterative method of searching for the minimum viable multiyear route is analogous to incrementally shrinking a rubber band stretched around the Moon. The rubber band naturally wants to minimize it total arc length and reduced to a point at the lunar pole. It is held in place by a set of waypoints acting like pins in a pincushion. Each iteration removes a single pin, and the rubber band shrinks incrementally to minimize its length subject to the remaining set of constraints. This process is continued as long as the path of the rubber band does not violate any constraints on lighting. The final result can be thought of as the shortest possible length of rubber band that circumnavigates the pole and satisfies all constraints. The minimum viable multiyear route is the shortest possible "rubber band" route.

The shortest multiyear route reveals both the maximum and minimum speeds required to execute such a route. The lowest possible maximum (min-max) drive speed

necessary could be computed by examining the lighting conditions as a function of time along the route. The method described relies on assumptions and simplifications, such as ignoring slope, that may invalidate the result. Additional formulation is needed to address these complications.

10.6 Planning a Sustainable Power Grid

Minimum Viable Solar Grid

A related concept to the minimum viable multiyear route is to estimate the minimum viable solar grid. This is defined as the smallest finite set of fixed points on the surface of a planetary body such that for all times, at least one points is illuminated by direct sunlight. If a solar power station were set up at each of these points, a network could be formed which supplies continuous solar power to nearby appliances, such as vehicles, habitats, or in-situ resource utilization infrastructure. The power grid could be connected either by cables or beaming power to solar receivers. Natural extensions include finding the minimum viable solar grid that minimizes the total length of electrical cable needed to form a complete network and finding the minimum viable solar grid such that a complete network can be formed through direct line of sight between power stations. Near the poles, continuous seasonal power is likely achievable with only two or three power stations and minimal distances between them. To achieve continuous annual power more stations will be needed. A first step toward generating viable, albeit sub-optimal, solutions might be to place stations along an already computed minimum viable multiyear route. Other possible techniques to solve the minimum viable solar grid include constrained optimization algorithms. Future research should build on prior related work in this area [92].

Chapter 11

Conclusion

11.1 Summary

This thesis asserts that 1) spatiotemporal routes exist near the geographic poles of the Moon that enable solar-powered rovers to operate for multiple lunar days; 2) these routes satisfy constraints on uninterrupted sunlight, direct-to-Earth communication, terrain slope, rover speed; and 3) these routes can be planned using high-fidelity predictive models based on lunar topography data.

This research implements planning algorithms and utilizes high-fidelity predictive models to generate route solutions that demonstrate sustained lunar polar roving. Initial results make simplifications to reduce the size and complexity of the planning problem. Subsequent results demonstrate methodology capable of efficiently solving increasingly relevant versions of the planning problem. This research builds on prior related work in the areas of sun-synchronous circumnavigation and mission-directed path planning. These notions combine the ideas of resource-constrained temporal planning with predictive models of how sunlight and shadows evolve over time on planetary surfaces. This thesis research generates large-scale, long-duration, shortest-distance routes that satisfy resource constraints on uninterrupted sunlight, direct-to-Earth communication, rover speed, and terrain slope. This work improves the resolution at which these routes are generated, taking advantage of the latest high-resolution topographic maps of the Moon.

Sustained lunar polar routes in this research are generated using deterministic grid-based graph search approaches, specifically A*. Constraints are enforced at plan time, using binary arrays representing spatiotemporal lighting, communication, and slope conditions. The solutions presented serve to demonstrate a valuable proof of concept—that moderately paced rovers can achieve multiple lunar days of solar-powered exploration by traversing sun-synchronous lunar polar routes. This thesis also applies elements of connected component analysis to aid route selection and computation time.

11.2 Conclusions

- The South Pole of the Moon features numerous examples of multi-lunar-day sunlight routes, some of which are achievable with maximum sustained rover speed of less than 1 cm/s. Many more are possible with speeds of less than 10 cm/s.

- On the South Pole of the Moon, there exist sun-synchronous routes that satisfy constraints on terrain slope, rover speed, and uninterrupted sunlight for up to 6 months. Six months of sun-synchronous lunar polar roving is achievable at speeds of less than 10 cm/s.

- There exist on the lunar South Pole spatiotemporal routes lasting multiple lunar days that maintain uninterrupted direct sunlight and feature a direct line-of-sight to Earth at all times when the rover is in motion.

- Polar routes that enforce hard constraints on both sunlight and direct-to-Earth communication when moving tend to dwell at local peaks for weeks at a time due to a lack of autonomous driving capabilities.

- Rovers constrained by a requirement for supervised teleoperation are susceptible to errors present in lunar topography models, since long, stationary dwells in sunlight are not guaranteed.

- Rovers that are permitted to selectively deploy limited use of autonomous driving capabilities during unavoidable communication blackouts may reduce overall mission risk by guaranteeing continuous solar power.

- Within close proximity to examples of multi-lunar-day rover routes, there exist numerous feasible landing sites that feature mild slope, sustained sunlight and Earth view, and a landing radius of at least 150 meters. These sites are important for successful deployment of lunar polar rovers and can be used to validate and seed sun-synchronous routes.

- Deterministic grid-based graph search methods such as A* are sufficient to plan paths of moderate spatial and temporal resolution that avoid steep slopes and maintain uninterrupted sunlight for multiple lunar days.

- Randomized sampling-based planning methods, such as RRT, facilitate the generation of longer-duration routes on larger models with higher spatial and temporal resolution than is possible with deterministic grid-based planning methods, such as A*.

- Connected component analysis can aid mission planning by informing the selection of waypoints that are likely to be reachable from a given starting state and eliminating a large subset of unreachable states.

- Connected component analysis can improve planner performance by pruning spatiotemporal branches of sunlit states that cannot lead to a valid solution and/or do not reach a desired mission duration.

11.3 Contributions

This thesis research contributes to future lunar polar missions in two major capacities: 1) the ability to plan detailed sun-synchronous rover traverses, defined by spatiotemporal routes and science activities, prior to launch that sustain solar-powered lunar polar roving for multiple diurnal cycles and 2) the ability to inform on-ground decisions during mission operations through better understanding of the global mission-level repercussions. This thesis focuses on the former but contributes to the latter as well. The primary contribution is a pair of ground-based route planning methods that handles dynamic resources and constraints characteristic of polar exploration and generates large-scale, long-duration, global routes that enhance and extend robotic missions. During mission design, this technology aids the selection of landing sites, rover routes, and science activities. During mission operations, it can provide anytime contingencies in response to new discoveries. The following contributions will improve the mission longevity, range, efficiency, safety, and scientific return of robotic rovers exploring the poles of the Moon.

1. A grid-based method to plan sun-synchronous routes that sustain solar-powered polar roving on the Moon to durations lasting multiple diurnal cycles while satisfying constraints on
   (a) direct exposure to sunlight
   (b) direct-to-Earth communication
   (c) maximum terrain slope
   (d) maximum rover speed
2. Identification and analysis of feasible sun-synchronous routes lasting multiple diurnal cycles on the Moon with direct relevance to resource prospecting missions.
3. A strategy to selectively employ limited rover autonomy to reduce risk of sun-synchronous lunar polar exploration.
4. A sampling-based method to efficiently plan sun-synchronous lunar polar routes lasting up to 6 months while satisfying constraints on sunlight, terrain slope, and rover speed.
5. A method of selecting landing sites amenable to lunar prospecting missions and used both to validate and seed sun-synchronous routes.

Appendix A

Acronyms

DEM Digital Elevation Map/Model

DOF Degree(s) Of Freedom

DSN Deep Space Network

DTE Direct-To-Earth

DTM Digital Terrain Map/Model

EVA ExtraVehicular Activity

GEO Geosynchronous Transfer Orbit

ISE Incremental Search Engine

ISPP In-Situ Propellent Production

ISRU In-Situ Resource Utilization

LEO Low Earth Orbit

LOLA Lunar Orbiter Laser Altimeter

LRO Lunar Reconnaissance Orbiter

LROC Lunar Reconnaissance Orbiter Camera

LRV Lunar Roving Vehicle

MMRTG Multi-Mission Radioisotope Thermoelectric Generator

MER Mars Exploration Rover

MESSENGER MErcury Surface, Space ENvironment, GEochemistry, and Ranging

MSL Mars Science Laboratory

NAC Narrow Angle Camera

RHU Radioisotope Heater Unit

RPS Radioisotope Power System

RRT Rapidly-exploring Random Tree

RTG Radioisotope Thermoelectric Generator

SEXTANT Surface Exploration Traverse Analysis and Navigation Tool

TEMPEST TEmporal Mission Planner for the Exploration of Shadowed Terrain

TRN Terrain Relative Navigation

TSP Traveling Salesman Problem

WAC Wide Angle Camera

Bibliography

[1] K.Fairchild and W. W.Mendell, "Report of the In Situ Resources Utilization Workshop," in *NASA Conference Publication 3017*. Lake Buena Vista, FL: NASA, nov 1988.

[2] A.Jain and N.Trost, "Current and Near-Future Space Launch Vehicles for Manned Trans-Planetary Space Exploration: Phobos-Deimos Mission Architecture Case Study," in *AIAA SPACE 2013 Conference and Exposition*. Reston, Virginia: American Institute of Aeronautics and Astronautics, sep 2013, pp. 1–8.

[3] J.Elliott, M.Fries, S.Love, R. G.Sellar, G.Voecks, and D.Wilson, "In-Situ Resource Utilization Experiment for the Asteroid Redirect Crewed Mission," in *European Planetary Science Congress*, vol. 10, 2015.

[4] SpaceX, "Capabilities and Services," 2017. [Online]. Available: http://www.spacex.com/about/capabilities

[5] E.Musk, "Status," feb 2018. [Online]. Available: https://twitter.com/elonmusk/status/963076231921938432

[6] C. M.Pieters, J. N.Goswami, R. N.Clark, M.Annadurai, J.Boardman *et al.*, "Character and Spatial Distribution of OH/H2O on the Surface of the Moon Seen by M3 on Chandrayaan-1," *Science*, vol. 326, no. 5952, pp. 568–572, oct 2009.

[7] A.Colaprete, P.Schultz, J.Heldmann, D.Wooden, M.Shirley *et al.*, "Detection of Water in the LCROSS Ejecta Plume," *Science*, vol. 330, no. 6003, pp. 463–468, oct 2010.

[8] D. J.Lawrence, W. C.Feldman, J. O.Goldsten, S.Maurice, P. N.Peplowski *et al.*, "Evidence for Water Ice Near Mercury's North Pole from MESSENGER Neutron Spectrometer Measurements," *Science*, vol. 339, no. 6117, pp. 292–296, jan 2013.

[9] T. N.Titus, H. H.Kieffer, and P. R.Christensen, "Exposed water ice discovered near the south pole of Mars," *Science*, vol. 299, no. 5609, pp. 1048–1051, 2003.

[10] J. P.Bibring, Y.Langevin, F.Poulet, A.Gendrin, B.Gondet *et al.*, "Perennial water ice identified in the south polar cap of Mars," *Nature*, vol. 428, no. 6983, pp. 627–630, 2004.

[11] P. R.Christensen, "Water at the Poles and in Permafrost Regions of Mars," *Elements*, vol. 2, no. 3, pp. 151–155, jun 2006.

[12] D. R.Andrews, A.Colaprete, J.Quinn, D.Chavers, and M.Picard, "Introducing the Resource Prospector (RP) Mission," in *AIAA SPACE 2014 Conference and Exposition*, no. August. San Diego, CA: American Institute of Aeronautics and Astronautics, aug 2014, pp. 1–9.

[13] D. R.Andrews, "Resource Prospector (RP) - Early Prototyping and Development," in *AIAA SPACE 2014 Conference and Exposition*, 2015, pp. 1–15.

[14] A.Colaprete, R.Elphic, D.An-Drews, J.Trimble, B.Bluethmann, J.Quinn, and G.Chavers, "Resource Prospector: Evaluating the ISRU Potential of the Lunar Poles," in *Lunar Exploration Analysis Group (LEAG) Annual Meeting*, Columbia, MD, 2017.

[15] J. E.Werner, S. G.Johnson, C. C.Dwight, and K. L.Lively, "Cost Comparison in 2015 Dollars for Radioisotope Power SystemsCassini and Mars Science Laboratory," Idaho National Laboratory, Tech. Rep., 2016. [Online]. Available: https://inldigitallibrary.inl.gov/sites/sti/sti/7267852.pdf

[16] M.Wall, "Full-scale production of plutonium-238 still years away," may 2016. [Online]. Available: http://spacenews.com/full-scale-production-of-plutonium-238-still-years-away/

[17] J.Foust, "Plutonium supply for NASA missions faces long-term challenges," Washington, oct 2017. [Online]. Available: http://spacenews.com/plutonium-supply-for-nasa-missions-faces-long-term-challenges/

[18] J.Foust, "NASA argues Resource Prospector no longer fit into agency's lunar exploration plans," Washington, may 2018. [Online]. Available: http://spacenews.com/nasa-argues-resource-prospector-no-longer-fit-into-agencys-lunar-exploration-plans/

[19] M.Wieczorek, "The gravity and topography of the terrestrial planets," *Treatise on Geophysics*, 2007.

[20] D. E.Smith, M. T.Zuber, G. A.Neumann, F. G.Lemoine, E.Mazarico *et al.*, "Initial observations from the Lunar Orbiter Laser Altimeter (LOLA)," *Geophysical Research Letters*, vol. 37, no. 18, pp. 1–6, 2010.

[21] F.Scholten, J.Oberst, K.-D.Matz, T.Roatsch, M.Wählisch, E. J.Speyerer, and M. S.Robinson, "GLD100: The near-global lunar 100 m raster DTM from LROC WAC stereo image data," *Journal of Geophysical Research: Planets*, vol. 117, no. E12, dec 2012.

[22] D. E.Smith, M. T.Zuber, G. B.Jackson, J. F.Cavanaugh, G. A.Neumann *et al.*, "The Lunar Orbiter Laser Altimeter Investigation on the Lunar Reconnaissance Orbiter Mission," *Space Science Reviews*, vol. 150, no. 1-4, pp. 209–241, jan 2010.

[23] A.Colaprete, R. C.Elphic, D.Andrews, G.Sanders, A.McGovern, R.Vaughan, J.Heldmann, and J.Trimble, "Resource Prospector: Mission Goals, Relevance and Site Selection," in *Annual Meeting of the Lunar Exploration Analysis Group*, Columbia, MD, 2015.

[24] N. D.Otten, H. L.Jones, D. S.Wettergreen, and W. L.Whittaker, "Planning routes of continuous illumination and traversable slope using connected component analysis," in *2015 IEEE International Conference on Robotics and Automation (ICRA)*. IEEE, may 2015, pp. 3953–3958.

[25] N.Otten, D. S.Wettergreen, and W. R.Whittaker, "Strategic Autonomy for Reducing Risk of Sun-Synchronous Lunar Polar Exploration," in *Field & Service Robotics*. Springer, 2017, pp. 465–479.

[26] D.Paige, "DIVINER lunar radiometer experiment: The lunar thermal environment," AbFab_Plot.png, May 2014. [Online]. Available: http://www.diviner.ucla.edu/science.shtml

[27] I.Thomas, "Measurement of properties of the lunar surface using the diviner lunar radiometer experiment on the nasa lunar reconnaissance orbiter," University of Oxford, Second Year Report, Aug. 2009.

[28] A. R.Vasavada, J. L.Bandfield, B. T.Greenhagen, P. O.Hayne, M. A.Siegler, J.-P.Williams, , and D. A.Paige, "Lunar equatorial surface temperatures and regolith properties from the diviner lunar radiometer experiment," *Journal of Geophysical Research*, vol. 117, 2012, e00H18, doi:10.1029/2011JE003987.

[29] G. H.Heiken, D. T.Vaniman, and B. M.French, *Lunar Sourcebook: A User's Guide to the Moon*. New York, New York, USA: Cambridge University Press, 1991.

[30] D. A.Paige, M. A.Siegler, J. A.Zhang, P. O.Hayne, E. J.Foote *et al.*, "Diviner Lunar Radiometer Observations of Cold Traps in the Moon's South Polar Region," *Science*, vol. 330, no. 6003, pp. 479–482, oct 2010.

[31] D. A.Paige, M. C.Foote, B. T.Greenhagen, J. T.Schofield, S.Calcutt *et al.*, "The Lunar Reconnaissance Orbiter Diviner Lunar Radiometer Experiment," *Space Science Reviews*, vol. 150, no. 1-4, pp. 125–160, jan 2010.

[32] A. R.Vasavada, J. L.Bandfield, B. T.Greenhagen, P. O.Hayne, M. A.Siegler, J. P.Williams, and D. A.Paige, "Lunar equatorial surface temperatures and regolith properties from the Diviner Lunar Radiometer Experiment," *Journal of Geophysical Research E: Planets*, vol. 117, no. 4, 2012.

[33] E.Mazarico, G.Neumann, D.Smith, M.Zuber, and M.Torrence, "Illumination conditions of the lunar polar regions using LOLA topography," *Icarus*, vol. 211, no. 2, pp. 1066–1081, feb 2011.

[34] D. E.Smith, "LRO-L-LOLA-4-GDR-V1.0," Goddard Space Flight Center, LOLA Gridded Data Record Shape Map LDEM_85S_10M, 12 2013, v2.0.

[35] S.Kassel, "Lunokhod-1 Soviet Lunar Surface Vehicle," The Rand Corporation, Tech. Rep., 1971. [Online]. Available: http://www.dtic.mil/docs/citations/AD0733960

[36] I.Karachevtseva, J.Oberst, F.Scholten, .Konopikhin, K.Shingareva, E.Cherepanova, E.Gusakova, I.Haase, O.Peters, J.Plescia, and M.Robinson, "Cartography of the Lunokhod-1 landing site and traverse from LRO image and stereo-topographic data," *Planetary and Space Science*, vol. 85, pp. 175–187, sep 2013.

[37] I.Karachevtseva, N.Kozlova, A.Kokhanov, A.Zubarev, I.Nadezhdina *et al.*, "Cartography of the Luna-21 landing site and Lunokhod-2 traverse area based on Lunar Reconnaissance Orbiter Camera images and surface archive TV-panoramas," *Icarus*, vol. 283, pp. 104–121, feb 2017.

[38] S.Blair, "Rovers return," *Engineering & Technology*, vol. 6, no. 3, pp. 48–50, apr 2011.

[39] National Air and Space Museum, "Lunar Roving Vehicle (LRV)." [Online]. Available: https://airandspace.si.edu/explore-and-learn/topics/apollo/apollo-program/spacecraft/lrv.cfm

[40] M.Wright, B.Jaques, and S.Morea, "A Brief History of the Lunar Roving Vehicle," in *History of the NASA Marshall Space Flight Center*. Huntsville, AL: Marshall Space Flight Center, 2002. [Online]. Available: http://history.msfc.nasa.gov

[41] Z.Sun, Y.Jia, and H.Zhang, "Technological advancements and promotion roles of Chang'e-3 lunar probe mission," *Science China Technological Sciences*, vol. 56, no. 11, pp. 2702–2708, 2013.

[42] S.Clark, "China's Yutu rover dies on the moon," aug 2016. [Online]. Available: https://spaceflightnow.com/2016/08/04/chinas-yutu-rover-dies-on-the-moon/

[43] E.Lakdawalla, "Bad news for Yutu rover," jan 2014. [Online]. Available: http://www.planetary.org/blogs/emily-lakdawalla/2014/01251527-bad-news-for-yutu-rover.html

[44] Xinhua, "China Exclusive: Control circuit malfunction troubles China's Yutu," Beijing, mar 2014. [Online]. Available: https://web.archive.org/web/20140309013421/http://news.xinhuanet.com/english/china/2014-03/01/c{_}133152096.htm

[45] Xinhua News Agency, "Chinese lunar rover alive but weak," Beijing, may 2014. [Online]. Available: http://www.spacedaily.com/reports/Chinese{_}lunar{_}rover{_}alive{_}but{_}weak{_}999.html

[46] J.Aron, "China's Jade Rabbit moon rover dead after 31 months on surface," aug 2016. [Online]. Available: https://www.newscientist.com/article/2099696-chinas-jade-rabbit-moon-rover-dead-after-31-months-on-surface/

[47] M.Wall, "The Moon's History Is Surprisingly Complex, Chinese Rover Finds," mar 2015. [Online]. Available: https://www.space.com/28810-moon-history-chinese-lunar-rover.html?adbid=10152690360766466{&}adbpl=fb{&}adbpr=17610706465

[48] M. T.Zuber, D. E.Smith, R. J.Phillips, S. C.Solomon, G. A.Neumann *et al.*, "Topography of the Northern Hemisphere of Mercury from MESSENGER Laser Altimetry," *Science*, vol. 336, no. 6078, pp. 217–220, apr 2012.

[49] D.Wettergreen, P.Tompkins, C.Urmson, M.Wagner, and W.Whittaker, "Sun-Synchronous Robotic Exploration: Technical Description and Field Experimentation," *The International Journal of Robotics Research*, vol. 24, no. 1, pp. 3–30, jan 2005.

[50] D. B. J.Bussey, P. D.Spudis, and M. S.Robinson, "Illumination conditions at the lunar South Pole," *Geophysical Research Letters*, vol. 26, no. 9, pp. 1187–1190, may 1999.

[51] W. L.Whittaker, G.Kantor, B.Shamah, and D. S.Wettergreen, "Sun-synchronous planetary exploration," in *AIAA Space*, 2000.

[52] P.Tompkins, A.Stentz, and D.Wettergreen, "Mission-level path planning and re-planning for rover exploration," in *Robotics and Autonomous Systems*, vol. 54, no. 2, feb 2006, pp. 174–183.

[53] J.Heldmann, A.Colaprete, R. C.Elphic, B.Bussey, A.McGovern, R.Beyer, D.Lees, M. C.Deans, N.Otten, H.Jones, and D.Wettergreen, "Rover Traverse Planning to Support a Lunar Polar Volatiles Mission," in *Annual Meeting of the Lunar Exploration Analysis Group*. NASA Ames Research Center, oct 2015.

[54] D.Wettergreen, P.Tompkins, C.Urmson, M. D.Wagner, and W. L.Whittaker, "Sun-synchronous robotic exploration: Technical description and field experimentation," *The International Journal of Robotics Research*, vol. 24, no. 1, pp. 3–30, January 2005.

[55] M.Maimone, Y.Cheng, and L.Matthies, "Two years of Visual Odometry on the Mars Exploration Rovers," *Journal of Field Robotics*, vol. 24, no. 3, pp. 169–186, Mar. 2007.

[56] V.Asnani, D.Delap, and C.Creager, "The development of wheels for the Lunar Roving Vehicle," *Journal of Terramechanics*, vol. 46, no. 3, pp. 89–103, Jun. 2009.

[57] P.Tompkins, "Mission-directed path planning for planetary rover exploration," Ph.D. dissertation, Robotics Institute, Carnegie Mellon University, Pittsburgh, PA, May 2005.

[58] A.Stentz, "Optimal and efficient path planning for partially-known environments," in *Proceedings of the 1994 IEEE International Conference on Robotics and Automation*. IEEE Comput. Soc. Press, 1994, pp. 3310–3317.

[59] E. W.Dijkstra, "A note on two problems in connexion with graphs," *Numerische Mathematik*, vol. 1, no. 1, pp. 269–271, dec 1959.

[60] P.Hart, N.Nilsson, and B.Raphael, "A Formal Basis for the Heuristic Determination of Minimum Cost Paths," *IEEE Transactions on Systems Science and Cybernetics*, vol. 4, no. 2, pp. 100–107, jul 1968.

[61] S. M.Lavalle and J. J.Kuffner, "Randomized Kinodynamic Planning," *The International Journal of Robotics Research*, vol. 20, no. 5, pp. 378–400, may 2001.

[62] S.Karaman and E.Frazzoli, "Sampling-based algorithms for optimal motion planning," *The International Journal of Robotics Research*, vol. 30, no. 7, pp. 846–894, jun 2011.

[63] J. D.Gammell, S. S.Srinivasa, and T. D.Barfoot, "Informed RRT*: Optimal Sampling-based Path Planning Focused via Direct Sampling of an Admissible Ellipsoidal Heuristic," *2014 IEEE/RSJ International Conference on Intelligent Robots and Systems*, pp. 2997–3004, apr 2014.

[64] J. D.Gammell, S. S.Srinivasa, and T. D.Barfoot, "Batch Informed Trees (BIT*): Sampling-based optimal planning via the heuristically guided search of implicit random geometric graphs," in *2015 IEEE International Conference on Robotics and Automation (ICRA)*. IEEE, may 2015, pp. 3067–3074.

[65] S.Choudhury, J. D.Gammell, T. D.Barfoot, S. S.Srinivasa, and S.Scherer, "Regionally accelerated batch informed trees (RABIT*): A framework to integrate local information into optimal path planning," in *2016 IEEE International Conference on Robotics and Automation (ICRA)*. IEEE, may 2016, pp. 4207–4214.

[66] A.Gilkey, R.Kobrick, R.Galvan, A.Johnson, J.Hoffman, D.Newman, and P.Melo, "Evaluation of a Surface Exploration Traverse Analysis and Navigation Tool," in *41st International Conference on Environmental Systems*, no. July. Reston, Virigina: American Institute of Aeronautics and Astronautics, jul 2011, pp. 1–9.

[67] A. W.Johnson, J. A.Hoffman, D. J.Newman, E. M.Mazarico, and M. T.Zuber, "An Integrated Traverse Planner and Analysis Tool for Planetary Exploration," Master's, Massachusetts Institute of Technology, 2010.

[68] C.Cunningham, H.Jones, J.Kay, K. M.Peterson, and W.Whittaker, "Time-dependent planning for resource prospecting," in *Proc. 12th International Symposium on Artificial Intelligence, Robotics and Automation in Space*, Montreal, Canada, Jun. 2014.

[69] C.Cunningham, J.Amato, H. L.Jones, and W. L.Whittaker, "Accelerating energy-aware spatiotemporal path planning for the lunar poles," in *2017 IEEE International Conference on Robotics and Automation (ICRA)*. IEEE, may 2017, pp. 4399–4406.

[70] A.Kelly, *Mobile robotics: Mathematics, models, and methods*. Cambridge University Press, 2013.

[71] D. E.Smith, "LRO-L-LOLA-4-GDR-V1.0," Goddard Space Flight Center, LOLA Gridded Data Record Shape Map LDEM_60S_240M, 12 2013, v2.1.

[72] "Viewing Malapert Massif Peak Potential Landing Site for ESA Lunar Lander DTM." [Online]. Available: http://wms.lroc.asu.edu/lroc/view{_}rdr/NAC{_}DTM{_}ESALL{_}MP1

[73] NASA, "Welcome to the Planetary Data System." [Online]. Available: https://pds.nasa.gov/

[74] Washington University in St. Louis, "PDS Geosciences Node Data and Services: LRO LOLA." [Online]. Available: http://pds-geosciences.wustl.edu/missions/lro/lola.htm

[75] LROC Team, "LRO MOON LROC 5 RDR V1.0," German Aerospace Center (DLR), LROC Special Data Record NAC Digital Terrain Map NAC_DTM_ESALL_MP1, 10 2012.

[76] C. H.Acton, "Ancillary data services of NASA's navigation and ancillary information facility," *Planetary and Space Science*, vol. 44, no. 1, pp. 65–70, 1996.

[77] A.Keller, "Instant radiosity," in *SIGGRAPH '97 Proceedings of the 24th annual conference on Computer graphics and interactive techniques*, 1997, pp. 49–56.

[78] Blender Foundation, "Blender," www.blender.org, 2013.

[79] E.Amoroso, H.Jones, N.Otten, D.Wettergreen, and W.Whittaker, "Quantitative Evaluation of a Planetary Renderer for Terrain Relative Navigation," in *Annual Meeting of the Lunar Exploration Analysis Group*. Columbia, MD: Lunar and Planetary Institute, 2016, p. 5037.

[80] LRO LROC Team, "LRO-L-LROC-2-EDR-V1.0," Arizona State University, EDR M138582948ME, 10 2013.

[81] LRO LROC Team, "LRO-L-LROC-2-EDR-V1.0," Arizona State University, EDR M124020663ME, 9 2013.

[82] LRO LROC Team, "LRO-L-LROC-2-EDR-V1.0," Arizona State University, EDR M147761957ME, 10 2013.

[83] L. R.Gaddis, J.Anderson, K.Becker, T.Becker, D.Cook *et al.*, "An Overview of the Integrated Software for Imaging and Spectrometers," in *Lunar and Planetary Science Conference*, 1997.

[84] V.Zammit, M.Rizzo, and K.Debattista, "CSM213 computer graphics," Department of Computer Science and A.I., University of Malta, pp. 27–29, Feb. 2001, 4.3.2 Flood-Fill Algorithm. [Online]. Available: http://staff.um.edu.mt/kurt/documents/grafx.pdf

[85] C. H.Acton, "Ancillary data services of NASA's navigation and Ancillary Information Facility," *Planetary and Space Science*, vol. 44, no. 1, pp. 65–70, jan 1996.

[86] C. Z.Mooney, *Monte Carlo Simulation*. SAGE Publications, 1997.

[87] G. S. P.Miller, "The definition and rendering of terrain maps," in *ACM SIGGRAPH Computer Graphics*, vol. 20, no. 4. ACM, aug 1986, pp. 39–48.

[88] J.Gaschnig, "Exactly how good are heuristics? Toward a realistic predictive theory of best-first search," *Proceedings of the Fifth International Joint Conference on Artificial Intelligence*, pp. 434–441, 1977.

[89] J.Gaschnig, "Performance Measurement and Analysis of Certain Search Algorithms," Ph.D. dissertation, Carnegie Mellon University, may 1979.

[90] M.Sutoh, M.Otsuki, S.Wakabayashi, T.Hoshino, and T.Hashimoto, "The Right Path: Comprehensive Path Planning for Lunar Exploration Rovers," *IEEE Robotics & Automation Magazine*, vol. 22, no. 1, pp. 22–33, mar 2015.

[91] M.Ai-Chang, J.Bresina, L.Charest, A.Chase, J.-J.Hsu *et al.*, "MAPGEN: mixed-initiative planning and scheduling for the Mars Exploration Rover mission," *IEEE Intelligent Systems*, vol. 19, no. 1, pp. 8–12, jan 2004.

[92] J. V.Henrickson and A.Stoica, "Optimal placement of solar reflectors at the lunar south pole," *2016 IEEE International Conference on Systems, Man, and Cybernetics, SMC 2016 - Conference Proceedings*, pp. 2006–2011, 2017.